No. 3/2016

HIDRAULICA

HYDRAULICS-PNEUMATICS-TRIBOLOGY-ECOLOGY-SENSORICS-MECHATRONICS

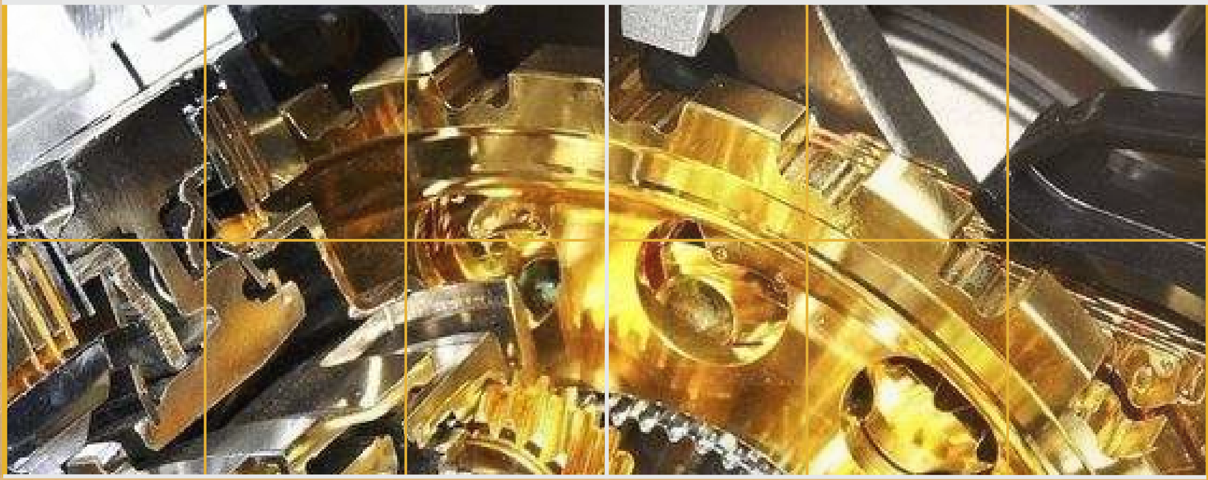

http://hidraulica.fluidas.ro

ISSN 1453 - 7303
ISSN-L 1453 - 7303

CONTENTS

BOARD

Published by:
Hydraulics and Pneumatics Research Institute, Bucharest-Romania
Address: 14 Cuţitul de Argint, district 4, Bucharest, 040558, Romania
Phone: +40 21 336 39 91; Fax:+40 21 337 30 40; e-Mail: ihp@fluidas.ro; Web: www.ihp.ro
with support from:
National Professional Association of Hydraulics and Pneumatics in Romania - FLUIDAS
e-Mail: fluidas@fluidas.ro; Web: www.fluidas.ro

HIDRAULICA Magazine is indexed by international databases:

ISSN 1453 – 7303; ISSN – L 1453 – 7303

EDITORIAL

The need for innovation

Ph.D.Eng. Petrin DRUMEA
DIRECTOR OF PUBLICATION

Many times in this corner of the magazine I approached, quite directly and in the simplest way, many issues of scientific research, considered from point of view of a person particularly interested in fluid power systems. This time also I will observe the rule and I will try in little words, without a desire for generalization, to discuss a subject of great interest among our partners, bringing in front of the reader only a few elements of a comprehensive process. Many times we find ourselves in the position to explain what innovation is and why it is said that without it hardly anything can be done in future. Obviously this editorial is only about innovation in the field of fluid power and related fields.

The first thing we usually clarify is that there are many differences between innovation and inventics, highlighting the importance and utility of both activities.

The second thing we point out is that innovation also relates to research, design, development and services within the field, thus going beyond technical innovation of products. Of course, invention is still very important, but for us it represents only a part of the innovation process, sometimes precisely the essential part, that's true; however the interest in the field is to ensure progress both in the area of research and development services and in all services involved in production and sale.

Thirdly we try to persuade the people with whom we discuss just how important in innovation partnership with specialists in other innovative entities is, be there specialists in the field or experts in related or complementary fields.

Fourthly we try to explain that innovation requires from us intimate knowledge of subdomains addressed, which leads automatically to building partnerships, various and specific to the issues approached. Partnerships that our research unit joins are based on fairly clear knowledge of the abilities and skills of those involved; often prior experiences are essential, and we assess them according to the results obtained. Of course we also admit the solution of building partnerships together with entities that we have not had the opportunity to collaborate with so far, but in this case what matters is the experience which they possess in the field and which they proved by the results obtained in recent years.

Another important thing for us (the fifth one) is how much contact with the real economy those who wish to participate in innovation within a field have, as we think that a "generally speaking innovation" process is not possible, or perhaps it could be only in very few cases, and those would be special cases.

Finally I would like to point out that innovation is not a trendy topic, it is a must to ensure progress in all fields of real life, and also I would like to say that innovation can only be done by people qualified and experienced in the field in which this process will be carried out.
Good luck in innovating to improve people's lives!

Use of Finite Taylor Developments Method to Determine the Flow Coefficient of Small Orifices

PhD. Eng. **Andrei VOINEA**[1], Assoc. Prof. PhD. Eng. **Lucian MÂNDREA**[2],
Prof. em. PhD. Eng. **Valeriu PANAITESCU**[3]

[1] University POLITEHNICA of Bucharest, Romania, e-mail: andreilucianvoinea@yahoo.com

[2] mandrea_lucian@hotmail.com

[3] valeriu.panaitescu@yahoo.com

Abstract: *This paper presents the finite Taylor developments method used to integrate the Navier-Stokes equations with the purpose of obtaining the hydrodynamic spectrum of the flow in a tank and also in the orifice contracted section of the liquid exit. The authors created a computing program which allows running also at high Reynolds numbers to determine the theoretical value of the orifice flow coefficient. An experimental installation was also made to obtain the practical value of the flow coefficient. Conclusions were obtained comparing the two values.*

Keywords: *flow coefficient, current lines, orifice, numerical methods.*

1. Introduction

The main objective of the paper is to determine the flow coefficient of an orifice using numerical methods. The authors solve the system of flow equations for different Reynolds numbers, first with Re = 1, then with the values 10 and 1000.
The finite Taylor developments method was used and different flow patterns where obtained, represented with the values of the current function ψ.
In the experimental research the Re number of the flow through circular orifices has been defined with the diameter d of the orifice to determine the variations of the flow coefficient μ,

$$\mathrm{Re} = \frac{d\sqrt{2gH}}{\upsilon} \tag{1}$$

$$\mu = \varphi_c \varphi_v \tag{2}$$

H is the orifice head and *υ* is the kinematic viscosity.
Synthesizing the experimental results, there is obtained a diagram that shows the dependence of the velocity coefficient φ_v, contraction coefficient φ_c, and flow coefficient μ with the Re number [1]. Subsequently the diagram was completed with their variation in laminar flow regime as in figure 1, [2], [3].

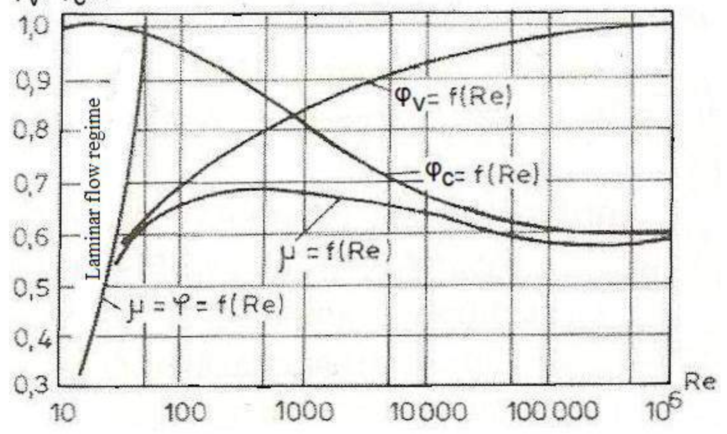

Fig. 1. Dependence of the φ_v, φ_c and μ coefficients according to Re

The μ coefficient dependence on the H head orifice is expressed implicitly by the Reynolds number. The numerical solution obtained can solve the problem of determining the contraction coefficient of an orifice and with the help of this value.
Then the orifice flow coefficient can be determined and finally the actual flow rate which flows out of the tank.

2. The numerical solution of the flow

It is considered a flow through a tank with free surface, fueled at the top and provided with a central orifice at the bottom. The bi-dimensional flow of the fluid is analyzed to estimate the contraction coefficient into the orifice at the bottom of the tank. It is considered that the movement of the liquid phase is permanent, axially symmetric. The dimensionless values are introduced [4], [5], [6], and [7]:

$$\begin{aligned} & r=\frac{R}{R_t},\ z=\frac{Z}{R_t}, \\ & v_r=\frac{V_r}{V_m},\ v_z=\frac{V_z}{V_m}, \\ & p=\frac{P}{\rho V_m^2},\ \psi=\frac{\Psi}{V_m R_t^2}=\frac{\Psi\pi}{Q},\ \mathrm{Re}=\frac{V_m R_t}{\upsilon} \end{aligned} \tag{3}$$

r and z are the dimensionless components of spatial variables, v_r and v_z are the dimensionless velocity components of the horizontal and vertical directions, p the dimensionless pressure, ψ the dimensionless stream function and Re the dimensionless Reynolds number used in the literature to determine the Re number in the tank.
Within formulas R is the radius and Z the share of the vertical point of interest, R_t is the maximum radius of the tank, Z_t maximum height of the tank, V_m the medium velocity, P the pressure, Q is the volumetric flow rate of the liquid and υ is the kinematic viscosity of the liquid.
Using the Reynolds number of the flow inside the tank as well as the previous dimensionless values in the Navier-Stokes equations system, the partial differential equation is obtained [4], [5], [6], and [7]:

$$\begin{aligned} & \psi^{IV}_{r^4}+2\psi^{IV}_{r^2z^2}+\psi^{IV}_{z^4}-2\frac{\psi^{III}_{r^3}+\psi^{III}_{rz^2}}{r}+\frac{3}{r^2}\left(\psi^{II}_{r^2}-\frac{\psi^{I}_{r}}{r}\right)= \\ & \mathrm{Re}\left(\frac{3\psi^{I}_{z}\psi^{I}_{r}}{r^3}+\frac{\psi^{II}_{rz}\psi^{I}_{r}-2\psi^{II}_{z^2}\psi^{I}_{z}-3\psi^{II}_{r^2}\psi^{I}_{z}}{r^2}+\frac{\psi^{III}_{r^3}\psi^{I}_{z}-\psi^{III}_{z^3}\psi^{I}_{r}-\psi^{III}_{r^2z}\psi^{I}_{r}+\psi^{III}_{rz^2}\psi^{I}_{z}}{r}\right) \end{aligned} \tag{4}$$

It is considered that the velocity is zero on the solid walls.
The next conditions for the stream function were imposed in order to solve the problem, $\Psi = 0$ on the solid wall of the tank.
The flow field is covered by a rectangular network with constant steps,
$\Delta r = h$ and $\Delta z = k$, as in figure 2.

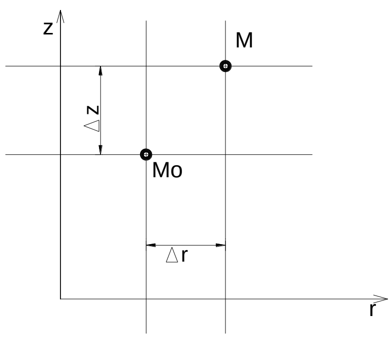

Fig. 2. The steps of the network

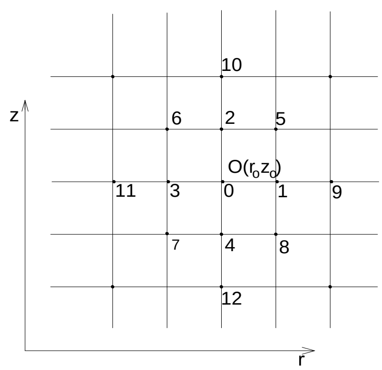

Fig. 3. The network and the nodes numbering

Finite Taylor developments for the current function Ψ were used, and the derivatives of this function up to order IV were obtained, including the values of the current functions in the nodes of the network

$$\begin{aligned}
&\psi^{I}_{r}=\frac{\psi_1-\psi_3}{2h}; && \psi^{I}_{z}=\frac{\psi_2-\psi_4}{2k};\\
&\psi^{II}_{r^2}=\frac{\psi_1-2\psi_0+\psi_3}{h^2}; && \psi^{II}_{z^2}=\frac{\psi_2-2\psi_0+\psi_4}{k^2};\\
&\psi^{III}_{r^3}=\frac{\psi_9-2\psi_1+2\psi_3-\psi_{11}}{2h^3}; && \psi^{III}_{z^3}=\frac{\psi_{10}-2\psi_2+2\psi_4-\psi_{12}}{2k^3};\\
&\psi^{III}_{r^2z}=\frac{\psi_5+\psi_6-\psi_7-\psi_8-2\psi_2+2\psi_4}{2h^2k};\\
&\psi^{IV}_{r^4}=\frac{\psi_9-4\psi_1+6\psi_0-4\psi_3+\psi_{11}}{h^4};\\
&\psi^{IV}_{r^2z^2}=\frac{\psi_5+\psi_6+\psi_7+\psi_8-2(\psi_1+\psi_2+\psi_3+\psi_4)+4\psi_0}{h^2k^2}
\end{aligned}\tag{5}$$

Ψ is the stream function value at the points 1, 2 ... n (nodes) [4], [5], [6], [7]. The relations (5) are replaced in the partial derivatives equation (4).
By distributing the corresponding terms of ψ_0 and Re, algebraic formula associated with partial derivatives equation is obtained

$$\alpha\psi_0=\beta+\mathrm{Re}\,\delta \tag{6}$$

The coefficients α, β and δ have the expressions:

$$\begin{aligned}
&\alpha=6\left(\frac{1}{h^4}+\frac{1}{k^4}-\frac{1}{r^2h^2}\right)+\frac{8}{h^2k^2}-\mathrm{Re}\left(\frac{3}{h^2}+\frac{2}{k^2}\right)\frac{\psi_2-\psi_4}{r^2k};\\
&\beta=\left[4\left(\frac{1}{h^2}+\frac{1}{k^2}\right)-\frac{3}{r^2}\right]\frac{\psi_1+\psi_3}{h^2}-\left[2\left(\frac{1}{h^2}+\frac{1}{k^2}\right)-\frac{3}{2r^2}\right]\frac{\psi_1-\psi_3}{rh}+\\
&+4\left(\frac{1}{h^2}+\frac{1}{k^2}\right)\frac{\psi_2+\psi_4}{k^2}-\frac{\psi_9+\psi_{11}}{h^4}-\frac{\psi_{10}+\psi_{12}}{k^4}-2\frac{\psi_5+\psi_6+\psi_7+\psi_8}{h^2k^2}+\\
&+\frac{\psi_9-\psi_{11}}{rh^3}+\frac{\psi_5-\psi_6-\psi_7+\psi_8}{rhk^2};\\
&\delta_1=\frac{\psi_1-\psi_3}{4hk}\left(3\frac{\psi_2-\psi_4}{r}-\frac{\psi_{10}-\psi_{12}}{k^2}-\frac{\psi_5+\psi_6-\psi_7-\psi_8}{h^2}+\frac{\psi_5-\psi_6+\psi_7-\psi_8}{2rh}\right);\\
&\delta_2=\frac{\psi_2-\psi_4}{k}\left(\frac{\psi_9-\psi_{11}}{9h^3}-3\frac{\psi_1+\psi_3}{2rh^2}-\frac{\psi_2+\psi_4}{rk^2}+\frac{\psi_5-\psi_6-\psi_7+\psi_8}{4hk^2}\right)\\
&\delta=\frac{\delta_1+\delta_2}{r}
\end{aligned}\tag{7}$$

h and *k* are the calculating steps on horizontal and vertical directions.
For the points located near the lower horizontal border, according to the reflection principle, $\psi_1=\psi_0$.
For the lower right corner (figure 4), $\psi_{12}=\psi_0$ and $\psi_9=\psi_0$, the coefficient *α* has the expression above [4], [5], the rest of the coefficients remains the same.

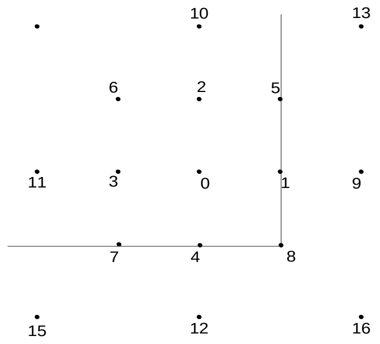

Fig. 4. Points of the network on the down right corner

$$\alpha = 6\left(\frac{1}{h^4} + \frac{1}{k^4} - \frac{1}{r^2h^2}\right) + \frac{8}{h^2k^2} - \mathrm{Re}\left(\frac{3}{h^2} + \frac{2}{k^2}\right)\frac{\psi_2 - \psi_4}{r^2k} + \frac{1}{k^2} - \\ - \mathrm{Re}\frac{\psi_1 - \psi_3}{4hk^3r} + \frac{1}{h^4} - \frac{1}{h^3r} - \mathrm{Re}\frac{\psi_2 - \psi_4}{9h^3kr}; \quad (8)$$

For the points located near the right wall of the tank, also based on the reflection principles, it is deduced that $\psi_9 = \psi_0$; for the points located near the right upper corner of the tank $\psi_9 = \psi_0$ and $\psi_{10} = -\psi_0$.

The values of the current function in the points on the borders were calculated with specific conditions and then within the network, which has not been affected by one of the above conditions.

Calculation was iterative, starting from the left bottom, each time using the values of the current function previously determined.

It is considered that the accuracy is good enough if the difference of two successive values of the stream function of each network point is below ε, which for hydrodynamic flow spectrum obtained was considered equal to 0.001.

3. Calculation example and the results interpretation

Calculation example corresponds to several Reynolds numbers, and the function ψ takes values between 0 and 1. For Re = 1 the flow occurs slowly approximately along the entire length of the tank, with the current lines approximately parallel.

Considering a plane flow and applying the method presented above, there was obtained the flow spectrum for Re = 1, Re = 10 (figure 5), Re = 100 and Re = 1000 (figure 6), results which opens new possibilities to study and solve problems related to the flow coefficient on the orifices.

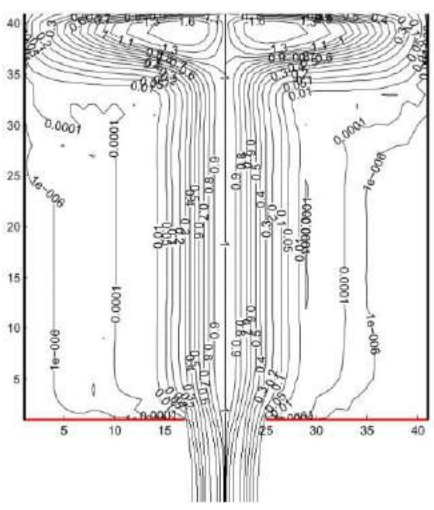

Fig. 5. The current lines for Re = 10

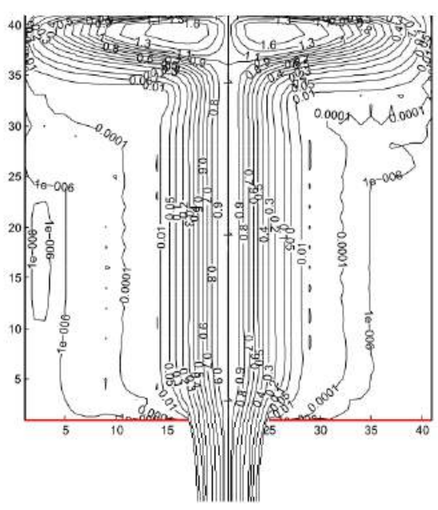

Fig. 6. The current lines for Re = 1000

It is considered that the upper part of the tank is supplied by water dripping and the flow is permanent.
It is determined the contracted section of the fluid jet at different distances from the orifice, namely, at *d*/3, *d*/2, 3*d*/4, and at the length *d*. In literature the maximum contraction considered is at *d*/2 [2] and 0.6*d* [10].
The contraction coefficient φ_c is obtained with the equation

$$\varphi_c = \frac{A_c}{A_g}, \tag{9}$$

A_c is the contracted area of the jet and A_g is the geometric area of the orifice.
The results are shown in Table 1 and inserted in figure 7.

TABLE 1: Dependence of the φ_c coefficient according to Re at different distances from the orifice

Re	1	10	100	1000
–	φ_c			
d/3	0.80210	0.75134	0.73085	0.71318
d/2	0.77951	0.70224	0.65999	0.64835
3*d*/4	0.76353	0.65480	0.58967	0.58752
d	0.76021	0.62853	0.57426	0.56626

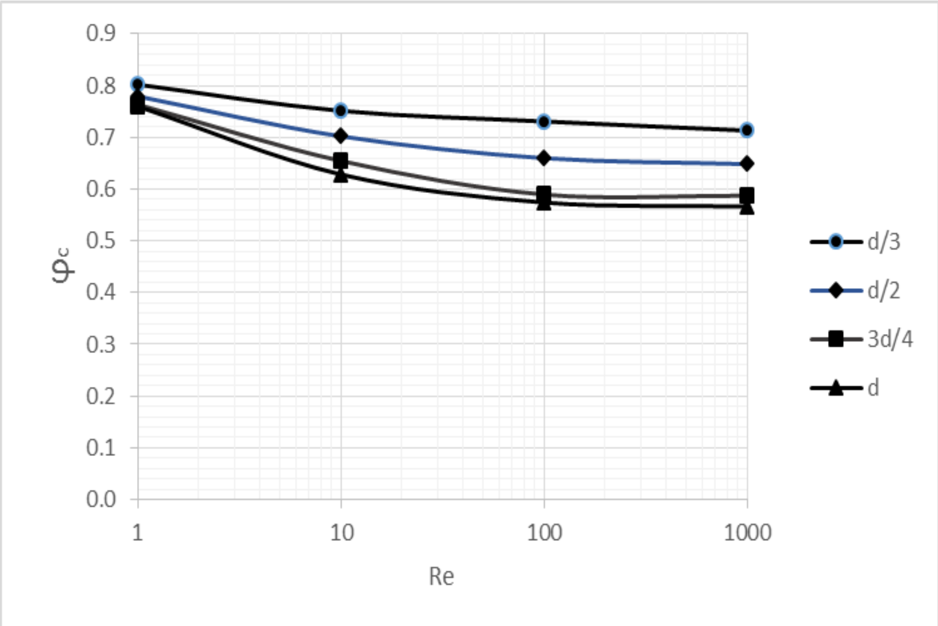

Fig. 7. The contraction coefficients resulted at different contracted areas and at different Re numbers

It is noticed that on the sides of the tank can be found “dead zones” because the liquid flow is concentrated towards the hole. In figure 7, for a better view the Re axis has a logarithmic scale, and it is noticed that the contraction coefficient and implicitly the flow coefficient is influenced by the number Re, decreasing with increasing flow regime.

4. Experimental research

To verify the numerical solution and to study the jet contraction an experimental installation has been designed (fig. 8). It is composed from a cylindrical transparent glass vessel with the inner diameter 187 mm, provided with a circular orifice at the bottom with a diameter *d* = 10 mm, respectively 20 mm.

The cylinder is supplied with water at the top, and to provide a symmetrical flow a vessel with a diameter approximately equal to the glass tank is used.
The vessel has at the bottom orifices equally spaced over the entire surface to ensure equal distribution of the flow over the free surface.
It is maintained a constant level of water H = 200 mm and it is determined the flow rate with the volumetric method.
A flow rate $Q = 1.1 \cdot 10^{-4}$ m^3/s was determined for a permanent flow and the Reynolds number in the tank was Re = 740. Finally, the flow coefficient μ = 0.706 of the circular orifice is determined with the diameter d = 10 mm.
Figure 9 corresponds to the numerical simulation associated with the experimental installation and contains both the flow spectrum in the tank and shape of the liquid jet at the output of the orifice.

Fig. 8. The experimental installation used to determine the flow coefficient.

From the contraction coefficient resulted from simulation φ_c = 0.713, and the velocity coefficient considered in the literature φ_v = 0.97 [11], results the flow coefficient μ = 0.691.
Keeping the same parameters of the experimental installation and by doubling the diameter of the circular orifice d = 20 mm, the flow rate resulted from the measurements is $Q = 0.428 \cdot 10^{-3}$ m^3/s, respectively the Reynolds number in the tank Re = 2850 (fig. 10). The flow coefficient obtained by the ratio resulted from the measured flow divided to the theoretical flow is μ = 0.688.

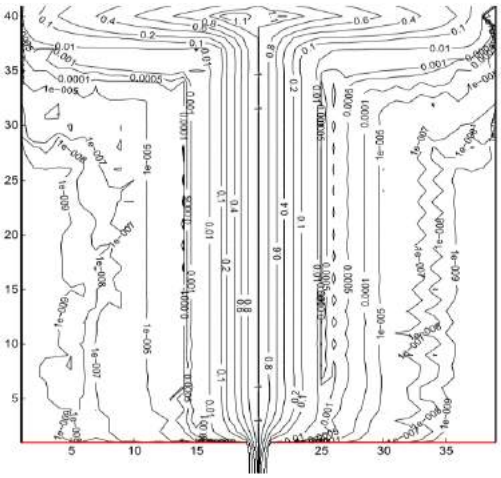

Fig. 9. Current lines for
Re = 740, d = 10 mm

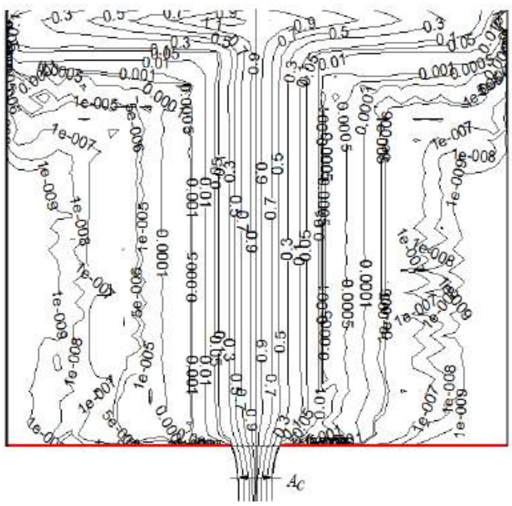

Fig. 10. Current lines for
Re = 2900, d = 20 mm

Using the same computing program and changing the diameter of the orifice, a contraction coefficient φ_c = 0.697 is obtained. Multiplying with the velocity coefficient mentioned above, the flow coefficient resulted is μ = 0.676.
For a better visualization of the flow spectrum in the experimental cylindrical tank a colored substance was introduced in the water supply.
The results can be seen in Figure 11, and one can observe that the flow focuses to the center of the tank and at the sides the flow is slow.

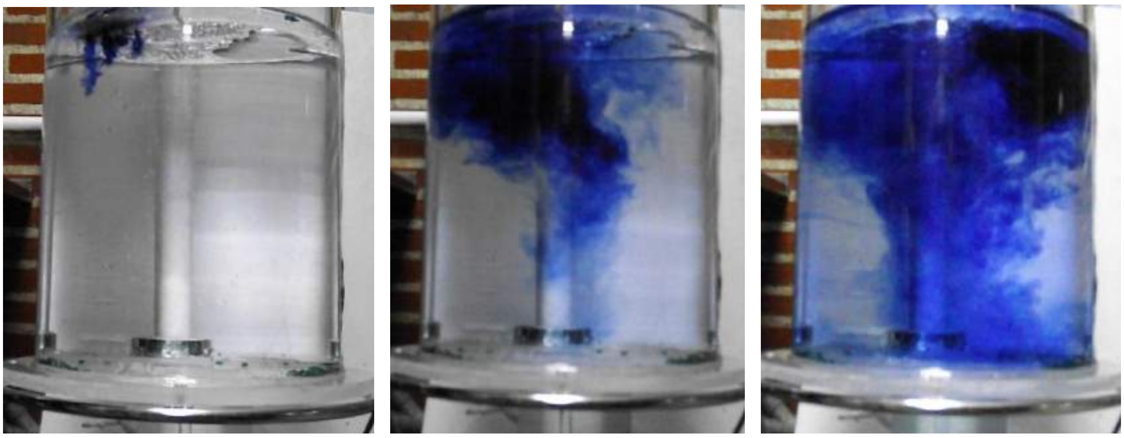

Fig. 11. View of the flow inside the experimental tank

It was obtained an error of −1.5 % for the orifice diameter *d* = 10 mm, respectively −1.2 % for *d* = 20 mm, thus it can be concluded that the values determined theoretically are comparable to those obtained experimentally.

5. Conclusions

The numerical solution obtained with the proposed numerical computer program can solve the problem of determining the contraction coefficient of an orifice and with the help of this value it can be determined the flow coefficient of the orifice and finally the actual flow rate which flows out of the tank.
Numerical treatment of the problem allows obtaining the flow spectrum into the tank and indicating areas of vortices, which can facilitate further information to other users.
Due to limited space, the authors could not present all the numerical results, even at higher Reynolds numbers. The authors can only say that the tendency already presented for the contraction coefficients in figure 7 continues.
The experimental installation was made in correspondence with the numerical simulations, and in the end it can be concluded that the values obtained theoretically by the numerical solution are comparable to those obtained experimentally.

References

[1] V. I. Kalitun, E. V. Drozdov, "Osnovî ghidravliki i aerodinamiki". Stroizdat, Moskva 1980, p. 118
[2] S. Hâncu, G. Marin, "Hidraulică teoretică şi aplicată (Theoretical and Applied Hydraulics)", vol. I, Bucharest, 2007, ISBN 978-973-731-476-5, p. 580;
[3] I. E. Idelcik, "Îndrumator pentru calculul rezistenţelor hidraulice (Guide for calculation of hydraulic resistances)", Editura Tehnică, Bucharest, 1984, p. 33;
[4] G. Băran, L. Mândrea, "Studiul curgerii în reactoarele de omogenizare (Study of the flow in homogenizing reactors)". J. Hidrotehnica no. 2, 1998, pp. 39-44;
[5] G. Băran, L. Mândrea, "Influenţa geometriei reactoarelor de omogenizare asupra curgerii (The geometry influence of the homogenizing reactors on the flow)", J. Hidrotehnica no. 8, 1998, pp. 147-149;
[6] G. Băran, L. Mândrea, "Optimizarea formei reactoarelor de omogenizare hidraulică (The shape optimization on hydraulic homogenizing reactors)", J. Hidrotehnica no. 6, 2001, pp.187-190;

[7] L. Mândrea, “Influența formei asupra curgerii în reactoarele de omogenizare (The shape influence on the flow for the homogenizing reactors)”, J. Hidrotehnica, no. 4-5, Vol 56, 2011, pp. 33-37;
[8] A. L. Voinea, L. Mândrea, V. Panaitescu. “The determination of an orifice contraction coefficient using numerical methods”, 7th International Conference on Energy and Environment CIEM 2015, Iași, October 22 – 23, 2015, CD-ROM, ISSN 2067-0893;
[9] G. Degrez, E. Dick, E. Grundmann, “Course of computational fluid dynamics”, Von Karman Institute for Fluid Dynamics, 1992;
[10] C. Mateescu, “Hidraulică (Hydraulics)”, Editura Didactică şi Pedagogică, Bucharest, 1963, pp. 471-475;
[11] N. Vasiliu, D. Vasiliu. “Acționări hidraulice şi pneumatice (Hydraulic and pneumatic drives)”, vol.1, Bucharest, ISBN 973-31-2248-3, 2005.

Evaluation of Nozzle Coefficients for Water Jet Used in Sewer Cleaning

PhD. Eng. **Nicolae MEDAN**

[1]Tech. Univ. Cluj-Napoca, North Univ. Center Baia Mare, Nicolae.Medan@cunbm.utcluj.ro

Abstract: *The purpose of this paper is to determine the discharge, speed and contraction coefficients for nozzle with three dimensions of diameter. To determine the speed of water jet at the nozzle exit, were measured the impact forces between the water jet and a flat and rigid surface in the potential core region of the water jets. In order to measure the impact forces of water jet, were designed and built a stand for generating pressure jets, as well as a device to measure the impact force.*

Keywords: *water jet, impact force, discharge coefficient, speed coefficient, contraction coefficient.*

1. Introduction

Industrial cleaning is a classic application of water jets technology. In the late 1950s, when reliable high pressure pumps were built, the usage of water jets spread widely in the field of pipes and sewerage cleaning. Phenomena that occur in the cleaning water jets are complex. Adler [1] describes mechanisms occurring at the impact of a jet with a surface. Leach et al [6], Leu et al [7] and Guha et al [5] analysed pressure distribution along centreline of the water jet. A number of papers have studied the influence of nozzle geometry on water jet [2, 3, 4, 8].
In order to be able to characterize the degree of efficiency of the nozzles has been defined the discharge coefficient μ. This coefficient is determined by the speed coefficient φ, the contraction coefficient ε and the compressibility coefficient ψ of the water from the jet.
To determine the coefficients for the nozzles used in this paper, were made a series of measurements for the determination of the impact force of the water jets.

2. Apparatus used and methodology of the measurements

In order to measure the impact forces of water jet, were designed and built a stand for generating pressure jets, as well as a device to measure the impact force [9].

2.1 Stand to generate pressure jet

Schematic diagram of the stand to generate pressure jet is shown in figure 1.

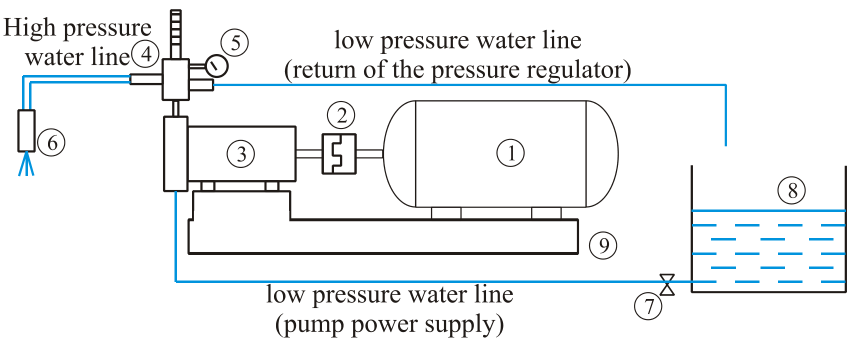

Fig. 1. Schematic diagram of the stand to generate pressure jet [9]

Component parts of stand: (1) electric motor (2) flexible coupling; (3) high pressure pump, 4) pressure regulator, 5) pressure gauge, 6) nozzle, 7) tap water, 8) water tank, 9) chassis.
Water coming out of the high pressure pump (3) goes into the pressure regulator (4). Through it adjusts the pressure and flow of water in the path of the high pressure water. This pressure corresponds to the one at the outlet of nozzle.

2.2 Device for the measurement of the impact force

In figure 2 is represented the principle diagram of the device for the measurement of the impact force of the water jet and a flat and rigid surface.

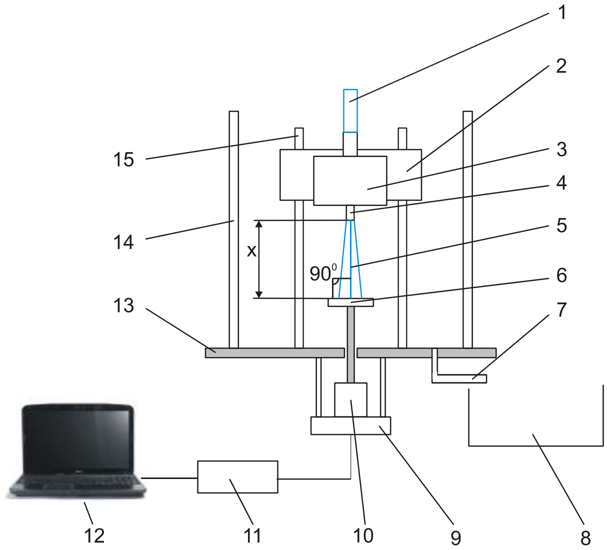

Fig. 2. Diagram of the device for the measurement of the impact force of the water jet [9]

Main component parts of the device are: 1) high-pressure water hose, 2) support nozzle, 3) nozzle block, 4) nozzle, 5) water jet, 6) flat and rigid target plate, 7) collection path water, 8) scaled container for measurement of the flow of water jet, 9) piezoelectric sensor mounting, 10) piezoelectric sensor, 11) data acquisition Personal Daq/3000, 12) computer for the processing of data; 13) support plate, 14) acrylic tube, 15) rods for adjusting distance x.

From high pressure water hose (1) come water at a certain pressure p desired. At the outlet of nozzle is generated a water jet (5) that striking target plate (6), who is located at a certain distance x in front of the nozzle. The jet (5) generates an impact force at a time when he meets target plate (6). This force produces axial movement of target plate. This movement is converted into an electric signal by the piezoelectric sensor (10). Electrical signal is collected by data acquisition Personal Daq/3000 (11), which forward data to a computer (12) using DaqView soft processes data actually obtained.

2.3 Geometric configuration of nozzles

Geometric configuration of the nozzles used is shown in figure 3.

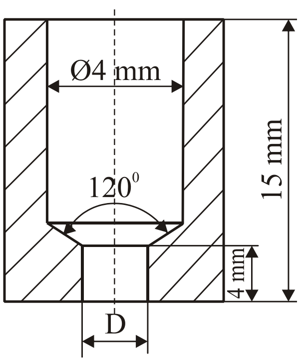

Fig. 3. Geometric configuration of the nozzles

The values used for diameter D of nozzle are D=1mm, 1.5 mm and 2 mm. The material for nozzles is stainless steel.

3. Results

The structure of the high speed water jets in air can be divided into three distinct regions [7,10]: 1) potential core region, 2) main region and 3) diffused droplet region.

It is known that in the potential core region, which has been determined as having a length of 6 to 8 times the diameter of the nozzle diameter [5], the water speed is relatively constant and equal to the speed of the water jet at the outlet of the nozzle. Thus, in order to be able to calculate the speed coefficient φ, were calculated the impact forces generated by the water jet at a distance of 8 mm for all three dimensions D of the nozzles, distance which corresponds to the potential core region of the water jet.

The Bernoulli equation of equilibrium, in the form of pressure for a water jet of under pressure is:

$$p_1 + \rho \cdot g \cdot h_1 + \frac{1}{2}\rho v_1^{\ 2} = p_2 + \rho \cdot g \cdot h_2 + \frac{1}{2}\rho v_2^{\ 2} + p_v \tag{1}$$

Starting on Bernoulli equation (1) can be expressed the velocity of the water speed V at the outlet of the nozzle, depending on pressure p of the water (upstream of the nozzle):

$$V = \sqrt{2\frac{(p-p_v)}{\rho}} = \sqrt{2\frac{p\left(1-\frac{p_v}{p}\right)}{\rho}} \text{ [m/s]} \tag{2}$$

where:

- p is the regulated pressure upstream of the nozzle;
- p_v is the loss pressure in the nozzle;
- ρ is the density of the water.

Is defined speed coefficient φ given by the relationship:

$$\varphi = \sqrt{1-\frac{p_v}{p}} \tag{3}$$

Replacing the relationship (3) in the relationship (2) the equation for the speed V becomes:

$$V = \varphi\sqrt{\frac{2p}{\rho}} \text{ [m/s]} \tag{4}$$

Considering the pressure loss in the nozzle p_v=0, resulting φ=1 and under these conditions, from the relationship (4), it is possible to calculate the theoretical speed V_{th} of the water at the outlet of the nozzle with relationship:

$$V_{th} = \sqrt{\frac{2p}{\rho}} \text{ [m/s]} \tag{5}$$

In accordance with the theoretical speed V_{th} of the water at the outlet of the nozzle may be calculated theoretical flow rate Q_{th} of the water at the outlet of the nozzle with relationship:

$$Q_{th} = \pi\left(\frac{D^2}{4}\right)V_{th} \text{ [m}^3\text{/s]} \tag{6}$$

where D is the diameter of the nozzles.

The pressures p used to perform the measurements have the values p=100 bar, p=120 bar, p=140 bar, p=160 bar, p=180 bar and p=200 bar.

They have measured the real flow rates Q_{mas} of water. Has been measured the flow rate of water for a period of 60 seconds for each diameter D of the nozzle and for the six established pressures. For the measurement of flow rate has been used a graduated container. For the accuracy of the

flow rate measurement for each set of parameters have been carried out a number of three measurements, and still has been used in the arithmetic average.
In table 1 are presented the theoretical flow rates Q_{th} with relationship (6) and the measured flow rates Q_{mas} (using the stand to generate pressure jet (fig.1) and the device for the measurement of the impact force (fig. 2).

TABLE 1: Theoretical and measured flow rates

Nozzle [mm] \ Pressure [bar]		100	120	140	160	180	200
1	Q_{th} [m³/s]	0.000107	0.000118	0.000128	0.000136	0.000145	0.000153
	Q_{mas} [m³/s]	0.00008	0.00008	0.00009	0.00010	0.00010	0.00011
1,5	Q_{th} [m³/s]	0.000242	0.000265	0.000287	0.000307	0.000326	0.000343
	Q_{mas} [m³/s]	0.00017	0.00019	0.00020	0.00022	0.00024	0.00025
2	Q_{th} [m³/s]	0.000431	0.000472	0.00051	0.000546	0.000579	0.00061
	Q_{mas} [m³/s]	0.00031	0.00035	0.00038	0.00041	0.00044	0.00046

According to the values presented in table 1, it should be noted that there is a difference between the theoretical flow rates Q_{th} and measured flow rates Q_{mas}. This difference is due to the discharge coefficient μ. Practically this coefficient provides information on the effectiveness of the nozzle. The discharge coefficient μ shall be expressed using the relationship [2]:

$$\mu = \frac{Q_{mas}}{Q_{th}} \tag{7}$$

Using the relationship (7) and the values obtained at the table 1, it was determined the values of discharge coefficient μ, values presented in table 2.

TABLE 2: The discharge coefficient μ

Nozzle [mm]	p [bar]					
	100	120	140	160	180	200
	μ					
1	0.687	0.689	0.693	0.689	0.698	0.694
1,5	0.676	0.692	0.687	0.707	0.718	0.715
2	0.707	0.716	0.715	0.730	0.732	0.727

Based on the values of discharge coefficient μ obtained in table 2, it was realised the graph presented in figure 4.

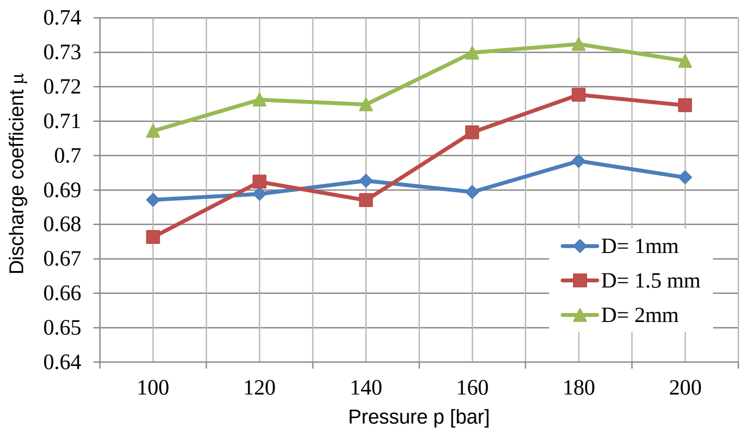

Fig. 4. Discharge coefficient μ

Conclusion: The discharge coefficient μ increases with pressure increasing. For the nozzle with diameter D = 2mm we are dealing with a higher efficiency than for the other two diameters of the nozzle. For all three dimensions of the nozzle the maximum value of the discharge coefficient μ appears for the pressure of 180 bar.
The discharge coefficient μ is given by the relationship (Anoni et al 4):

$$\mu = \varphi \cdot \varepsilon \cdot \psi \tag{8}$$

where:

- φ is the speed coefficient;
- ε is the contraction coefficient;
- ψ is the compressibility of the water.

In this paper, the volume of flow variation has values between 3.438x10^{-7} [m^3/s] for p=100 bar and 4.11x10^{-6} [m^3/s] for p=200 bar. Therefore the coefficient of compressibility ψ can be neglected (ψ=1).
The speed coefficient φ is given by relationship [2]:

$$\varphi = \frac{V_r}{V_{th}} \tag{9}$$

where:

- V_r is the real speed of water jet at the outlet of the nozzle;
- V_{th} is the theoretical speed of water jet at the outlet of the nozzle.

The impact force of a water jet is given by the relationship [2]:

$$F = \rho \cdot Q_{mas} \cdot V_r \ \text{[N]} \tag{10}$$

From relationships (9) and (10) result:

$$\varphi = \frac{F\sqrt{\rho}}{\rho \cdot Q_{mas}\sqrt{2p}} \tag{11}$$

In table 3 are presented the values of impact forces measured for a standoff distance x=8 mm.

TABLE 3: The measured impact forces for x=8 mm

Nozzle [mm]	p [bar]					
	100	**120**	**140**	**160**	**180**	**200**
	F [N]					
1	10.78	12.40	14.59	16.46	18.89	21.47
1,5	23.14	28.11	31.83	37.39	43.32	48.09
2	39.84	48.55	57.78	64.22	74.57	85.67

Using the relationship (11) and the values of measured impact forces from table 3 shall be calculated the speed coefficient φ. In table 4 are presented the determined values of speed coefficient φ.

TABLE 4: The speed coefficient φ

Nozzle [mm]	p [bar]					
	100	**120**	**140**	**160**	**180**	**200**
	φ					
1	0.999	0.955	0.958	0.950	0.957	0.985
1.5	0.968	0.957	0.936	0.936	0.949	0.952
2	0.897	0.899	0.919	0.875	0.900	0.937

Based on the values of speed coefficient φ obtained in table 4, it was realised the graph presented in figure 5.

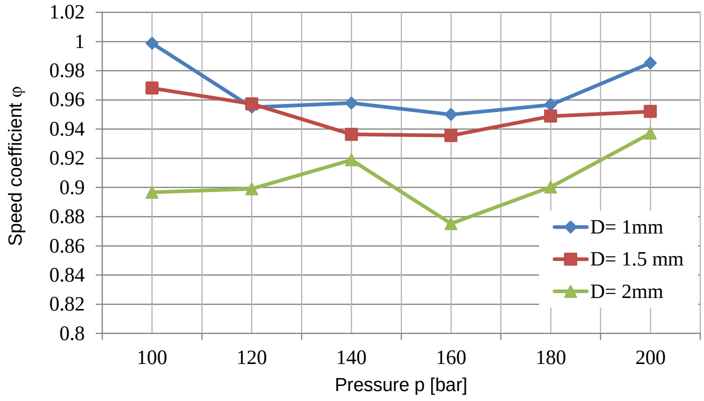

Fig. 5. Speed coefficient φ

Conclusion. The speed coefficient φ decreases with increasing of the diameter of the nozzle. For values of diameters D=1 mm and D=1.5 mm the speed coefficient φ is maximum for pressure p=100 bar and for Diameter D=2 mm is maximum for p=200 bar.
After they have been calculated the discharge coefficients μ and speed coefficients of φ, using the relationship (8) may be calculate the contraction coefficient ε for all three dimensions of the nozzle:

$$\varepsilon = \frac{\mu}{\varphi} \tag{12}$$

The calculated values for the contraction coefficient ε are presented in the table 5.

TABLE 5: The contraction coefficient ε

Nozzle [mm]	p [bar]					
	100	**120**	**140**	**160**	**180**	**200**
	ε					
1	0.688	0.721	0.723	0.726	0.730	0.704
1.5	0.699	0.723	0.734	0.755	0.756	0.751
2	0.789	0.797	0.778	0.834	0.814	0.776

Based on the values of contraction coefficient ε obtained in table 5, it was realised the graph presented in figure 6.

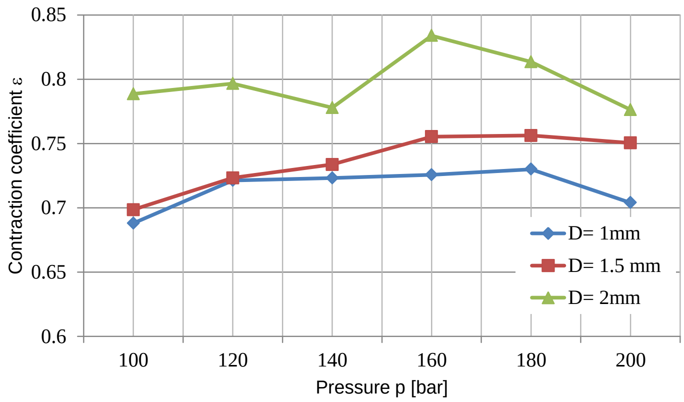

Fig. 6. Contraction coefficient ε

Conclusion: From the graph 5 it is observed that for the nozzles D=1 mm and D=1.5 mm minimum value of the contraction coefficient appears for p=100 bar and the maximum value appears for p= 180 bar, while for the nozzle with D= 2 mm minimum value of the contraction coefficient appears for p= 140 bar and the maximum value appears for p= 160 bar.

4. Conclusions

In this work it is presented a methodology for the determination the efficiency of the nozzles used to sewer cleaning. In order to be able to determine the effectiveness of the nozzles were determined: discharge coefficient μ, speed coefficient φ and contraction coefficient ε.
By determining the theoretical and practical of mass flow of the water jets has been determined the discharge coefficient μ, coefficient which practically represents the efficiency of the studied nozzles.
In the experimental domain of this work, the compressibility coefficient ψ of the water in the jet shall have the value of 1. Therefore the coefficient of compressibility ψ can be neglected.
In order to determine the speed coefficient φ were carried out the measurements of the impact forces in potential core region of the water jet (where the water speed is relatively constant and equal to the speed of the water jet at the outlet of the nozzle).
After the determination of the discharge coefficient μ and the speed coefficient φ could been determined the contraction coefficient ε.
The efficiency of the nozzles concerned depends by the diameter of the nozzles and the pressure of a water jet at the outlet of the nozzle.
For all three dimensions of the nozzles maximum efficiency appears for pressure p= 180 bar.

References

[1] W. F. Adler, ”The Mechanics of Liquid Impact”, Treatise on Materials Science and Technology, 1979. pp. 127-183;
[2] M. Annoni, L. Cristaldi, M. Faifer, M. Norgia, ”Orifice Coefficients Evaluation for Water Jet Application”, Sept. 22-24, 2008, Florence, Italy, 16th IMECO TC4 Symposium, ”Exploring New Frontiers of Instrumentation and Method for Electrical and Electronic Measurement”, pp. 761-766;
[3] A., Cotetiu, R., Cotetiu, N. Ungureanu, ”Research about automatic adjustment solution of the advance force at the perfusion drills using fluid elements”, January 2014,”Archives of Mining Sciences”, Volume 58, Issue 4, ISSN (Print) 0860-7001, pp. 1201–1208;
[4] S. Dimitrov, S. Simeonov, S. Cvetkov, ”Static Characteristics of the Orifices in a Pilot Operated Pressure Relief Valve”, “Hidraulica” (No. 2/2015) Magazine of Hydraulics, Pneumatics, Tribology, Ecology, Sensorics, Mechatronics, ISSN 1453 – 7303, pp.35-39;
[5] A., Guha, R. M., Barron, R. Balachandar, ”An Experimental and Numerical Study of Water Jet Cleaning Process”,2011, ”Journal of Materials Processing Technology”, pp. 610-618;
[6] S. J., Leach, G. L. Walker, ”Some Aspects of Rock cutting by High Speed Water Jets”, July 1966, Philosophical Transactions of the Royal Society of London, Series A, Vol. 260, pp. 295-308;
[7] M. C. Leu, P. Meng, E. S. Geskin, L.Tismeneskiy, ”Mathematical modelling and experimental verification of stationary waterjet cleaning process”, August 1998,”Journal of Manufacturing Science and Engineering”, Vol. 120, Issue 3, pp.571-579;
[8] Y. Liu; F. Ma; H. Xie; Y. Li, ”Development of Impact Test System for Waterjet Descaling Nozzles with LabVIEW”, October 23-24, 2010, International Conference ”Web Information Systems and Mining (WISM)”, Vol.1, pp.3-7;
[9] N. Medan, PhD thesis ”Research and Contributions to the Functioning of Cleaning Head-Sewer System”, November 29, Baia Mare, Romania;
[10] N. Rajaratnam, C. Albers, ”Water Distribution in Very High Velocity Water Jets in Air”, June 1998, Vol. 124, No. 6, ”Journal of Hydraulic Engineering”, ISSN (print): 0733-9429, pp. 647-650.

Diagnostic and Correction of the Spreader´s Inclination Hydraulic Circuit of the Transtainer Crane

Dr. Ing. **Genovevo MOREJÓN VIZCAINO**[1], Prof.**,** Ing. **Julio Ernesto HERNÁNDEZ MARTÍNEZ**[2]

[1] Department of Applied Mechanics, Faculty of Mechanical Engineering, Superior Polytechnic Institute "José Antonio Echeverría" (Cujae), Marianao, Cuba, gmvizcaino@mecanica.cujae.edu.cu

[2] Department of Applied Mechanics, Faculty of Mechanical Engineering, Superior Polytechnic Institute "José Antonio Echeverría" (Cujae), Marianao, Cuba, jhernandezm@mecanica.cujae.edu.cu

Abstract: *This paper exposes the diagnosis and correction suggestion to the hydraulic circuit of inclination of the spreader of a crane transtainer, type Rail Mounted Gantry of a containers terminal that frequently was out of service. The questions: why happen and how to solve them. We applied the deductive-inductive method and inferred that the mishaps were caused by dynamic loads as a consequence of the free fall of the container broken by the rope. We carried out a mathematical modeling the phenomenon; we obtained models with a combination of mechanical variables and the behavior of the fluid in the pipes. We have carried out an algorithm and it was programmed in MATLAB, and through the result of the simulation we obtain the parameters to make the new components of the modification proposed. It consists of adding relief valve type cartridge of short time response and an accumulator to dampen the picks.*

Keywords: *Spreader, antisnag, mathematical modeling, transtainer crane, hydraulic oil.*

1. Introduction

The main questions in this article: Why happen? and How to solve the mishaps? We expose diagnosis and correction proposal to the hydraulic circuit of inclination of the spreader of a crane transtainer, type Rail Mounted Gantry of a containers terminal due to frequent and accidental mishaps caused by picks of pressure of very high values (load dynamic), causing efforts bigger than acceptable in the materials of the screws and the body of the valves, destroying them, figure 1.

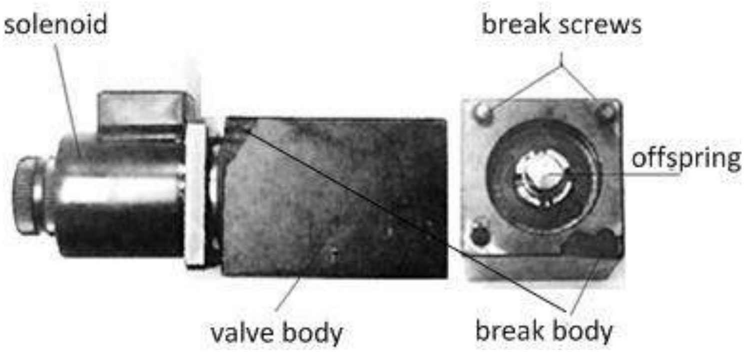

Fig. 1. Valve out of service

The assembling of figure 2: cylinders of the mechanism of deviation of the spreader, elevation drums, the rope and the pulleys that support to the spreader, in charge of fixing the contender when introducing and to rotate the spinning tops in the holes of the corners, co axial is required between the axes of spinning tops and holes, say otherwise, it is necessary parallelism between spreader and container.
When there is not parallelism, for example by irregularities on the floor, the mechanism of inclination of the sprider has the function of solving this inconvenience. It is a hydraulic system with eight cylinders whose stems notice the cables, when extending or to retract the stem it varies their longitude, to consequence, the spreader rotates with regard to the Cartesian axes (trim, list, skew) to reach the position. In figure 3 a segment of the hydraulic circuit is shown.

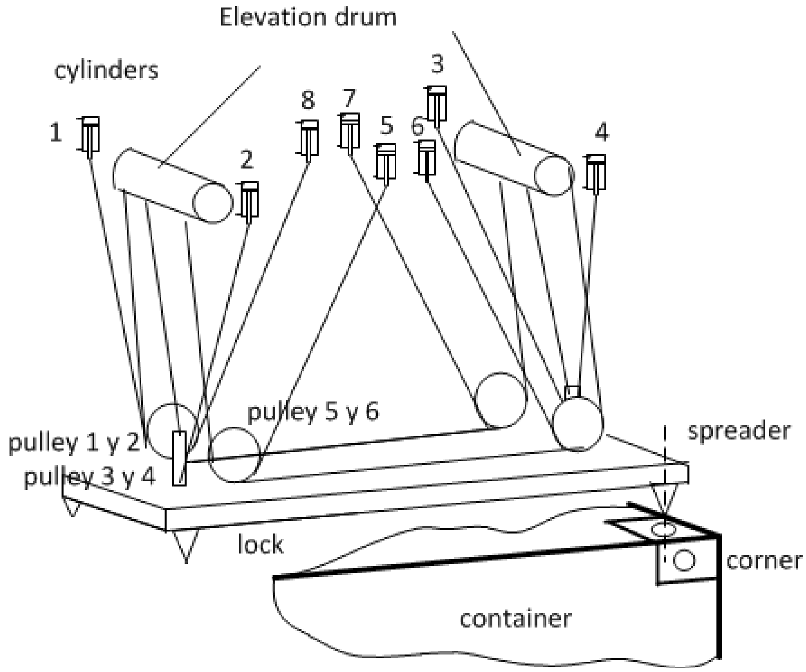

Fig. 2. Spreader and cylinders of the mechanism of inclination

The revised literature [1,2] picks up two effects that produce dynamic loads in the hydraulic circuit of inclination of the spreader: the <sway> effect is the one provoked for the spreader swinging and the <snag> effect, where dynamic loads of traction or compression, unaware to the process, are applied in the ends of the stem by the cables, transforming the cylinders into bombs; the theoretical power reached by the cylinder is superior to 600 Kw; this is transformed into heat [pamphlet of TCH].

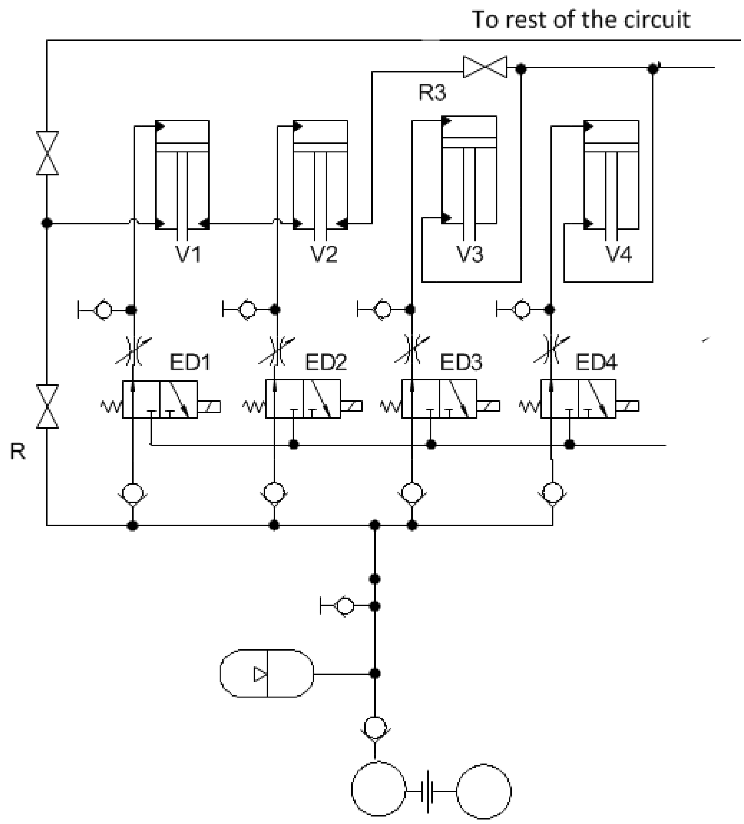

Fig. 3. Original circuit

To eliminate these effects the designers [3,4,5,6,7] have established solutions anti-sway and anti-snag in the hydraulic circuits. For the latter they used valves constrainers of pressure, the conventional ones [8] in advance of response of 100 milliseconds are not recommended, valves cartridge are recommended or logical in advance of opening among 15 -20 milliseconds.
Figure 4 shows the operation of an antisnag. The load applied in the cable, firstly they elongate it and later on the residual load applied in the stem's end deforms the column of hydraulic oil in the cylinder when it is being pumped, generating a pick of pressure, the valve of security opens up, allowing the offspring's displacement. Also, it shows the time from the beginning of the application of the force in the stem until reaching the pick of pressure and the time consumed by the valve to open up totally.
Using the deductive-inductive method we assume that the origin of the causing dynamic loads of the mishaps was the fall free of the container, when being broken by the cable it caused an event Snag. It was modeled and it was simulated the event. The main conclusion: to modify the circuit adapting to it an anti-snag (valve cartridge constrainer of pressure and accumulator as a damper to end the picks of pressure).

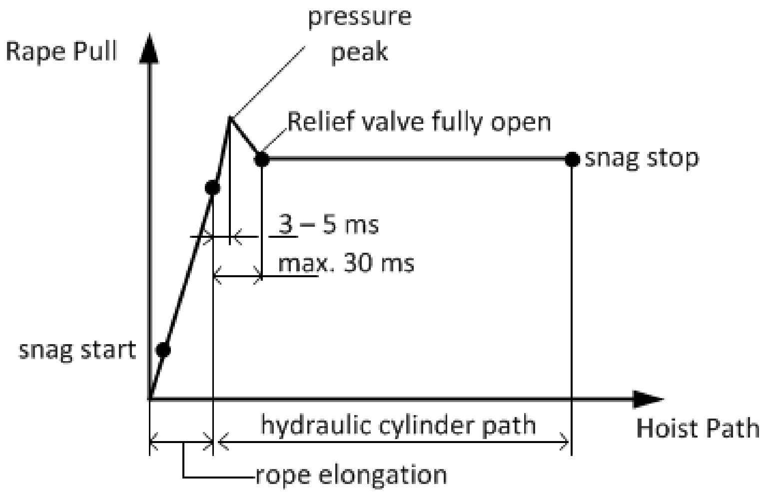

Fig. 4. To come from the antisnag (taken and edited [8])

2. Fall free of the container

When applying the deductive-inductive method it was found that the causing dynamic loads of the mishap were consequence of the fall free of the container when for an erroneous manipulation this was supported for other, later on it slips for the interaction with the cable and it fell.
When studying the original hydraulic circuit it was determined that this didn't possess protection antisnag since the valves of security they aren´t action express and the distance to those that the elements are located they don't allow the protection.
The expressions (1) and (2) model the longitude of the cable L_{CD} when being loosened by the operative.

$$L_{CD} > \overline{ab} + \overline{bc} + 2H \tag{1}$$

$$L_{CD} \leq \overline{ab} + \overline{bc} + 2H \tag{2}$$

In the situation (1) the free fall concludes with the impact of the container because h is bigger than H, (see figure 5), in the (2) h is smaller than H and the container is braked by the cable being suspended, the kinetic energy is transferred, firstly, it produces an elastic deformation of the cable; later on the load remainder acts on the stem making an event of Snag.

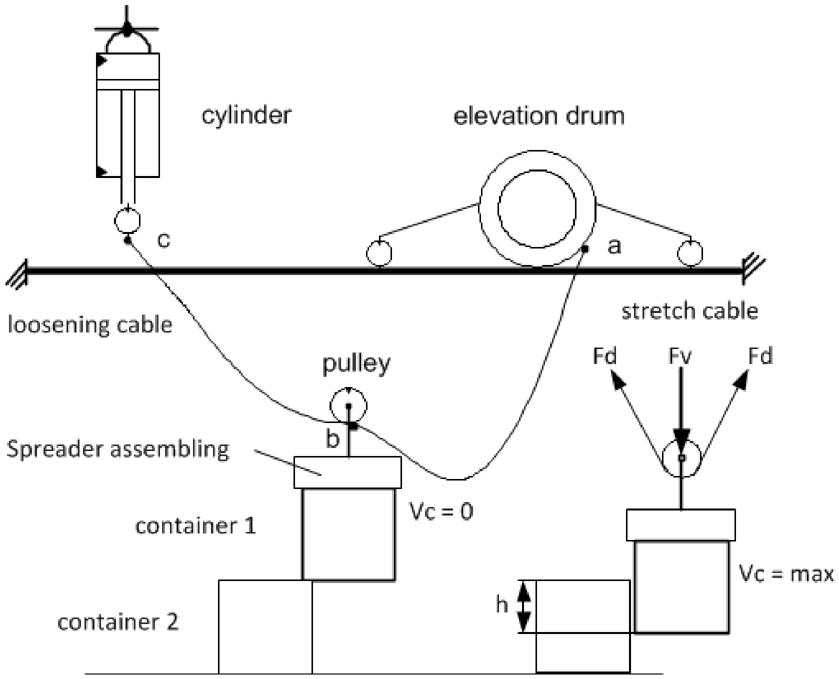

Fig. 5. Fall free of the container

Suppose the force Fv (originated by the free fall) is distributed equally among each brunch of the cable Fd, with two components: one to deform the cable Fdc and the other one for interaction axially in the stem's end Fdv [N]. It is supposed that:

$$Fdv = 0.3 \cdot Fv \tag{3}$$

Applying the impulse law and quantity of movement, also, the principle of energy conservation, referred to figure 5 and substituting in (3), it is:

$$Fdv = 0.424 \cdot \frac{m_{unitaria} \cdot \sqrt{g \cdot h}}{\Delta t} \tag{4}$$

The $m_{unitaria}$ [Kg] is the mass associated to the most loaded cable, it is the sum of the mass of the sprider support, that of the sprider and the one of the container to full load divided by the number of cylinders and multiplied by the coefficient k = 1.2; keep in mind the eccentricity of the load in the container. g[m/s^2] is gravity, h[m] is the distance made by the container in the free fall and Δt [s] the time in the free fall.

$$munitaria = \frac{k(mps + ms + mc)}{8} \tag{5}$$

3. Event Snag

The event Snag a consequence of the effect of the compressibility of the hydraulic oils, the force is Fdv it makes to the piston pump (see figure 6) generating a deformation X, which implies a variation of the volume of oil ΔV and the emergence of a pressure pd according to (6), in [9].

$$pd = -E\frac{\Delta V}{V} \tag{6}$$

The pressure pd and E: module of elasticity [Pa ΔV: variation of volume [m^3].
The pressure spreads from the inferior face of the piston of the cylinder A to its homologous d. The effect of the pressure on the piston of the cylinder B causes the deformation ΔX_1, does this deformation generate the pressure pd1, if when arriving to the point **f**it takes a superior value to the acceptable one for the valve **V1** this collapses. Otherwise it creates a damped harmonic movement between the points **a** and **f**.

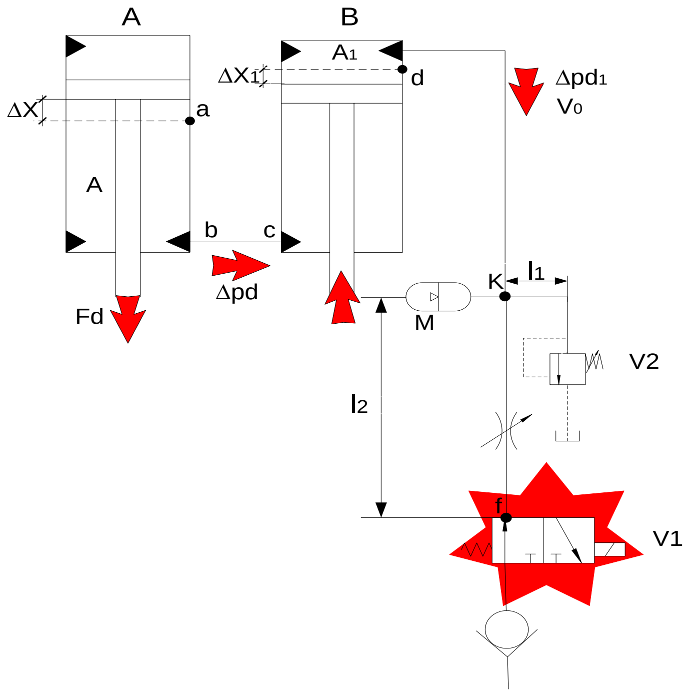

Fig. 6. Section of circuit

To protect to the valve **V1** it does intend to add a valve constrainer of pressure **V2** at a distance smaller than the point K (l1< l2) so that the wave of pressure arrives first to the valve **V2**; also, an effective method [10] of reducing the overpressure directed by the battering ram blow is the installation of hydraulic accumulators; the incorporation of both elements is the solution antisnag.
The pressure is the relationship between the force Fdv and the area of the cylinder; substituting (4) it is:

$$pd1 = 0.54 \cdot \frac{m_{unitaria} \cdot \sqrt{g \cdot h}}{\Delta t \cdot dc^2} \tag{7}$$

The flow that moves from d to f qd1 is the relationship between the ΔV [m^3] and the time of opening of the valve of security tap [s], dc is the diameter of the cylinder [m]. Clearing of (6) and substituting (7), it is obtained:

$$qd1 = 0.424 \cdot \frac{h_{aceite} \cdot m_{unitaria} \cdot \sqrt{g \cdot h}}{tap \cdot \Delta t \cdot E} \tag{8}$$

The parameter h_{aceite} [m] is the height of the column of hydraulic oil in the cylinder and E coefficient of elasticity of the oil [Pa]. The theoretical power in the cylinder Ntc [kW] is determined for:

$$Ntc = \frac{pd1 * qd1}{1000} \tag{9}$$

4. Results and discussion

In figures 7, 8 and 9 are shown the graphs of theoretical power, pressure and the flow of the event Snag in the section d - f of the simulated circuit starting from (7,8,9) through a program written in MATLAB with the following data: mc = 30000; ms = 1000; mps = 3000; dc = 0.1; tap =0.030; h_{aceite} = 0.5; E = 12500x10^5;Δt = (0.005... 0.03) and h = (0.05… 1.5). The units of pressure and flow were converted to coordinate with the catalogs of hydraulic elements.
The three analyzed variables have a common behavior: they are bigger while higher is the kinetic energy accumulated by the container (bigger height and smaller time of fall).

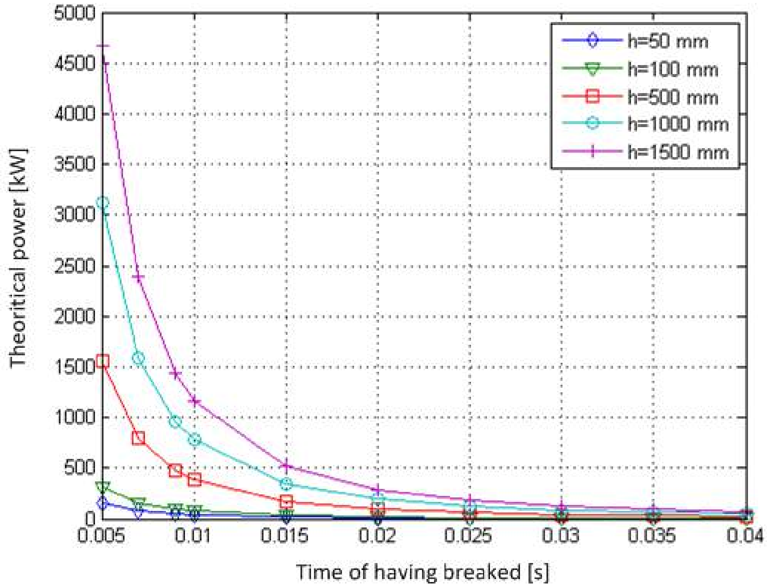

Fig. 7. Behavior of the theoretical power

Figure 7 allows determining the interval of time to protect the hydraulic circuit from fallen free of containers to full capacity of same heights or smaller than meter and half. In [pamphlet of TCH] "the theoretical power reached by the cylinder is superior to 600 Kw." Fixing the limit in 1000 kW, the interval of time for the biggest analysis is 10 milliseconds.
The remaining figures allow determining the values of the necessary parameters for sizing the elements of the antisnag starting from interval of defined time (bigger at 10ms). In figure 8 the value of the pressure pd1 of 1000 bar is determined in the accumulator to plane the picks of pressure. In figure 9 the value of the flow qd1 of 600 l/min is determined for the valve logical constrainer of pressure.

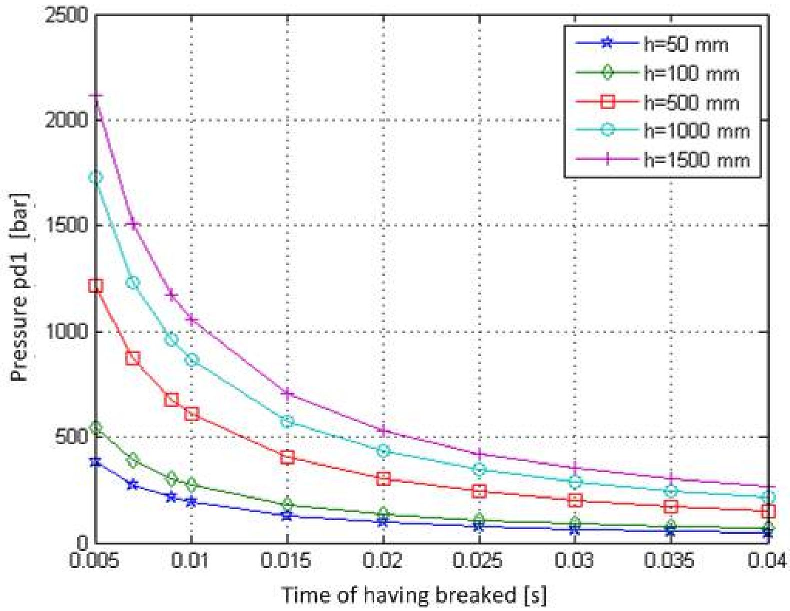

Fig. 8. Behavior of the pressures

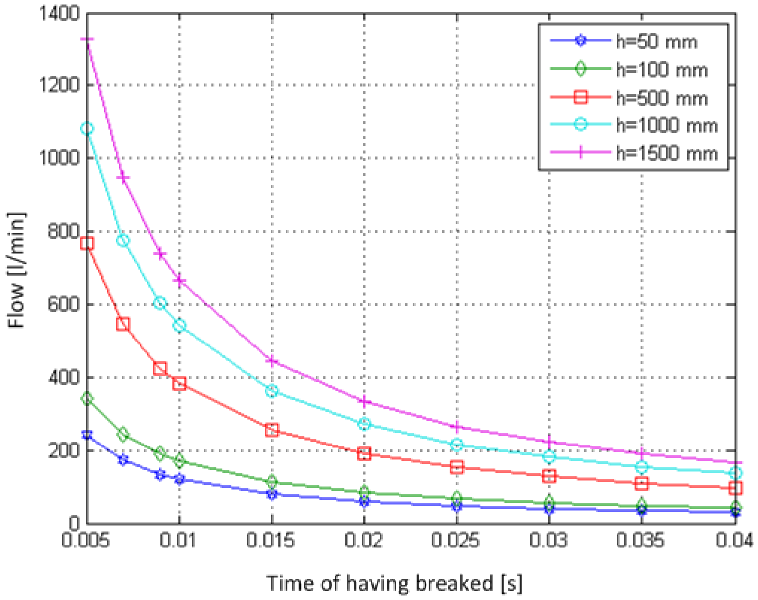

Fig. 9. Behavior of the flows

The knowledge founded during this investigation allowed to propose a modification to the original circuit (see figure 3), for the necessary correction, they intend two sub circuits and in each one to install a valve logical constrainer of pressure and an accumulator to plane the picks of pressure, uncoupled of the rest of the circuit with valves check like sample the outline of the circuit, figure 10.

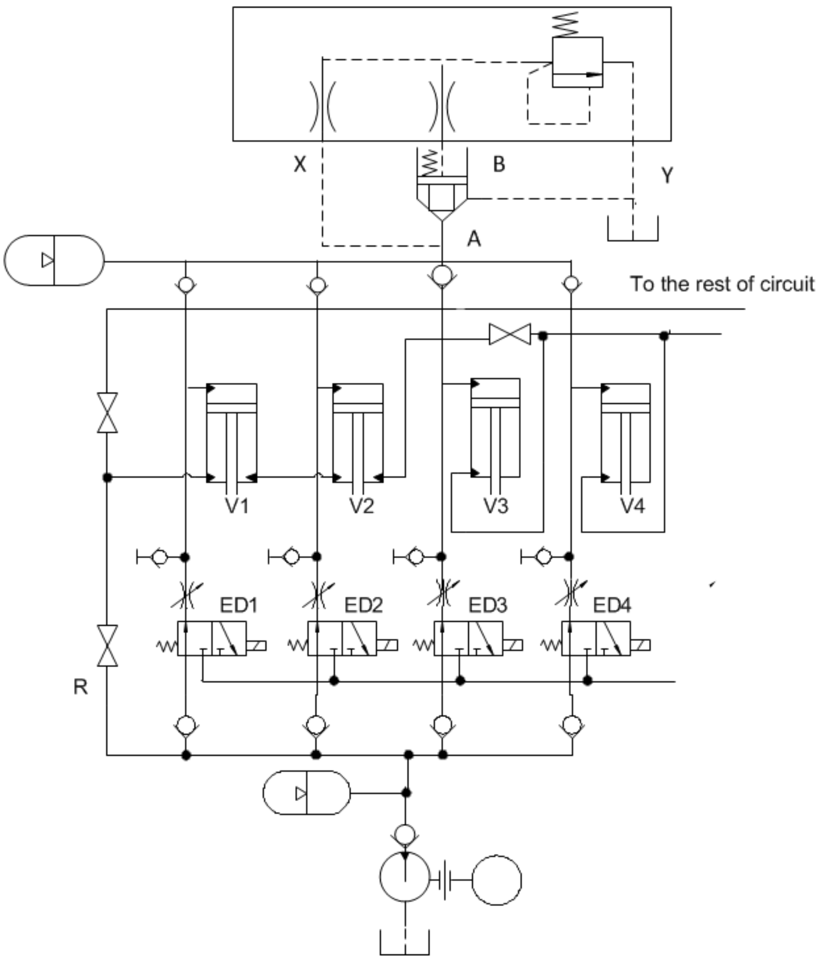

Fig. 10. Circuit modified with antisnag

Conclusions

The present work when applying the deductive-inductive method has been diagnosed the causes of the mishaps, the dynamic loads generated by an event Snag caused by the fall free of the container by an erroneous manipulation, also, the hydraulic circuit doesn't possess antisnag protection since the valves of security are not of fast response, neither the distance of location of the elements allows the protection.
A methodology has been developed based on the mathematical modeling and simulation to evaluate the event Snag caused by the fall free of the container in a crane transtainer, type Rail Mounted Gantry in a terminal container support; you can use this methodology in many other applications.
The simulation allows obtaining the values of the variables for sizing the components of the antisnag solution proposed to correct the circuit and to protect it before fallen free of containers to full load capacity and same heights or smaller than meter and half.
The weak points of the work are: the time to calculate the flow of the Snag the same as that of opening of the valve and to fix the limit of the theoretical power in 1000 kW.

References

[1] J. Verschoof, "Cranes-Design, Practice, and Maintenance". Editorial London and Bury St Edmundo, UK 1999, pp 158-257;
[2] J. Erb, W. Jones,. "Cargo Handling: coping with snags". Cargo System Journal, Feb 1993;
[3] J. Piriou, "Anti-Sway: controlling the swaying of the load" https://www.schneider-electric.fr/documents/original-equipment-manufacturers/pdf/Anti-Sway-controlling-the-swaying-of-the-load.pdf;
[4] "antisway-systems", http://www.rimagroup.com/pdf/antisway-systems.pdf;
[5] "tls-antisnag-systems", http://www.rimagroup.com/pdf/tls-antisnag-systems.pdf;
[6] "pb_feederserver_es", http://www.kranunion.de/fileadmin/Downloads/Kocks/brochures/pb_feederserver_es.pdf;
[7] C. A. "Development of Feedforward Anti-Sway Control for Highly Efficient and Safety Crane Operation", Mitsubishi Heavy Industries, Ltd Technical Review Vol 38 No 2, Jun 2001;
[8] "New dimensions in materials handling: Container quay cranes" Bosch Rexroth S.A.I.C, La Havana Nov 2002;
[9] E. Codina, S.de la Hera, "Modelización de Sistemas Fluidos mediante BONDGRAPH." Editorial Cordellach Copies-CBS S. A. Terrassa, España;
[10] Nekrasov, B. "Hidráulica". Editorial MIR, Moscú,1968.

Computerized System for a Steering Box Testing Stand with Automatic Data Record and Report Issuing

PhD.eng. **Radu RĂDOI[1],** PhD.eng. **Cătălin DUMITESCU[1],** PhD.eng. **Iulian DUȚU[2]**

[1] Hydraulics and Pneumatics Research Institute INOE 2000 – IHP Bucharest, radoi.ihp@fluidas.ro

[2] University Politehnica of Bucharest, Faculty of Biotechnical Systems Engineering, iulian.dutu23@gmail.com

Abstract: *Assisted steering systems are present in almost all modern vehicles even in the small class and compacts. Besides driver discomfort due to mechanical wear, these systems can produce unwanted effects such as: environmental contamination with hydraulic fluid and reduction of car's steering assistance. A defective steering box will no longer respond to driver's manoeuvres and can lead to potential life threatening situations due to traffic accidents.*
Main subject of the paper is describing a computerized testing stand designed for a steering box testing stand. This facilitates quick and easy testing of steering boxes before and after maintenance / repairing operations. The computerized system that authors propose can be used for upgrading existing steering box testing stands. Main system equipments are: data acquisition board, electronic transducers for pressure, flow, torque, temperature, speed and displacement, a servomotor for steering box driving and an inverter for dynamic speed control of a hydraulic pump. The authors have also designed a computer software that allows testing stand's full functionality, such as testing sequences control, testing data record in a database and automatic testing report issuing (including printing).
The computerized testing system that the authors describe can automatically determine the current state of the sealing elements of the hydraulic directional valve of the steering box through measuring the oil flow during testing. The testing report contains records regarding pressure values at travel ends and in an intermediary position having the rod blocked, as well as oil temperature, torque value at hydraulic directional valve's shaft during manoeuvres, steering box serial number, testing operator name and testing company name.
The computerized system for steering box testing provides the user with a friendly interface that allows simple and fast testing of steering boxes of vehicles. The system can be used as a part of a new testing stand or as an upgrade for an existing one. Main beneficiaries are vehicle repair workshops or companies specialized in maintenance or repairing hydraulic assisted steering boxes.

Keywords: *computerized test, transducers, steering box, DAQ system*

1. Introduction

Assisted steering systems are present in almost all modern vehicles even in the small class and compacts. Besides driver discomfort due to mechanical wear, these systems can produce unwanted effects such as: environmental contamination with hydraulic fluid and reduction of car's steering assistance. A defective steering box will no longer respond to driver's manoeuvres and can lead to potential life threatening situations due to traffic accidents. One of the causes of failure of hydraulic assisted steering boxes can be hydraulic fluid contamination with impurities [1].
Main subject of the paper is describing a computerized testing stand designed for a steering box testing stand. This stand facilitates fast and easy realization of the tests for steering boxes, before and after maintenance / repairing operations. The computerized system that authors propose can be used for upgrading existing steering box testing stands.
Main beneficiaries can be vehicle repair workshops or companies specialized in maintenance or repairing hydraulic assisted steering boxes.

2. System description

The system contains several sensors for parameters of interest to test the steering boxes. The transducers used are: a pressure transducer 0...160 bar (11), a flow transducer 0.18...18 l/min (10), a rotary encoder for step by step motor (18), a torque transducer 0...500 Nm (17) and a force transducer 2000 daN (20). Connecting transducers to the computer was done through a data acquisition board [2] from the National Instruments, model NI USB-6211 (22). In **figure 1** can be seen the location of the various transducers in the scheme of test stand. To control the speed of the pump from test stand, via a variable speed drive in order to adjust the flow, was used an output of analog signal 0…10V, from data acquisition board. Another analog output of data acquisition board is used for voltage control of driver of the stepper motor which drives the rotary valve of steering box. The hydraulic installation is located behind the front panel of stand for testing of steering boxes (Fig.2). The stand is equipped with a section for testing of pumps for power steering, which has not been drawn in this scheme.

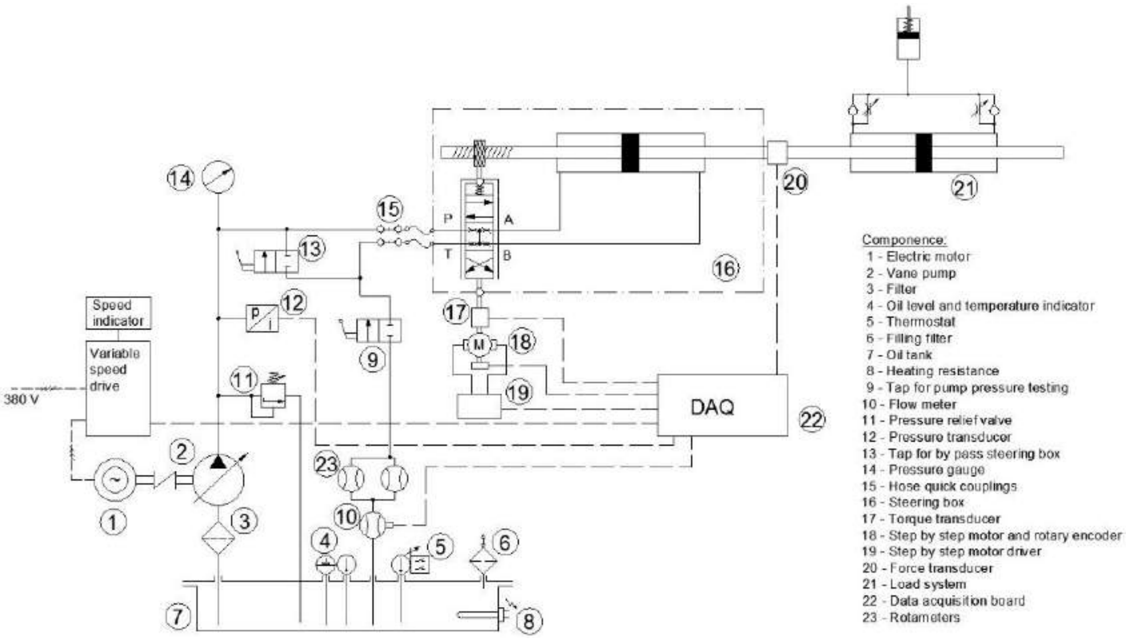

Fig. 1. Schematic of steering box testing stand

Fig. 2. Front panel of steering box testing stand

In **figure 3** it can be seen the mounting plate on which are mounted the contacter which starts the electric motor which drives the pump, a three phase automatic circuit breaker and a variable speed drive for regulating the rotational speed of the electric motor. Also on mounting plate is found the automatic circuit breaker of thermostating system for hydraulic liquid.
The test stand scheme contains a tank (7) for hydraulic liquid on which are mounted the next components: temperature and oil level gauge (4), sheath for thermostat probe (5), electrical resistance for heating (8) and tank venting and filler filter (6). The pump of the stand aspire oil through the filter (3).

In **figure 4** we can see the location of heating resistance, thermostat and connections for suction and return line. In the scheme is also found the relief valve (11) for limiting the maximum working pressure, adjusted to 110 bar, pressure gauge (14), valve (13) for steering box by-pass, valve (9) for testing the pressure raised by the power steering pump from the test stand, plug-in coupling connections (15) for hoses that connect the steering box and steering box for testing (16). The hydraulically assisted steering box is mounted on the test stand by a device equipped with a load system (21) [3] for the steering rod, useful for determining the efficiency of the steering box. For viewing the flow are mounted two rotameters (23).

Fig. 3. Electric enclosure

Fig. 4. Tank connections

3. Performing the tests

Testing is done with a software application developed in LabVIEW that generates test sequences and allows plotting of the test diagrams for steering box. The software communicates through data acquisition card with transducers, variable speed drive for regulating the rotational speed of the electric pump of test stand and with driver for step by step motor that controls the rotary valve of steering box. From the software control panel (fig. 5) can be set pump flow according to the steering box model, the number of pulses per rotation of the rotary encoder and the number of steering wheel turns to move the rod of the steering box from one end to the other end (left-right stroke). At control panel of software it also sets the serial number of the steering box, name of the operator that perform testing, beneficiary of the test report, date and registration number of the test report. In manual regime the rod of steering box can be moved using a cursor from control panel on PC screen, and in automatic regime the software determine the rate of oil leakages at the stroke ends of steering box. Blocking the steering rod by using the load system (21) (e.g. in the middle zone) can determine the leakage flow due to wear of piston seal. In manual regime it can plot a diagram of pressure of the test stand pump, to see if still provide the nominal pressure. On the control panel of the software application there are two indicators for torque at rotation of shaft from rotary valve of steering box and for force performed at the rod of steering box.
In **figure 6** there is a record of the flow of hydraulic fluid lost by steering box at the end of the stroke. If the flow of loss at the end of stroke is above 1.5 l / min is recommended to replace or repair the steering box. A steering box worn, with large internal losses, will lead to disturbance in handling the steering. [4,5]. In **figure 7** there is a record for the pressure raised by the pump of the test stand. After recording the chart of loss of hydraulic fluid for steering box, it can be printed in a report containing identification data from front panel of application and recorded diagram.

Fig. 5. Software panel

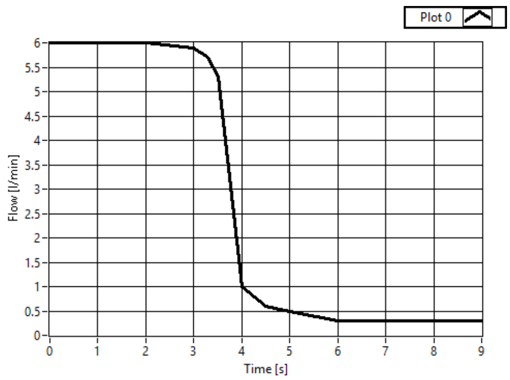

Fig. 6. Flow record

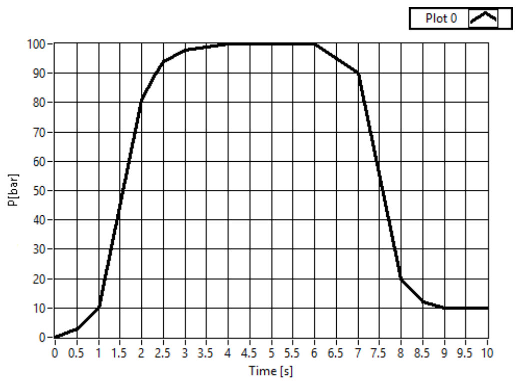

Fig. 7. Pump pressure record

4. Conclusions

The test stand equipped with data acquisition system enables rapid testing of steering boxes and issuing the test reports.

The test stand is equipped with thermostatic circuit for hydraulic fluid in order to ensure identical conditions for testing, regardless of the outside temperature.
The stand allows adjusting operating parameters [6,7,8] and contains a variety of sensors for registering the operating characteristics of the tested steering.
The test stand has an electric motor for driving the rotary valve of hydraulically assisted steering box, which allows automation of testing.
The system can be improved by increasing the degree of automation introducing in the scheme in place of manual valves electrically controlled valves, which can receive commands according to the test sequence.

References

[1] P.A. Adegbuyi, I.L. Marcu, "Hydraulic and pneumatic cylinder failures, the effect of fluid cleanliness on component life", Hidraulica Magazine, ISSN 1453-7303, Romania, no.1, pp. 27-30, 2013;
[2] I. Dutu, G. Matache, "Computer assisted electro-hydraulic stand for testing servovalves", Hidraulica Magazine, ISSN 1453-7303, Romania, no.3-4, pp. 73-77, 2012;
[3] G. Matache, St. Alexandrescu, Gh. Sovaiala, I. Pavel, I.C. Girleanu, "Testing of linear pneumatic actuators with hydraulic load", Hidraulica Magazine, ISSN 1453-7303, Romania, no.3, pp. 53-56, 2013;
[4] G. Matache, St. Alexandrescu, A. Pantiru, Gh. Sovaiala, M. Petrache, "The analysis of flow losses through dynamic seals of hydraulic cylinders", Hidraulica Magazine, ISSN 1453-7303, Romania, no.1, pp. 52-60, 2013;
[5] C. Cristescu, C. Dumitrescu, G. Vranceanu, L. Dumitrescu, "Considerations on energy losses in hydraulic drive systems", Hidraulica Magazine, ISSN 1453-7303, Romania, no.1, pp. 36-46, 2016;
[6] T.C. Popescu, C. Dumitrescu, I. Bordeasu, "Aspects Concerning the Use of Plastics in Developing Test Stands for Experimental Models of Hydraulic Turbine Blades ands Rotors", MATERIALE PLASTICE Bucharest - Romania Chem. Abs.: MPLAAM 53 (1) (1 - 184) ISSN 0025 / 5289 Vol. 53, no. 1, March, 20, pp. 174-178, 2016;
[7] T.C. Popescu, R. Radoi, M. Blejan, S. Nicolae, "Considerations on the experimental testing means of axial hydraulic turbine models", 15th International Multidisciplinary Scientific GeoConference SGEM 2015, www.sgem.org, SGEM2015 Conference Proceedings, ISBN 978-619-7105-38-4 / ISSN 1314-2704, June 18-24, Book4, pp.137-144, DOI: 10.5593/SGEM2015/B41/S17.018, 2015;
[8] T.C. Popescu, M. Blejan, "Means and Methods for Conducting Experimental Tests on Hydraulic Turbine Models", The Romanian Review Precision Mechanics, Optics & Mechatronics 48 , ISSN 1584-5982, pp.133-141, 2015.

Characterization of Rainfall Regime in Bucharest (2009-2015)

Carmen Otilia RUSĂNESCU[1], Gigel PARASCHIV[1], Sorin Ștefan BIRIȘ[1], Gheorghe VOICU[1], Marin RUSĂNESCU[2]

[1] Polytechnic University of Bucharest, Faculty of Biotechnical Engineering, otiliarusanescu@yahoo.com

[2] Valplast Industry Bucharest

Abstract: *This paper analyzes rainfall in Bucharest in 2009-2015. There are analyzed monthly average amounts of precipitation, distribution of quantities, seasonal rainfall, annual rainfall regime, the number of days with rainfall, the annual number of days with rainfall between certain limits, precipitation in the hot semester, and precipitation in the cold semester.*

Keywords: *Seasonal rainfall, monthly average amounts, half-yearly, yearly*

1. Introduction

Ecometrici climatic indices are formulas for climatic suitability, taking into account the actual amounts of key climate factors.
Monthly precipitation values are different depending on the circulation of air masses, altitude, slope orientation of landforms, local conditions.
Rainfall is an important meteorological parameter in assessing air quality by cleaning air in the lower layer, where industrial activities take place [1]. Knowing precipitation scheme was annual and multiannual, the variability over time, frequency form and intensity with falling presents practical interest, application and theory to provide usable reserves of soil moisture as a source of food rivers and prevent and combat the negative effects.
The energy that contain rainfall is divided into two, the kinetic energy of rainfall that is their strength impactor with direct role in the destruction of aggregates from soil and their energy potential, energy runoff on slopes and whites, with important role in detachment and transport parts of broken rock in its path [2].
Bucharest territorial sat on the periphery of anticyclonic influences aisatic and cyclone ocean and Mediterranean peculiar frontal and convective precipitation.
According rainfall from weather stations on the territory of Bucharest that the annual average rainfall varies between 600-700 mm annually, where the amount of aerosols is higher due to industrialization [1].
During recording a maximum rainfall in May-June. Heavy precipitation falling during the warm season of the year due to advection of moist air masses coming from the Atlantic Ocean, and thermo-convective processes that produce torrential rains sometimes accompanied by hail. Heavy rains occur over Bucharest because thermal convection is stronger. High frequency of rainfall in warm semester continental climate highlights the character of this country. They are generated by a high moisture air of intense activity and convection heat, which stimulates the development of clouds and rainfall intensification [1].

2. Results and discussion

Rainfall was recorded by the weather station at the Biotechnical Faculty of Engineering of the UPB, analyzed interval is 2009, 2010, 2011, 2012, 2013, 2014, 2015. And the comparison was made with data from the years 1961-1990 rainfall data ANMH site.
The least amount of rainfall between January and March due to the predominance anticyclone regime, preventing the development of thermal convection, the driest month of February. Starting in March, the precipitation increases progressively from May to June, for an annual maximum rainfall (197.4 mm). Rainfall this month are generated by the high frequency of cyclones ocean.

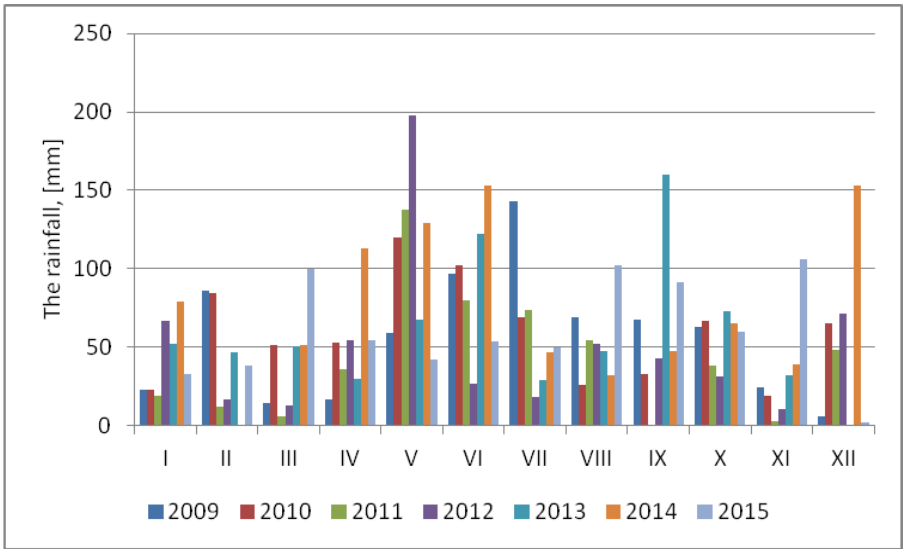

Fig. 1. The graphical representation of the average amount of rainfall in the period 2009-2015 compared with 1961-1990

The average amount of rainfall registered in Bucharest in 2009 was within normal limits (658.6 mm) compared to the period 1961 to 1990 (596.2 mm).
In the first months of the year (January, February, and March) precipitation likely prevail front; the local is very low, with small fluctuations from month to month. In January masses of air from the anticyclone Eurasian have a high frequency, coming cold, common cold, dry in their way, there aren't any obstacles orographic major and systems cloudy related fronts cyclones Mediterranean are routed mainly over the Pannonian Plain, orographic barrier east of the eastern Carpathians, rarely failing to get all these lead to the recording of very small average amounts of precipitation.
Since April, rainfall almost doubled. Between May and June, the amount of rainfall recorded a sharp rise and continues to rise until July. In July, the work cyclone intensifies the northern outskirts of Ridge and the anticyclone of the Azores extended to the south of Romania, bringing air masses wet and unstable and convection heat is considered as a supplement moisture of brought the movement west on stretches of ocean in western Europe. Higher levels of rainfall in the June-July is due primarily produce thermal convection (besides processes Front), which causes strong rain showers.
In August, September, rainfall is decreasing because of lower thermal convection with temperature decrease. In October, November and December convection heat disappears and precipitation are caused not only by cold advection of air masses, coming from the continental north and east, resulting in very low amounts and largely solid. These variations have a normal progression, ascending in the first half to record maximum in May, after which values decrease progressively until December, so in January to register the minimum [1].
The average amount of rainfall in Bucharest in 2009 (669 mm) exceeded the climatological normal (596.2 mm) with a positive deviation of 3.12%. The annual amount of precipitation in 2010 in Bucharest was 713 mm below the climatological norm (596.2 mm) with a positive deviation of 19.59%.
Overtaking the highest of standards climate monthly quantities of precipitation in Bucharest occurred in May 2012 (exceeded normal climatological a positive drift of 181.20%). The annual amount of precipitation on average in 2011 in Bucharest was 507.8 mm below the climatological norm (596.2 mm) with a negative deviation (-14.83%) due to the poor rainfall in most months except the months: May (with misconduct positive 95.73% compared to normal climatological), June (with a positive drift of 3.10% compared to the climatological normal) in July (with a positive drift of 15.40% compared to normal climatological), October (with a positive drift of 20.50% compared to climatological normal) and December (with a positive deviation of 10.85% compared to the climatological normal). In the other eight months of the year deviations were negative in the months: January rainfall was 52.02% lower than the climatological normal April rainfall was 21.74% lower than the climatological normal August rainfall was with 7.03% less than normal largest

deficits were registered in March (with a deviation of 84.82% in September (100% rainfall lower than normal climatological), November (94.26%).
Precipitation recorded in Bucharest in 2012 under normal climatological were in the months of February (16.8 mm by 53.59% lower than the climatological normal), March (5.8 mm to 38.2 mm by 65.45 % lower than the climatological normal), June (37.6 mm to 77.4 mm by 51.42% lower than the climatological normal), July (28.3 mm versus 64.3 mm by 55.99% lower than the climatological normal), August (38.3 mm to 58.3 slightly deficient rainfall with 34.31% lower than normal climatological), November (low rainfall quantitatively 10.3 mm to 48.8 mm by 78.89% lower than the climatological normal processes of vegetation species autumn were slowed. the fruit trees and vines and continued yellowing and leaf fall, farm work in the field, crop residues release land, plowing, were made in good condition).
The annual amount of precipitation in Bucharest in 2014 was 953 mm beyond the standard climatological normal (1961-1990) (596.2 mm), with 59.85%. Deviations were positive in the months: March (33.77%), April (145.65%), May (83.90%), June (97.67%), July (1.09 %), September (12.32%), October (103.79 %), August (1.20 %), December (253.12%) deviations were negative in: January (98.74%), February (98.90%), July (26.75%), August (26.6%), November (20.49%), the annual amount of precipitation in Bucharest in 2015 was 730.8 mm beyond the standard climatological normal (1961-1990) (596.2 mm), with 22.58% (Figure 1 and table 1).

TABLE 1: Deviations from the years 2009-2015 (%)

	Deviations from the years 2009-2015 rainfall against the normal climatological (1961-1990) (%)					
	I	**II**	**III**	**IV**	**V**	**VI**
2009	-52.02	0.55	-47.64	-63.48	-15.38	25.32
2010	-42.42	134.25	33.51	14.35	70.37	32.30
2011	-52.02	-65.75	-84.82	-21.74	95.73	3.10
2012	68.18	-53.59	-65.45	17.83	181.20	-51.42
2013	51.52	35.36	70.16	-35.87	23.93	67.96
2014	98.74	-98.90	33.77	145.65	83.90	97.67
2015	-17.68	6.08	161.52	19.13	-30.20%	-22.48%

TABLE 1: Deviations from the years 2009-2015 (%) *(continued)*

	Deviations from the years 2009-2015 rainfall against the normal climatological (1961-1990) (%)						
	VII	**VIII**	**IX**	**X**	**XI**	**XII**	**annual**
2009	122.40	18.70	60.19	98.74	-50.41	-87.07	3.12
2010	7.62	-55.06	-21.33	110.73	-60.25	50.12	19.59
2011	15.40	-7.03	-100.00	20.50	-94.26	10.85	-14.83
2012	-55.99	-34.31	1.18	-22.08	-78.89	64.67	0.87
2013	-56.45	2.92	110.90	149.21	-13.93	-99.31	-20.56
2014	1.09	1.20	12.32	103.79	-20.49	253.12	59.85
2015	-6.69%	50.60%	100.00%	90.22%	108.40%	-95.61%	22.58%

Seasonal precipitation amounts distribution

Seasons as a feature of temperate continental climate, summer fall the highest amounts of rainfall (16% - 46%) and winter fewest (9.93% - 25.76%) of the year. Spring (16.92% - 44.09%) and autumn (16.61% -35.56%) intermediate amounts of rainfall recorded compared to the other two seasons (Table 2).
Annually there are two maximum and two minimum rainfalls. The major peak in May-June occurs as a result of increased thermal convection and the deepening work polar front and the secondary November-December due to the development of Mediterranean cyclones that bypass the country from the west and southwest. Lows rainfall is related to drought periods from late winter-early

spring and the late summer-early autumn. In the summer season there are high amounts of rainfall compared to the winter season where there was a decrease theirs, but increases in summer occurs generally in the form of rain, which often cause flooding.

TABLE 2: The amount of rainfall in spring multiannual period 2009-2015

The analyzed period	Winter	percentage of the annual average	Spring	percentage of the annual average	Autumn	percentage of the annual average	Summer	percentage of the annual average
2009	81.4	12.17%	113.2	16.92%	154.8	23.14%	309.4	46.25%
2010	172.6	24.21%	223.2	31.31%	119.4	16.75%	197.8	27.75%
2011	79.4	15.64%	179.2	35.29%	118.7	23.38%	208.2	41.00%
2012	154.7	25.76%	264.8	44.09%	77.7	12.94%	97.1	16.17%
2013	109.3	15.39%	181.5	25.55%	210	29.56%	199.1	28.03%
2014	232	24.69%	293.2	32.30%	150.8	16.61%	231.8	25.53%
2015	72.9	9.93%	203.7	27.75%	246.4	33.56%	206.3	28.10%

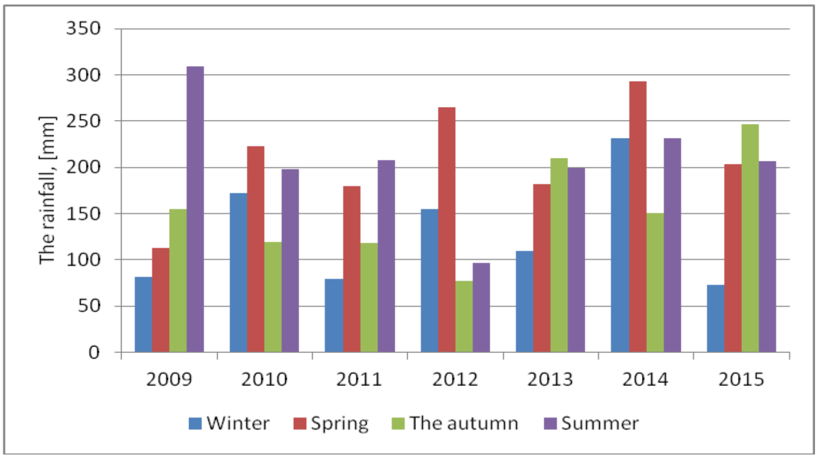

Fig. 2. The amounts of rainfall in the four seasons of the year

The annual rainfall regime in Bucharest between 2009-2015

The annual rainfall regime in Bucharest in the period 2009-2015 compared with 1961-1990 average climatological records a major peak in May, the average amounts of precipitation are over 197.4 mm in 2012, 129.1 mm in 2014. In May fall in the range 2009-2015, 778.9 mm rainfall 659.8 mm compared to June. And July is characterized by a rich rainfall in third place after May, June and the annual minimum in November (239.2 mm) and February (237.8 mm).

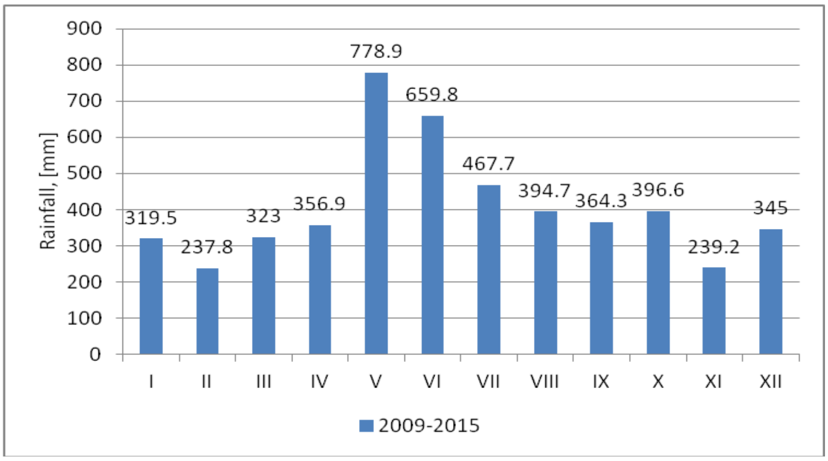

Fig. 3. Distribution yearly rainfall in Bucharest between 2009-2015

The number of days with precipitation in Bucharest between 2009-2015

For the analysis of rainfall days were used daily rainfall data recorded by the weather station at the Biotechnical Faculty of Engineering U.P.B. on 2009-2015.
The average annual number of days with precipitation is over 100 in four years, so raining about 3-3.5 months of the year (2010, 2013, 2014, 2015), and the average monthly number of days with precipitation has a maximum in May, 87 days. The average monthly number of days with precipitation has a minimum in August, 33 days (Figure 3).

The annual number of days with rainfall between certain limits

We calculated for years 2009, 2010, 2011, 2012, 2013, 2014, 2015, the annual number of days with precipitation amounts, it appears that precipitation ≥ 0.1 mm in Bucharest are 477 days, decreasing as threshold of increase amounts to 271 days if ≥ 0.5 mm rainfall; 199 days for those that ≥ 1.0 mm rainfall; 188 days for precipitation ≥ 2.0 mm; 98 days if ≥ 5.0 mm rainfall; 48 days in case of rainfall diurnal ≥ 10.0 mm, 9 days when daytime precipitation ≥ 20 mm and 4 days with rainfall amounts ≥ 30 mm.
On the same day rainfall was 0.1 mm and 1.0 mm and 2.0 mm and. In Bucharest prevails ≥ 0.1 mm precipitation.

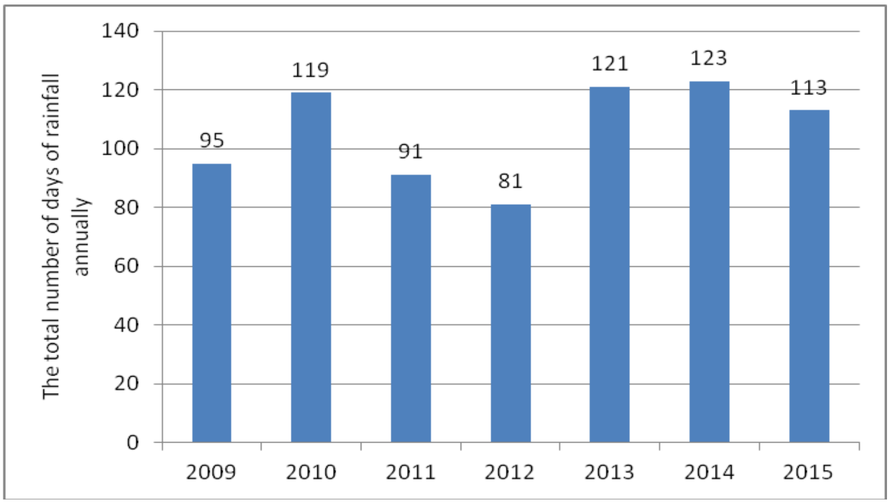

Fig. 4. The total number of days of rainfall annually

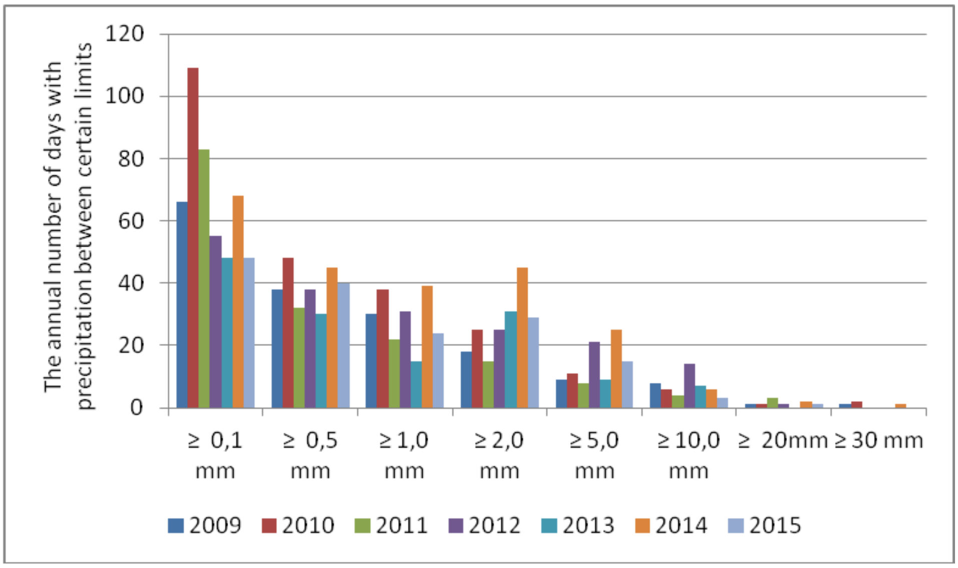

Fig. 5. The annual number of days with precipitation between certain limits in Bucharest (2009-2015)

Precipitation in the warm semester

Precipitation during the period of maximum consumption is the amount of precipitation that corresponds to the interval from May to September, when registered the highest thermal values. Generally, this period is characterized by long periods of drought and intensive [4].
Precipitation in the warm semester are between 381.6 mm (2011) and 566.5 mm (2014).
The average amounts of precipitation in the warm half of the year (months IV-IX) in the city of Bucharest in 2009-2015 were calculated based on weather data recorded by the weather station at the Faculty of Biotechnical Systems Engineering from Polytechnic University of Bucharest, their values are given in table 5. it is noted that the highest amounts of rainfall were recorded in June 2014 (153 mm).
In terms of precipitation, June 2014 was rich in rainfall, which amounted on average to the level of Bucharest an amount of 153.5 mm, compared to the 1961-1990 climatological reference, the average is 77, 4 mm.
In June, on almost the whole country recorded the highest amounts of rainfall throughout the year [3].
Quantities significant rainfall Specific June is mainly due to intense activity of Ridge and the Azores High, extended south of Romania, which brings air masses wet oceanic and unstable, which on contact with air tropical covering and area of our country causes production of precipitation particularly abundant. They may be the result of crossing the area examined by weather fronts (or their peripheries) or local factors that may cause considerable vertical development generating rainfall. Heavy rains falling in Romania are dependent on elevation, landform, Carpathian orographic blocking role to advection of moist air to solar radiation as well as other local conditions and time.
The average intensity of heavy rains is the main characteristic of them; it gradually decreases with altitude up to 3 mm in high mountain regions. A torrential rain if its intensity is average
It is 0.2 mm / min and the average intensity excessive rain if it is 0.45 mm / min over a period of 121-180 minutes [7].
Below in figure 6 are presented precipitation analysis specific ecological factors. It is characterized during water accumulation in a biologically active horizon (X-III) or maximum biological activity period (IV-IX).
For spontaneous vegetation, these low precipitation can be an indicator illuminating in terms of the character and xeromezofite xerophit vegetation that grows in all areas of the steppe.
Moisture deficit characteristic of this period, the drying effect of trees and shrubs green spaces, decreasing habitat comfort internally and externally, the rising cost of living.

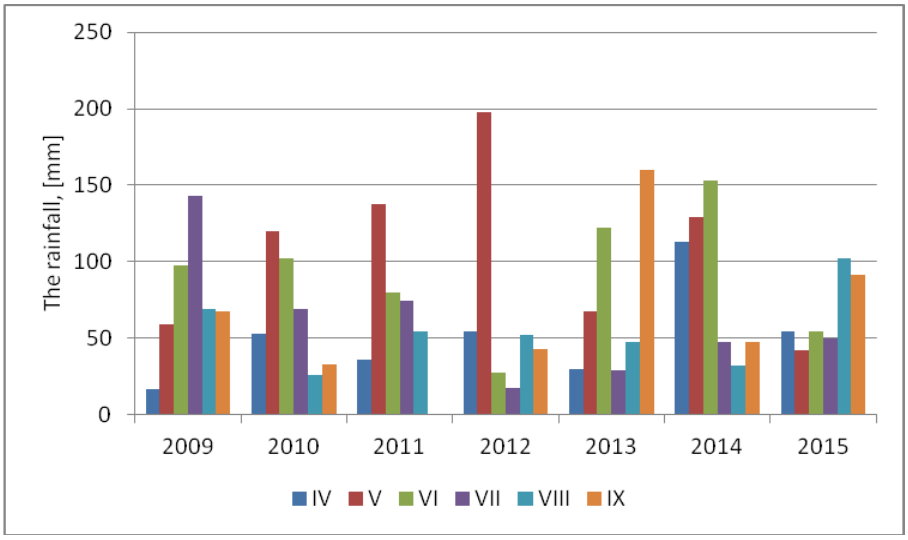

Fig. 6. The amount of rainfall in warm semester in Bucharest, between 2009-2015

Precipitation in the cold semester

In cold fall semester between 205.6 mm (2009) and 334.8 mm (2015).
Precipitation semester cold are less abundant than those recorded in the warm semester of the year due to high-frequency air masses continental cold and dry (with a low water vapor) and because clouds and precipitation convection heat have development lower than in summer. Above our country anticyclone prevailing regime of no rainfall [9].
In January masses of air from the anticyclone Eurasian have a high frequency, coming cold, common cold, dry in their way neinterpunându into any obstacles orographic major and systems cloudy related fronts cyclones Mediterranean are routed mainly over the Pannonian Plain, orographic barrier east of the eastern Carpathians, rarely failing to get all these lead to the recording of very small average amounts of precipitation [9].
October-March period is a period of excess water in the soil, it is necessary accumulation of vegetation structure in the first two phases of the vegetative cycle (germination and sprouting).
High temperatures in this period leading to high levels of actual evapotranspiration. Given and full development of foliage, plants needs are maximized, resulting in depletion of ground water. The amount of rainfall during the cold season of the year is the total amount of water resulting in solid and liquid precipitation. Winter important in terms of rainfall, as it ensures the water reserve in the soil, which is then used during the first phenological phases [4]. The amounts recorded in this period represents approximately 24.85% (cold semester 2011) – 45.85 % (cold semester 2015) of the annual average (Figure 7) are lower than in the first half of the year hot.
These low values illustrate droughts, which occurs due to reduced amounts of rainfall in this period especially important for agriculture because now formed into useful soil water reserve required beginning of the growing season. Limited rainfall and lead to a higher concentration of pollutants in the atmosphere [1].

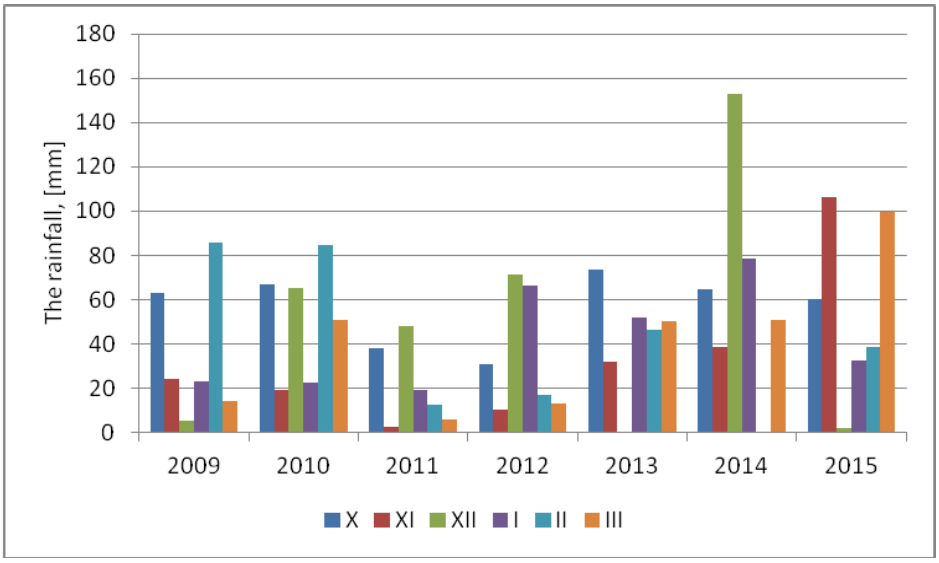

Fig. 7. Showed average values of rainfall semester cold in Bucharest 2009-2015, based on data from the weather station.

3. Conclusions

Cold precipitation semester are less abundant than those recorded in the warm semester of the year. The average annual number of days with precipitation is over 100 in four years, i.e. raining about 3-3.5 months a year, and the average monthly number of days with precipitation has a maximum in May 87 days. The average monthly number of days with precipitation has a minimum in August 33 days.
The annual rainfall regime in Bucharest in the period 2009-2015 compared with 1961-1990 average climatological records a major peak in May, June and July followed by an annual minimum in November, February and March.

Seasons as a feature of temperate continental climate, summer fall the highest amounts of rainfall and lowest in winter of the year. Spring and autumn intermediate amounts of rainfall recorded compared to the other two seasons.
In the summer season there are high amounts of rainfall compared to the winter season where there was a decrease theirs, but increases in summer occurs generally in the form of rain, which often cause flooding.

References

[1] I. Iojă, "Metode și tehnici de evaluare a calității mediului în aria metropoliatană a municipiului București" 2009;
[2] V. Tufescu, "Modelarea naturală a reliefului şi eroziunea accelerată", Editura Academiei Republicii Socialiste România, Bucureşti, 618 p., 1966;
[3] Clima Romaniei - Administraţia Naţională de Meteorologie, Ed. Academiei Române, Bucureşti, 2008;
[4] A. Vlăduţ, "Ecoclimatic indexes within the Oltenia plain*",* Forum geografic.- Studii și cercetări de geografie și protecția mediului, Year 9, No. 9/ 2010, pp. 49-56;
[5] A. Vlăduţ, "Deficitul de precipitaţii în Câmpia Olteniei în perioada 1961-2000", Forum Geografic – Studii şi cercetări de geografie şi protecţia mediului, Year III, No. 3, Editura Universitaria, Craiova, pp. 99-104, 2004;
[6] C.-O. Rusănescu, I. N. Popescu, M. Rusanescu, L. David , "Analysis of variation in relative humidity in autumn 2009", In: International Journal of Energy and Environment, Issue 4, Volume 4, 2010, pp.113-121, ISSN: 1109-9577;
[7] Scientific Journal of the National Meteorological Administration, Bucharest, 2012-2013;
[8] C.-O. Rusănescu, G. Paraschiv, Gh. Voicu, M. Rusănescu, "Comparative analysis of atmospheric temperature values, relative humidity in 2009 and 2010 in west side of Bucharest city", In: Bulletin UASVM Agriculture, 68(2)/2011, Print ISSN 1843-5246; Electronic ISSN 1843-5386, pp. 130-138;
[9] V. Sorocovschi, T. Tudose, H. Selagea, P. Roman, "Variația în cursul anului și repartiția teritorială a precipitațiilor medii din Podișul Someșean", Geographia Napocensis, Year IV, No. 2/2010;
[10] C.-O. Rusănescu, M. Rusănescu, "Some aspects regarding the global warming", In: Hidraulica **no.** 4 (2013), pp. 7-11;
[11] C.-O. Rusănescu, "Îndrumar de meteorologie și climatologie", Editura Matrix Rom, Bucuresti, 2013;
[12] N. Mărunţelu, L. Istode, A. Coman, "Indicii ecometrici, instrumente moderne folosite pentru monitorizarea evoluției ecosistemelor, conservarea biodiversității şi optimizarea conceptului de casă ecologică", București, 2013.

A Review of Combustion Process

Vikaram SINGH[1], Sujoy NAIR [2]

[1] Indus University, India, sn2008@rediffmail.com

[2] Indus University, India

Abstract: *Combustion based noise plays an important role in emissions in engines. In this work these emissions have been analyzed and various factors affecting it have been discussed.*

Keywords: *Piston secondary motion, liner system*

1. Introduction

Combustion noise generated mainly depends on rapid rise of cylinder pressure due to ignition delay period in combustion engines. Design of combustion chamber as well as variations in various injection parameters like injection pressure, amount of fuel injected and its timings also play a crucial role in noise emissions [1]. Depending upon type of engine and various operational parameters, overall noise emissions from a typical engine are in range 80-110dBA [2]. Anderton has investigated the effects of turbo charging on noise emissions from engines [3] .Split injection using electronic control reduces the premixed combustion and hence is an effective way to reduce overall noise emissions by about 5-8dBA [4]. Head and Wakes have shown that during transient operational conditions, overall noise levels are 4-7dBA higher as compared with steady state operations [5]. Cold starting conditions lead to higher ignition delay period which in turn causes more premixed combustion and hence an increase in noise emissions [6]. Quality of fuel also affects combustion noise emissions from engines. It has been seen that reduction of centane number of diesel from 50 to 40 causes a rise of 3 dBA in combustion based noise [7]. In gasoline engines, the ignition delay period is longer due to lesser compression ratio which leads to lower temperature of charge and hence more noise [7]. For a naturally aspirated engine the combustion noise depends upon amount of fuel that mixes with air charge during injection delay period and hence compression ratio of engine also plays a vital role [7].

2. Background

Due to high efficiency, diesel engines have been a favorite choice for heavy duty applications including trucks [8].However they suffer from drawbacks of high noise, weight and vibrations. These engines are of two types: > Direct Injection (D.I.) Engines; > Indirect Injection Engines
In the D.I. engines, the fuel is directly injected inside combustion chamber and due to lesser time for mixing, a heterogamous mixture consisting of both rich and lean parts is formed in the chamber.

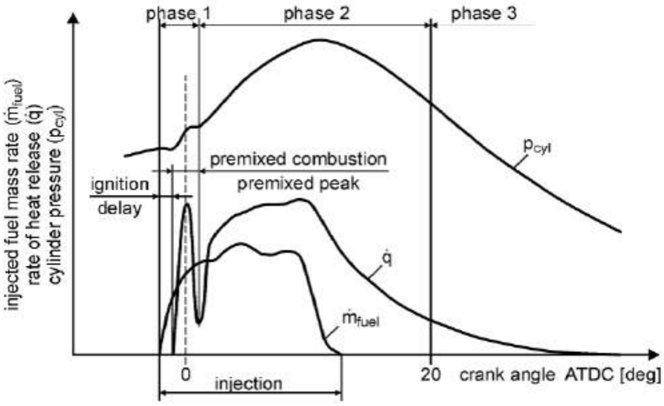

Fig. 1. Phases of Diesel Engine Combustion

Figure no 1 shows the three phases of combustion in a conventional diesel engine. The first phase starts with start of injection process and ends with premixed combustion phase. The direct injection of fuel into combustion chamber begins some crank angle degree before top dead center positions depending upon engine operational conditions. As soon as cold jet of fuel penetrates into chamber, it mixes up with hot compressed air. The droplets begin to vaporize forming a sheath of vaporized fuel-air mixture around jet periphery. When temperatures reach around 750K, the first break down of Cetane fuel occurs. Further reactions produce C_2H_2, C3H3, C2H4, CO2 and water vapors [9].
Resulting rise in temperature causes complete combustion of fuel-air mixture. This sudden combustion causes rise in heat release rate and high pressure gradient $\frac{dP}{d\theta}$ which further leads to high temperatures in pre-mixed zone and NO_x production. The premixed combustion consumes all mixture around inner spray region where temperatures of ranges 1600-1700K are reached and all oxygen available for combustion is consumed [8]. Now various partial burnt particles diffuse to outer layers and are burnt in a thin reaction region at periphery of spray which leads to formation of diffusion flame.
This kind of combustion is known as diffusion controlled combustion and is depicted by region 2 and 3 in the above figure. The high temperatures along with lack of oxygen is ideal for soot formation.

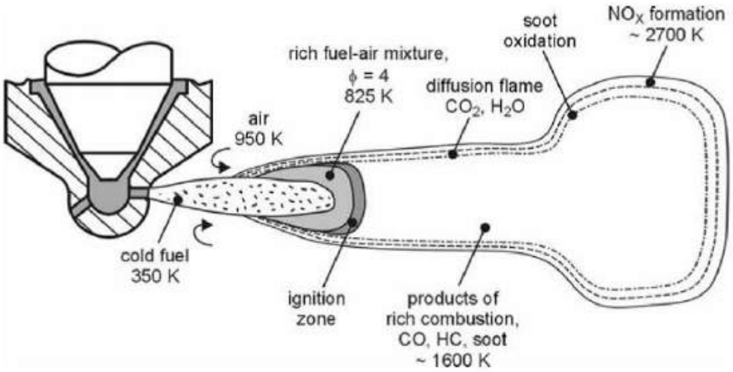

Fig. 2. Conventional diesel engine spray formation

The diffusion flame is fed with oxygen from surrounding environment and high temperatures of range 2700K is reached consuming all the soot formed. At outer region of flame there is enough oxygen content for formation of NO_x.
Figure no 3 shows soot formation concentration as a function of crank angle. Most of soot produced at early crank angles is consumed later and final exhaust emissions have only a fraction of initial one. As seen from figure no 1, the diffusion controlled combustion can be divided into two sub phases. During phase 2 of combustion the burning rate is controlled by mixing of fuel fragments and air and rate of reaction is must faster. During the phase 3 the final oxidation of remaining unburnt particles and soot takes place, however due to decrease of gas temperature during expansion stroke and lack of oxygen the reaction rate is much slower.

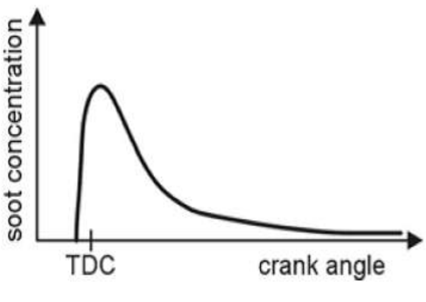

Fig. 3. Rate of soot formation

NO_X and soot formation in combustion engines show an opposite trends as shown in figure no 4. In order to reduce NO_x ,it is necessary that local temperatures must not rise above 2000K.A possible way to do so is to inject fuel late in cycle inside combustion chamber which shifts combustion phase towards expansion phase and hence significant reduction in chamber temperatures. However consumption of fuel and soot formation increases due to late combustion.

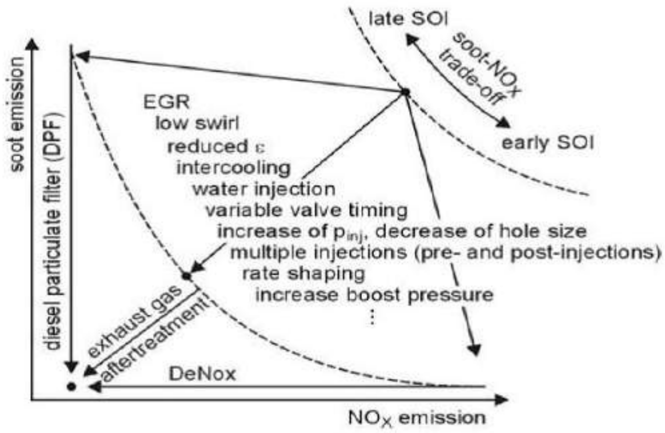

Fig. 4. Soot & NOx trade off

Hence modern injection systems use multiple injection techniques in order to reduce both soot as well as NO_x emissions as seen from figure no 5[8, 10, 11].

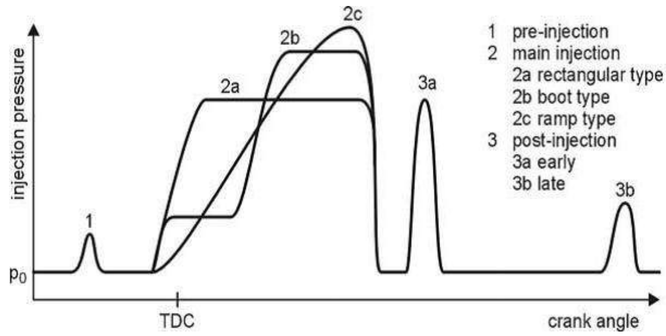

Fig. 5. Multiple injection methods adopted for modern diesel engines

These generally use three phases of injection namely pre-injection Period, Main –Injection Period & Post injection period as seen from figure no 5.There is delay period between the start of ignition process and fuel injected inside diesel engine. More this ignition delay more is the temperature during combustion and hence better condition for NOx formation. To shorten the delay period, small amount of fuel is pre-Injection before main injection during the phase pre-Mixed combustion phase. The torque and power produced in engine depends upon main injection period. It is advantageous to vary injected fuel mass with time to reduce the specific fuel consumption. This method is known as rate shaping. Rate shaping may be rectangular, step or boot in shape. Post-injection of fuel is done to reduce soot emissions and in some cases may be useful for Exhaust gas recirculation treatment of gases [12]. It has been reported that post injection reduces soot by about 70% without increasing the fuel consumption [13].

3. Phase analysis

This part of work presents experimental data in which signals from accelerometers and cylinder pressure transducers are used for analysis of combustion behavior of engines. Previous works have shown that engine vibrations are sensitive towards change in engine injection parameters. Accelerometer signals have been able to locate the important features of combustion process in diesel engines [14, 15]. The aim of present part of work is to explore the relationship between block vibrations and in cylinder pressure development process. Experiments were done at various load and speed conditions to explore the sensitivity of vibration data.

Combustion process monitoring and analysis is an important feature in NVH feature improvement of diesel engines since a major portion of noise is attributed towards the combustion process occurring inside cylinders. Use of in cylinder pressure transducers and other non-intrusive methods of monitoring form an important methodology of combustion analysis. Microphones located at a distance from engine also provide information about engine performance; however there is risk of contamination of signals during engine operational conditions [16-19].The combustion process in diesel engines have various phases as discussed in previous section. The frequency spectrum of combustion noise form diesel engines is divided into three regions as discussed later in this work. The aim of this work is to establish a relationship between engine vibrations and in cylinder pressure development.

4. Results and discussions

The aim of this part is to provide an overview of combustion noise generation process. This was done by analyzing the methodology provided in previous works done. Engine combustion noise originates from combustion process taking place in cylinder. When fuel is injected inside the combustion chamber where high pressure air is present, then part of ignitable gas starts to burn causing a rapid rise in pressure as well as temperatures inside combustion chamber. The pressure wave thus generated also strikes the walls of combustion chamber causing resonance of structure. The vibrations are radiated in air through engine structure and are perceived as combustion noise.

In actual practice it is difficult to distinguish between combustion noise and piston slap as both coincide near top dead center positions. For sake of convenience it is assumed that combustion noise originates due to pressure vibrations inside engine cylinder and is transmitted to cylinder cover, piston, connecting rod, crank shaft and engine surroundings. Mechanical noise includes noise from piston-liner impact, valve operations, pump operations, injector operations as well as operation of various accessories and valve trains. Generally for indirect injection diesel engines and gasoline engines, the combustion process is less severe as compared with diesel engines; hence the combustion noise is lesser as compared with mechanical noise.

The cause of combustion noise is rapid change in cylinder pressure during combustion process. The effects of combustion process consist of high frequency gas vibrations and dynamic load due to rapid pressure change. The intensity of combustion noise (I) is dependent upon the values of maximum pressure value (P_{max}) and maximum rate of pressure rise as [20]:

$$I\alpha[(\frac{dP}{dt})_{max}P_{max}]^2 \quad (1)$$

In a direct injection diesel engine, combustion process occurs in following four phases: retarded, rapid, early and late phase. Combustion noise is mainly generated during rapid phase of combustion however retarded phase has an indirect effect on combustion noise. During this phase of combustion, the firing and fuel propagation results in impulsive pressure wave that gets reflected multiple times after striking walls of chamber. This process causes high frequency oscillations. The frequency (f_g) can be estimated from engine bore diameter (D) &Wave propagation speed (C_c) by:

$$f_g = \frac{C_c}{2D} \quad (2)$$

Further the spectrum plot of cylinder pressure can be obtained from acquired about in cylinder as seen in figure no 6.

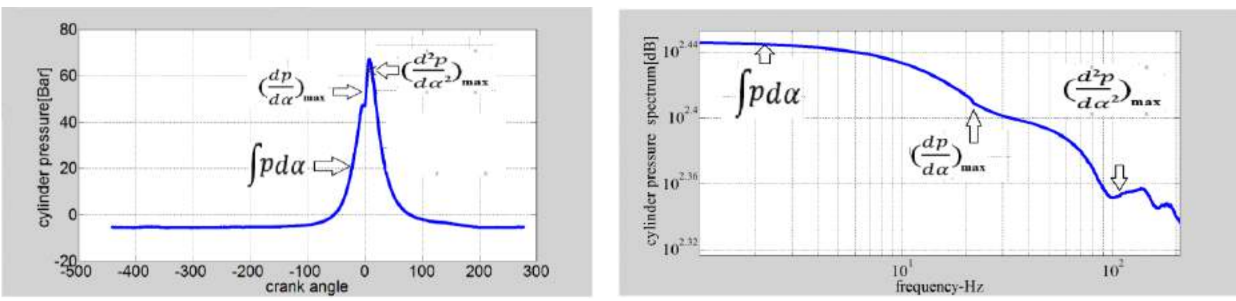

Fig. 6. Regions of combustion noise

The graph is marked by following three distinct regions [20]:
a) Region of low frequency-in this region the curve depends upon peak cylinder pressure. Higher the maximum value of cylinder pressure, higher is the peak in low frequency range.
b) Medium frequency range-in this part the pressure levels decrease in logarithmic range with slope depending upon rate of cylinder pressure Larger the value of pressure gradient, steeper is the slope of curve.
c) High frequency range –in this range rapid evolution of in cylinder pressure occurs due to onset of combustion process which results in high frequency vibrations of cylinder structure having amplitude dependent on second cylinder pressure derivative.
Combustion noise is not only dependent upon cylinder pressure but also upon the structural response and damping effects of engine. The difference between in cylinder pressure and outside noise radiated in engines is characterized by a decay which reflects the structural attenuation of engine structure. Figure no 7 shows a typical plot of structural attenuation of an engine which is independent of exciting forces and cylinder pressure spectrum. Various operational parameters of engine e.g. load, speed & fuel injection parameters have no significant effects on structural attenuation property.

5. Conclusions

This work considers the effects of combustion process on various parameters of noise generated in engines. The various phases and regions of combustion noise in frequency domain were considered.

References

[1] S. C. Tung, M. L. McMillan, “Automotive tribology overview of current advances and challenges for the future”, In: Tribology International 2004;37:517–35;
[2] D.F. Li, S.M. Rhode, H.A. Ezzat, “An automotive piston lubrication model”, ASLE Transactions 1983;26(2):151–60;
[3] V.W. Wong, T. Tian, H. Lang, J.P. Ryan, Y. Sekiya, Y. Kobayashi, *et al.*, “A numerical model of piston secondary motion and piston slap in partially flooded elasto hydrodynamic skirt lubrication”, SAE paper no. 940696, 1994;
[4] S. Jiang, J. Cho, “Effects of skirt profiles on the piston secondary movements by the lubrication behaviors”, In: International Journal of Automotive Technology, 2004;5(1):23–31;
[5] A. Gupta,S. Narayan, "Electrical Analogy of Liquid Piston Stirling Engines", In: Hidraulica no. 2 (2016): 58;
[6] S. Narayan, V. Gupta, "Overview of working of Striling engines", In: Journal of Engineering Studies and Research, 21.4 (2015): 45;
[7] A. Gupta, S. Narayan, "A Review of Heat Engines", In: Hidraulica no. 1 (2016): 67;
[8] S. Narayan, "Analysis of noise emitted from diesel engines", In: Journal of Physics: Conference Series, vol. 662, no. 1. IOP Publishing, 2015;
[9] A. Gupta, S. Narayan, "Effects of turbo charging of spark ignition engines", In: Hidraulica no. 4 (2015): 62;
[10] S. Narayan, "Designing of liquid piston fluidyne engines", In: Hidraulica no. 2 (2015): 18;
[11] S. Narayan, “Effects of various parameters on piston secondary motion”, no. 2015-01-0079. SAE Technical Paper, 2015;
[12] S. Narayan, "Analysis of Noise Radiated from Common Rail Diesel Engine", In: Tehnički glasnik, 8.3 (2014): 210-213;
[13] S. Narayan, "Time-frequency analysis of Diesel engine noise", In: Acta Technica Corviniensis-Bulletin of Engineering, 7.3 (2014): 133;
[14] S. Narayan, A. Gupta, R. Rana, "Performance analysis of liquid piston fluidyne systems", In: Mechanical Testing and Diagnosis, 5.2 (2015): 12;
[15] S. Narayan, V. Gupta, "Motion analysis of liquid piston engines", In: Journal of Engineering Studies and Research, 21.2 (2015): 71;
[16] S. Narayan, “Modeling of Noise Radiated from Engines”, no. 2015-01-0107. SAE Technical Paper, 2015;
[17] B. V. Hubballi, V. B. Sondur, "Experimental investigation on transient response of two stage pressure relief valve", In: Hidraulica no. 3 (2015): 42;
[18] V. Gupta, S. Sharma, S. Narayan, "Review of working of Stirling engines", In: Acta Technica Corviniensis-Bulletin of Engineering, 9.1 (2016): 55;

[19] A. Singh, S. Bharadwaj, S. Narayan, "Review of how aero engines work", In: Tehnički glasnik , 9.4 (2015): 381-387;
[20] S. Narayan, "A review of diesel engine acoustics", In: FME Transactions, 42.2 (2014): 150-154;
[21] S. Narayan, "Noise Optimization in Diesel Engines", In: Journal of Engineering Science and Technology Review, 7.1 (2014): 37-40;
[22] V. Gupta, S. Sharma, S. Narayan, "Review of working of Stirling engines", In: Acta Technica Corviniensis-Bulletin of Engineering, 9.1 (2016): 55;
[23] A. Singh, S. Bharadwaj, S.Narayan, "Analysis of Various NHV Sources of a Combustion Engine", In: Tehnički glasnik, 10.1-2 (2016): 29-37;
[24] X. Meng, Y. Xie, "A new numerical analysis for piston skirt–liner system lubrication considering the effects of connecting rod inertia", In: Tribology International, 47 (2012): 235-243;
[25] S. Narayan, *et al.*, "A priority based exploration algorithm for path planning of an unmanned ground vehicle", In: Embedded Systems (ICES), 2014 International Conference on. IEEE, 2014.

The Analysis of the Black Sea Waves Features in order to Capitalize their Hydropower Potential

Assoc.Prof. PhD **Sanda BUDEA[1]**, Prof. PhD **Mariana PANAITESCU[2]**, Prof. PhD **Viorel PANAITESCU[2]**

[1] Department of Hydraulics, hydraulic machines and environmental protection, University Politehnica of Bucharest, Romania, e-mail: sanda.budea@upb.ro

[2] Department of Engineering Sciences in Mechanics and Environment, Maritime University of Constanta, e-mail: marianapan@yahoo.com

Abstract: *This paper presents the waves characteristics near the Romanian coastline of the Black Sea, based on a large set of data from National Institute of Meteorology and Hydrology. The main wave's characteristics are: wave height, wavelength, period, wave celerity, Strouhal's number to study the similarity. Analyze is made in order to estimate the waves hydropower potential. From the polynomial integration of the wave's height results this variation during a year. The average height of waves near the Romanian coastline of the Black Sea is about 2.5-3 m in cold seasons and about 1.5-2 m in warm seasons. This paper estimates the hydropower wave's potential for a plant with 5 meters mounted at three different deeps – 10 m, 20 m and 30 m. For waves with average height of about 2 m, it can obtain 58-65 KW. Catching the wave energy near the shoreline is useful to reduce Romanian shoreline erosion*.

Keywords: *wave features, hydropower potential, marine current, shoreline*

1. Introduction

The Black Sea is located at 40°- 46° North Latitude and 27°- 41° East Longitude and has a surface of 423488 km^2. The Romanian coast, at the west side of the Black Sea, is about 245 km long, including the Danube delta. The Black Sea's climate characteristics are influenced by the North Atlantic Oscillation (NAO) and El Nino-Southern Oscillation (ENSO), which from a cyclone over the Black Sea basin [1]. For this reason, the Black Sea level is higher on winters than it is on summers [2].

Marine Black Sea currents generate traveling waves. There are two major ring streamline in horizontal circulation, rotating counterclockwise, having a velocity from 0.08-0.18 m /s (Fig.1). In the Black Sea, the vertical circulation is very slow, "it takes hundreds of years for the waters at the surface to be replaced by near-bottom waters from the deep-sea depression" [3]. "Daily tidal oscillations in the Black Sea do not exceed several centimeters. Severe storms accompanied by waves up to 8-10 m high occur often in winter season. The water temperatures at the surface of the Black Sea extends from –1.2ºC in winter to +31ºC in summer with mean annual level varying from 12ºC in the northwest to 16ºC in the southeast of the basin. Below 500 m the waters have a constant temperature of about 9ºC" [3].

This paper analyses the characteristics of the waves on the Black Sea Coast, regarding their height, wavelength, wave period and velocity, in order to capitalize their hydropower potential.

There are significant fluctuations in the water depth at the Romanian coast – from 1.5-2 m in the northern part of the coast (Mamaia, Constanta), to 150 m offshore and from 2 m in the southern coast area (Mangalia) to 50 m offshore. Current wave - shore interactions cause an erosion rate of 2.4 m per year in Mamaia and 1.5 m per year in Mangalia. Capitalization of wave energy by catching and converting them into energy could reduce this erosion.

Wave geometry is characterised by:

- λ - wavelength (m);
- h - wave height (m);
- T - wave period (s);
- L_i – shore width (m);
- H - static water level (m);

Sh – Strouhal number

c – wave velocity / celerity (m/s)

The erosion rate is linked with Strouhal's number - representing the ratio between the height of a wave and the wavelength. This Strouhal's number – specified to the Black Sea is between 0.2÷0.05.

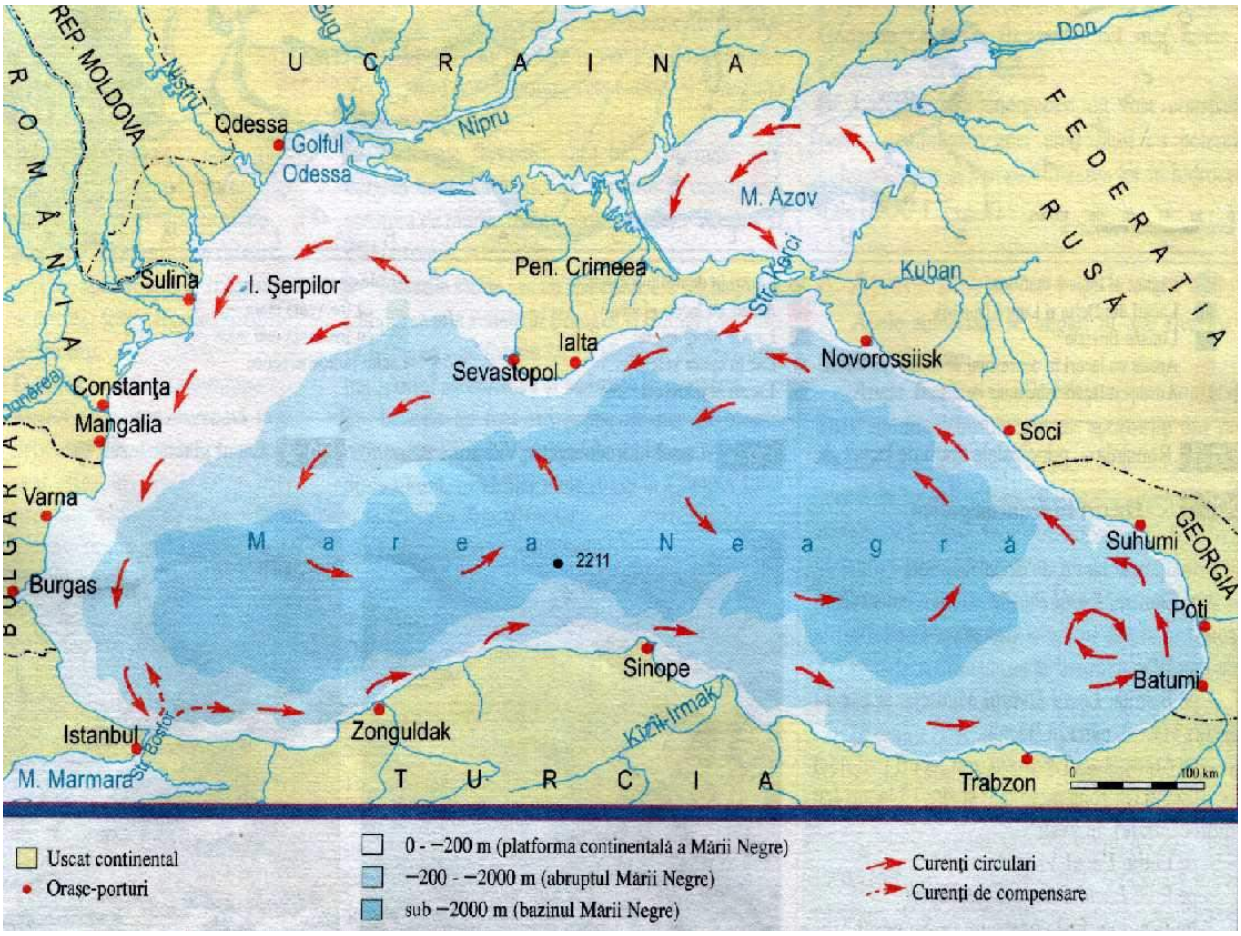

Fig. 1. Black Sea marine currents

Waves' features are important to analyse their hydropower potential, as it is presented in the following paragraphs.

2. Waves features near the Romanian coastline of the Black Sea

Several Research Institutes in Romania (National Institute of Meteorology and Hydrology, Aquaproiect, The Research and Power Engineering Institute etc.) have conducted measurements to determine wave characteristics on the Black Sea Coast (heights, wavelengths, displacement period and velocity, celerity) in Constanta, Mamaia, Sulina. Some results of their measurements are presented in the graphs below. In this paper, fig. 2 (a), (b) and fig. 3 show the wave height, taking into account the wavelength $h(\lambda)$. In fig. 4, it can identify the time period $T(\lambda)$, while fig. 5 shows the wave celerity $c(\lambda)$ for the three deeps of 10 m, 20 m and 30 m. The graphs were drafted for the Constanta shore. In Sulina, the wave periods and the wavelengths were lower [4], compared to the ones recorded in Constanta.

As you can see in fig. 1, the highest waves were measured on the N, NE and NW directions, in correlation with the directions of sea currents.

In table 1 one can see the heights recorded on each month of the year and on the main directions. In fig. 2.a) and b) also can be seen the variation of wave heights on each month of the year and the polynomial integration of these values.

TABLE 1: Wave height (m) for principal directions

Month	N	NE	E	SE	S	SW	W	NW
1	2.47	2.24	1.19	1.94	1.95	1.68	1.72	2.61
2	3.42	2.67	0.55	2.26	2.33	0.98	1.39	3.07
3	2.86	1.61	0.68	1.23	1.23	1.4	1	1.52
4	1.25	2.23	0.92	1.67	1.72	1.33	1.41	1.8
5	1.81	1.07	0.92	0.7	1.31	0.61	0.85	1.07
6	1.33	1.06	1.52	1.16	1.43	0.94	0.85	1.28
7	1.29	1.84	1.03	1.95	1.23	1.22	1.54	1.16
8	1.51	1.23	0.88	1.67	1.54	1.73	1.13	1.48
9	1.66	2.95	1.96	0.84	1.9	0.88	1.93	1.33
10	2.09	2.54	2.09	1.37	2.16	1.6	1.92	2.42
11	2.78	3.03	1.7	1.31	1.3	1.55	1.39	1.98
12	3.3	3.1	2.06	1.63	2.52	1.71	1.17	1.63

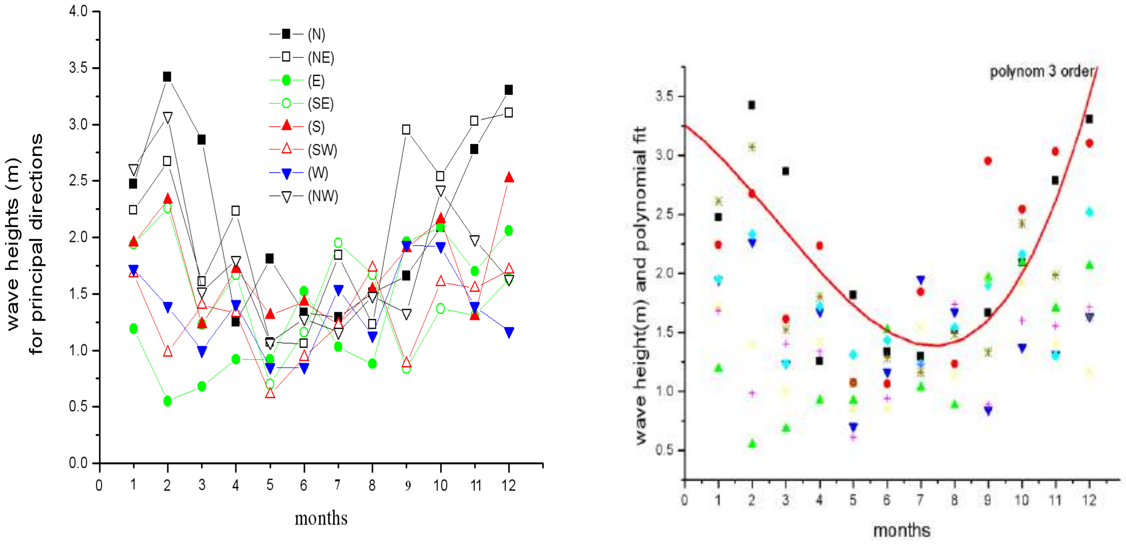

a) b)

Fig. 2. Wave heights recorded on each month of the year and on the main directions (a); polynomial integration (b)

Thus it can be seen that the average height of waves near the Romanian coastline of the Black Sea is 2.5-3 m in cold seasons and 1.5-2 m in warm seasons.

TABLE 2: Waves height, waves length, period and celerity at the water surface for three deeps of 10m, 20m and 30m

h(m)	λ10(m)	λ20(m)	λ30(m)	T(s)	c10(m/s)	c20(m/s)	c30(m/s)
0.5	14.04	14.05	14.05	3	4.68	4.68	4.68
1	24.69	24.97	24.98	4	6.17	6.24	6.24
2	45.24	50.12	50.67	5.7	7.93	8.79	8.88
3	65.55	79.08	83.71	7.4	8.85	10.68	11.31
4	81.23	101.16	110.92	8.7	9.33	11.62	12.74
5	99.49	126.12	142.13	10.2	9.75	12.36	13.93
6	113.76	144.43	164.71	11.3	10.06	12.78	14.57
7	130.84	165.94	190.97	12.6	10.38	13.17	15.15
8	147.39	185.99	215.03	13.8	10.68	13.47	15.58
9	164.53	206.25	239	15	10.96	13.75	15.93
10	182.27	226.78	262.97	16.2	11.06	14	16.23

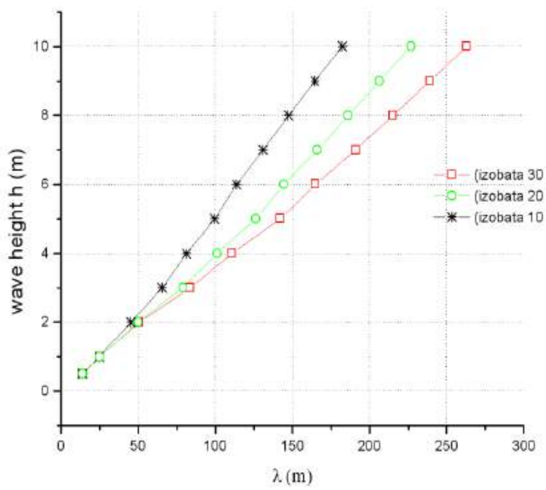

Fig. 3. Wave height depending on the wavelength

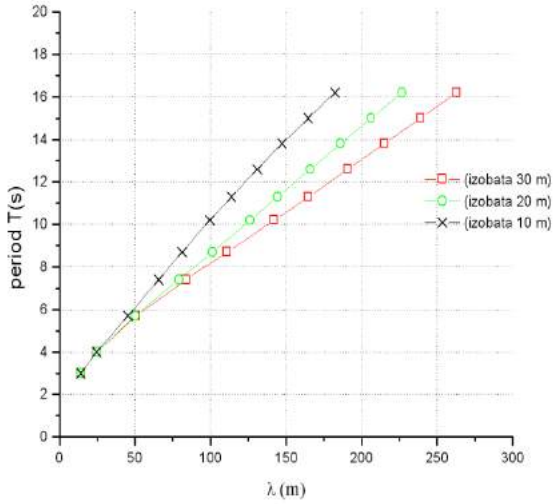

Fig. 4. Wave period depending on the wavelength

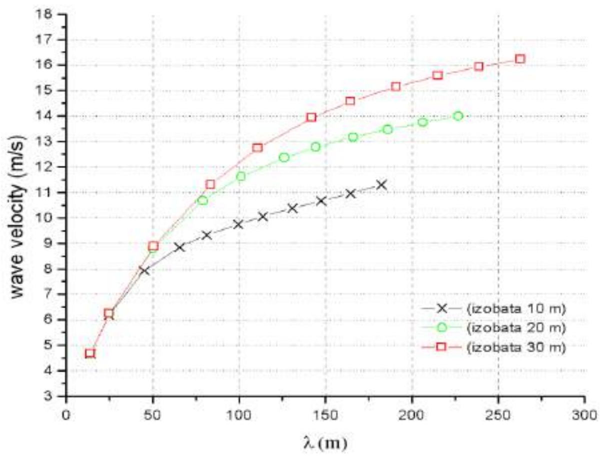

Fig. 5. Wave velocity depending on the wavelength

3. Wave's hydropower potential

Studies regarding the capitalization of hydropower potential of the waves near Romanian Black Sea shore ware made also by other authors [5-9].
Wave celerity is in relationship with the wavelength like in relation (1). Strouhal's number represents the ratio between the height of a wave and the wavelength, like in relation (2).
To capitalize the waves potential near the Romanian coastline of the Black Sea are used relations (3) and (4), assuming the efficiency of the system of 30% [5-6].

$$c = \frac{\lambda}{T} \tag{1}$$

$$Sh = \frac{h}{\lambda} \tag{2}$$

$$P_w = \frac{\gamma h^2}{8}\frac{\lambda}{T}L_i \quad (W) \tag{3}$$

$$P_c = \eta \cdot P_w \tag{4}$$

It can be seen in Table 3 and also in Fig. 6 the power that could be extracted from the wave energy by the systems fitted to each of the three deeps.

TABLE 3: Power of waves and power cached from waves according to the wavelength of the three deeps

h (m)	λ10 (μ)	λ200 (μ)	λ300 (μ)	T (s)	Pw 10 (kW)	Pc 10 (kW)	Pw 20 (kW)	Pc 20 (kW)	Pw 30 (kW)	Pc 30 (kW)
0.5	14.04	14.05	14.05	3	1.43	0.43	1.44	0.43	1.44	0.43
1	24.69	24.97	24.98	4	7.57	2.27	7.65	2.30	7.66	2.30
2	45.24	50.12	50.67	5.7	38.93	11.68	43.13	12.94	43.60	13.08
3	65.55	79.08	83.71	7.4	97.76	29.33	117.94	35.38	124.84	37.45
4	81.23	101.16	110.92	8.7	183.19	54.96	228.13	68.44	250.14	75.04
5	99.49	126.12	142.13	10.2	299.02	89.71	379.06	113.72	427.17	128.15
6	113.76	144.43	164.71	11.3	444.42	133.33	564.24	169.27	643.46	193.04
7	130.84	165.94	190.97	12.6	623.94	187.18	791.33	237.40	910.69	273.21
8	147.39	185.99	215.03	13.8	838.20	251.46	1057.72	317.32	1222.87	366.86
9	164.53	206.25	239	15	1089.48	326.84	1365.74	409.72	1582.60	474.78
10	182.27	226.78	262.97	16.2	1379.68	413.90	1716.60	514.98	1990.54	597.16

For example, catching the wave energy with hydro-pneumatic modules based on air piston, in hypothesis of wave height h = 1 m, with a wavelength of λ = 50 m and a wave period T = 6 s, we can obtain a raw power of 51 kW and a collection power of 15 kW, in the event of a η = 30 % collection efficiency rate, per each five meters of installation width L_i = 5 m [5-8].

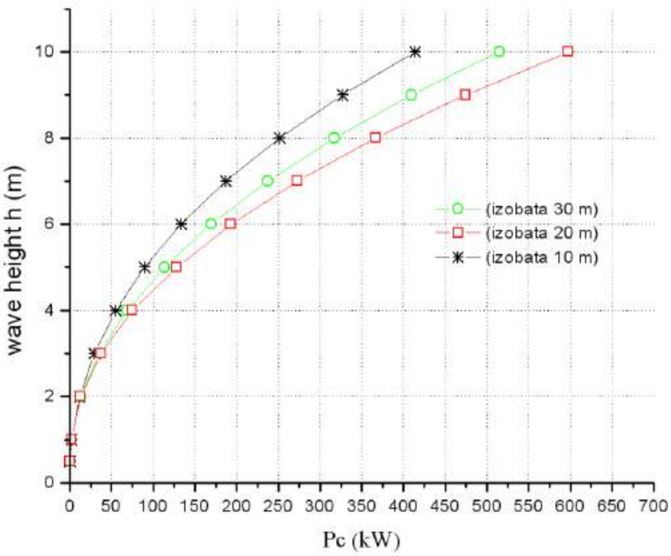

Fig. 6. Estimation of cached Power from wave's energy with hydro-pneumatic modules

For waves of about 2 m, as shown in Fig. 6 can be obtained 58-65 KW in any of the three mounting options. As waves are higher, the power is higher. For h = 8 m, can be obtained 250-370 kW. The plant mounted at 30 m deep provides more power.

4. Conclusions

This paper presents waves features near the Romanian coastline of the Black Sea, based on a large set of data from National Institute of Meteorology and Hydrology and Aquaproiect.
The average height of waves near the Romanian coastline of the Black Sea is 2.5-3 m in cold seasons and 1.5-2 m in warm seasons. Wave's velocity, wavelengths and periods depend on deeps. Strouhal's number – specified to the Black Sea is between 0.2÷0.05.
For waves with average height of about 2 m, it is estimated that can be obtained 58-65 KW for each 5 meter of wave's catching plant, in any of the three mounting options. As waves are higher, the power is higher. The plant mounted at 30 m deep provides more power. Catching the wave energy near coastline is useful also to reduce Romanian shoreline erosion.

References

[1] V.V. Efimov, M.V Shokurov, s.o, "Numerical simulation of a Quasi_Tropical Cyclone over the Black Sea", Izv Atmos Ocean Phy+, vol 43, 2007, pp. 723-743;
[2] V. Maslova, s.o,, "Variability of the Cyclone activity in the Mediterranean-Black sea region", Journal of Environmental Protection and Ecology, vol. 11, 2010, pp.1366-1372;
[3] *** Marine litter in the Black Sea Region, 2009, http://www.blacksea-commission.org/_publ-ML-CH1.asp;
[4] I. Constantin, "Combaterea eroziunii marine, (Tackling marine erosion)", Ed. Tehnica, Bucharest, ISBN 973-0-03924-0, 2005, pp.185-201;
[5] Gh. Olaru, "Captarea si conversia energiei valurilor, (Collecting and converting wave energy)", Ed. Printech, Bucharest, 2010, pp. 45-50;
[6] I. Constantin, "Utilizarea energiei valurilor, (Using wave energy)", Editura Tehnică, Bucharest, 1990, pp. 70-75;
[7] I. Constantin, P.D. Lazăr, "Energia valurilor – captare şi conversie, (Wave energy – collection and conversion)", Ed. Ştiinţifică şi Enciclopedică, Bucharest, 1982;
[8] S. Budea, M.D.Cazacu, "Metoda si instalatie de captare eficienta a energiei cinetice a valurilor calatoare, (Method and plant for effective collecting of horizontal kinetic energy of travelling waves)", *Patent* Number(s): RO128403-A2, Bucharest 2011, [Web of Science ®];
[9] V. Panaitescu, M. Panaitescu, S. Budea, "Optimization of Waves Flow On Slopes in view of the Problematic Hydroelectric Energy Conversion", IJARSE, vol 4 (1), Sept. 2015, pp. 433-443.

A Geometrical Model of Piston-Liner System

Sunny NARAYAN[1], Aman GUPTA[2]

[1] Indus University, India, sn2008@rediffmail.com

[2] Indus University, India

Abstract: *A numerical model for the skirt is studied to consider the effects of the connecting rod inertia on the piston skirt–liner system lubrication. The piston motion, the oil film lubrication model and the friction losses of the system have been studied and compared. The results on a dual cylinder diesel engine show that inertia of connecting rod also affects system lubrication as well as the piston motion, especially at higher speeds.*

Keywords: *Piston secondary motion, liner system*

Nomenclature

BTDC-Before Top Dead Center
F_t-Side Thrust Force
T.S.-Thrust Side
A.T.S.-Anti Thrust Side
F_h-Hydo dynamic oil force
T_G-Gas Torque
T_f-Frictional torque around pin
F_{icr}-Connecting rod inertial force
h-Oil film thickness
η-Oil Viscosity
Fs-Side thrust force
m_R-Mass of connecting rod
m_p-Mass of pin
m_{piston} -Mass of piston
u-Piston Velocity

1. Introduction

Piston Skirt –liner system contributes a major amount in combustion engines [1]. Simulation of lubrication between skirt and liner is needed from tribological system of engine. Li et al was first to consider plot of piston motion versus crank angle [5].Skirt surface roughness effects were later considered by Wong et al[6].Later piston design parameters were considered [7]. Inertial forces were never considered which can never be neglected typically at high speeds. In present work these effects have been considered for lubrication mode.

2. Numerical model

Motion of piston may be expressed as:

$$\begin{bmatrix} m_{pin}\left(1-\frac{b}{L}\right)+m_{pis}\left(1-\frac{a}{L}\right) & m_{pin}\left(\frac{b}{L}\right)+m_{pis}\left(1-\frac{a}{L}\right) \\ m_{pis}\left(1-\frac{a}{L}\right)(b-a)+\left(\frac{J_{pis}}{L}\right) & m_{pis}\left(\frac{a}{L}\right)(b-a)-\left(\frac{J_{pis}}{L}\right) \end{bmatrix}\begin{bmatrix} e''_t \\ e''_b \end{bmatrix}$$
$$=\begin{bmatrix} F_S+F_{SK}\,Tan\,\phi+S \\ M_S+M_{fSK}+M \end{bmatrix} \tag{1}$$

Various forces and moments can be expressed in form:

$$Fs = (F_g+m_pg+Y_p''m_p)Tan\phi \tag{2}$$

$$Ms = (F_g Cg - m_{piston}\, g\, Cp - Y_p'' m_p) \quad (3)$$

Taking into account inertial forces the new system of equations can be written as:

$$F_{ic} + F_{BX} + S + F_{ip} \;\; = \;\; 0 \quad (4)$$

$$F_g Cg + M_{pis} + M + M_{fSK} + (F_{ic}^{-} - m_p g)Cg + F_{ic}(C_B - C_A) = 0 \quad (5)$$

Where

$$F_{ic} = -m_{\,pis} \left(e_t^{\,''} - \left(\frac{a}{L}\right)\left(e_t^{\,''} - e_b^{\,''}\right) \right) \quad (6)$$

$$F_{ip} = -m_{\,pis} \left(e_t^{\,''} - \left(\frac{a}{L}\right)\left(e_t^{\,''} - e_b^{\,''}\right) \right) \quad (7)$$

$$F_{ic}^{-} = -m_{\,pis}\, Y_p'' \quad (8)$$

$$F_{ip}^{-} = -m_{\,pin}\, Y_p'' \quad (9)$$

For connecting rod various forces may be expressed as:

$$F_{BX} = (F_{BY} + j\, Y_p''\, m_R + jgm_R)tg\phi - j\, X_p''\, m_R - \frac{\phi'' I_R}{L\cos\phi} \quad (10)$$

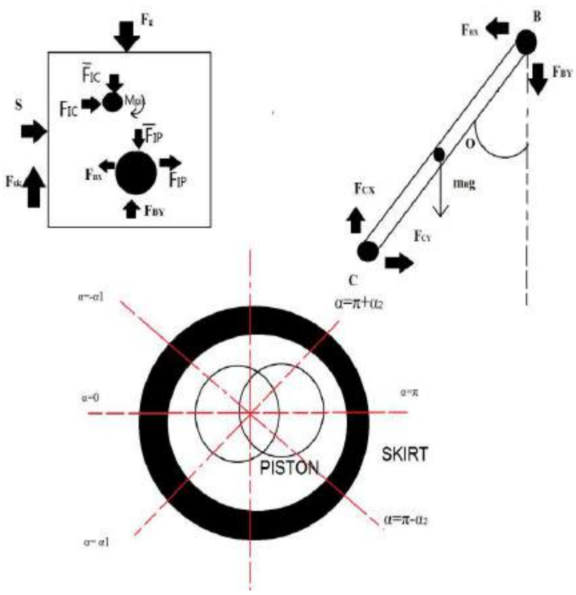

Fig. 1. Force equilibrium

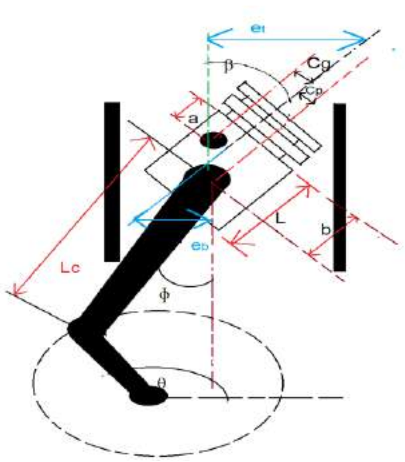

Fig. 2. Piston Motion

Hence piston dynamics equations can be written as:

$$\begin{bmatrix} m_{pin}\left(1-\frac{b}{L}\right)+m_{pis}\left(1-\frac{a}{L}\right)+j^2m_R\left(1-\frac{b}{L}\right) & m_{pin}\left(\frac{b}{L}\right)+m_{pis}\left(\frac{a}{L}\right)+j^2m_R\left(\frac{b}{L}\right) \\ m_{pis}\left(1-\frac{a}{L}\right)(b-a)+\left(\frac{J_{pis}}{L}\right) & m_{pis}\left(\frac{a}{L}\right)(b-a)-\left(\frac{J_{pis}}{L}\right) \end{bmatrix}\begin{bmatrix}(e_t^{\prime\prime} \\ (e_b^{\prime\prime}\end{bmatrix}$$

$$=\begin{bmatrix} F'_S+F_{SK}\,Tan\,\phi+S \\ M_S+M_{fSK}+M \end{bmatrix} \quad (11)$$

$$F'_s=(F_g+m_pg+Y_p''m_p+jm_RY_R''+jgm_R)Tan\phi-\frac{\phi''I_R}{Lcos\phi}-J\text{Sin}\theta\Theta''^2r(1-j)m_R \quad (12)$$

Connecting rod inertial force may be written as:

$$F_{icr}=(jm_RY_R''+jgm_R)Tan\phi-\frac{\phi''I_R}{Lcos\phi}-J\text{Sin}\theta\Theta''^2r(1-j)m_R \quad (13)$$

3. Hydro dynamic lubrication

Reynolds equation can be used to calculate the lubrication oil pressure between skirt and liner as:

$$\frac{\delta}{\delta x}\left(\frac{\rho h^3\phi_x}{12\eta}\frac{\delta P}{\delta x}\right)+\frac{\delta}{\delta y}\left(\frac{\rho h^3\phi_y}{12\eta}\frac{\delta P}{\delta y}\right)=\rho\frac{\delta h}{\delta t}\phi_c-\frac{u}{2}\left(\frac{\delta h}{\delta y}\phi_c\rho+\sigma\frac{\delta(\rho\phi_s)}{\delta y}\right) \quad (14)$$

The average shear stress on skirt can be expressed in terms of shear stress factors ϕ_f, ϕ_{fs} as :

$$\tau=-\eta\frac{u}{h}(\phi_f+\phi_{fs})-\phi_{fP}\frac{\delta P}{\delta y}\frac{h}{2} \quad (15)$$

Various forces and moments can be expressed as

$$S=R\iint[(p+pc)cos\alpha d\alpha dy] \quad (16)$$

$$M=R\iint[(p+pc)cos\alpha d\alpha dy(y-b)] \quad (17)$$

$$F_{SK}=R\iint[\tau d\alpha dy] \quad (18)$$

$$M_{fSK}=R\iint[\tau d\alpha dy(Rcos\alpha-Cp)] \quad (19)$$

4. Results and discussions

Piston motion equations are stiff and non linear differential equations which were solved using time step Runger Kutta method using various engine parameters used are listed in table no 1.

TABLE 1: Engine Parameters

Parameter	Value
a	31.3250 mm
b	36.9mm
C	0.05mm
Cg	0mm
Cp	0mm
J_{piston}	6.6200X 10^{-07} Kg-m^2
R	30.3mm
I_{rod}	7.8540X10^{-09}Kg-m^2
r	34mm

TABLE 1: Engine Parameters *(continued)*

Parameter	Value
j	0.12
L	62.65mm
m_R	200 g
m_{pin}	81g
m_{piston}	363 g
η	0.03 Pa-S
L_c	121mm

Figure no 3 shows plots of side thrust forces. Values of side thrust forces increases while taking into consideration connecting rod inertia. Figure no 3 shows the plots of lubrication oil pressure with as well as without taking into consideration connecting rod inertia. Both plots show same trend, however peak value of pressure taking into account inertia force (Figure 3,b) is lesser than normal oil pressure (Figure 3,a).

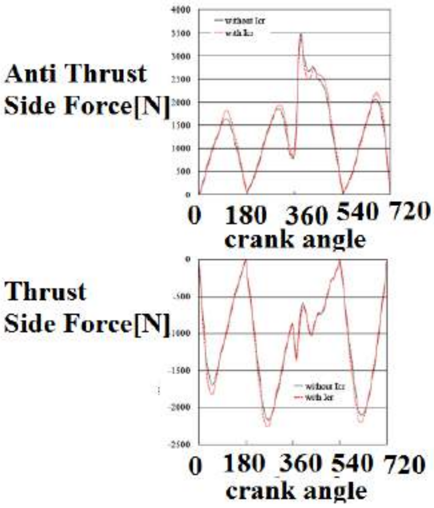

Fig. 3. Schematic representation of side force [24]

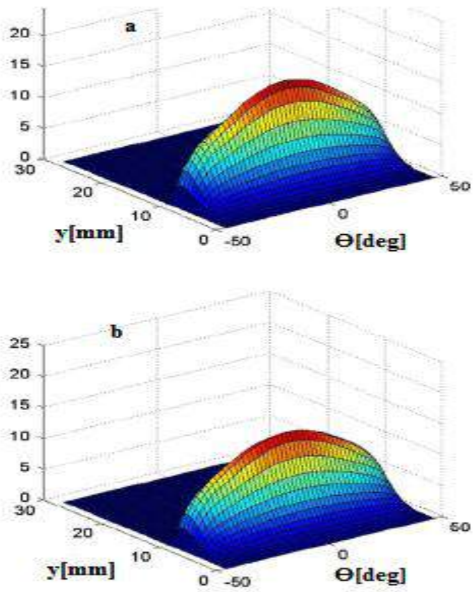

Fig. 4. Oil pressure distribution [24]

Figure no 4 shows top eccentricity of piston (e_t) calculated by solving piston dynamics equations considering various forces and moments. It can be seen that piston displacement increases while taking into connecting rod inertial forces after TDC position. Figure no 8 shows plots of oil film thickness as a function of crank angle. It can be seen that oil film thickness is thick enough and engine runs at full film lubrication. Oil film thickness is greater while taking into account connecting rod inertial force.

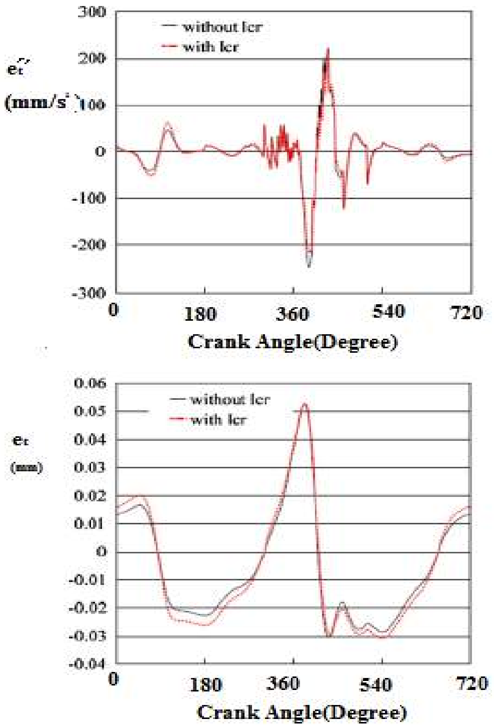

Fig. 5. Piston motion [24]

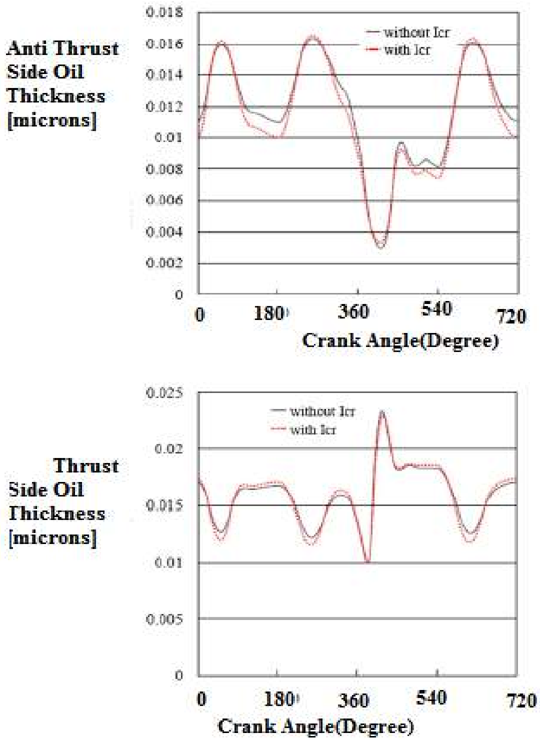

Fig. 6. Oil film thickness [24]

5. Conclusions

This work considers the effects of connecting rod inertial force on various parameters of piston-liner model. This force increases with speed. Side thrust forces as well as piston secondary motion increases while taking into account inertial forces.

References

[1] S.C. Tung, M.L. McMillan, “Automotive tribology overview of current advances and challenges for the future”, In: Tribology International, 2004; 37:517–35;
[2] D.F. Li, S.M. Rhode, H.A. Ezzat, “An automotive piston lubrication model”, ASLE Transactions 1983;26(2):151–60;
[3] V.W. Wong, T. Tian, H. Lang, J.P. Ryan, Y. Sekiya, Y. Kobayashi, *et al.*, “A numerical model of piston secondary motion and piston slap in partially flooded elasto hydrodynamic skirt lubrication”, SAE paper no. 940696, 1994;
[4] S. Jiang, J. Cho, “Effects of skirt profiles on the piston secondary movements by the lubrication behaviors”, In: International Journal of Automotive Technology 2004;5(1):23–31;
[5] A. Gupta, S. Narayan, "Electrical Analogy of Liquid Piston Stirling Engines", In: Hidraulica no. 2 (2016): 58;
[6] S. Narayan, V. Gupta, "Overview of working of Striling engines", In: Journal of Engineering Studies and Research, 21.4 (2015): 45;
[7] A. Gupta, S. Narayan, "A Review of Heat Engines", In: Hidraulica no. 1 (2016): 67;
[8] S. Narayan, "Analysis of noise emitted from diesel engines", In: Journal of Physics: Conference Series. Vol. 662. no. 1. IOP Publishing, 2015;
[9] A. Gupta, S. Narayan. "Effects of turbo charging of spark ignition engines", In: Hidraulica no. 4 (2015): 62;
[10] S. Narayan, "Designing of liquid piston fluidyne engines", In: Hidraulica no. 2 (2015): 18;
[11] S. Narayan, “Effects of Various Parameters on Piston Secondary Motion”, No. 2015-01-0079. SAE Technical Paper, 2015;
[12] S. Narayan, "Analysis of Noise Radiated from Common Rail Diesel Engine", In: Tehnički glasnik, 8.3 (2014): 210-213;
[13] S. Narayan, "Time-frequency analysis of Diesel engine noise", In: Acta Technica Corviniensis-Bulletin of Engineering, 7.3 (2014): 133.
[14] S. Narayan, "Wavelet Analysis of Diesel Engine Noise", In: Journal of Engineering and Applied Sciences, 8.8 (2013): 255-259;
[15] S. Narayan, V. Gupta. "Motion analysis of liquid piston engines", In: Journal of Engineering Studies and Research, 21.2 (2015): 71;
[16] S. Narayan, “Modeling of Noise Radiated from Engines”, No. 2015-01-0107. SAE Technical Paper, 2015;
[17] S. Narayan, A. Gupta, R. Rana, "Performance analysis of liquid piston fluidyne systems", In: Mechanical Testing and Diagnosis, 5.2 (2015): 12;
[18] V. Gupta, S. Sharma, S. Narayan, "Review of working of Stirling engines", In: Acta Technica Corviniensis-Bulletin of Engineering, 9.1 (2016): 55;
[19] A. Singh, S. Bharadwaj, S. Narayan, "Review of how aero engines work", In: Tehnički glasnik, 9.4 (2015): 381-387;
[20] S. Narayan, "A review of diesel engine acoustics", In: FME Transactions, 42.2 (2014): 150-154;
[21] S. Narayan, "Noise Optimization in Diesel Engines", In: Journal of Engineering Science and Technology Review, 7.1 (2014): 37-40;
[22] V. Gupta, S. Sharma, S. Narayan. "Review of working of Stirling engines", In: Acta Technica Corviniensis-Bulletin of Engineering, 9.1 (2016): 55;
[23] A. Singh, S. Bharadwaj, S. Narayan, "Prikaz rada motora zrakoplova", In: Tehnički glasnik, 9.4 (2015): 381-387;
[24] X. Meng, Y. Xie, "A new numerical analysis for piston skirt–liner system lubrication considering the effects of connecting rod inertia", In: Tribology International, 47 (2012): 235-243.

ISSN 1453 – 7303 "HIDRAULICA" (No. 3/2016)
Magazine *of Hydraulics, Pneumatics, Tribology, Ecology, Sensorics, Mechatronics*

Temperature Analysis in Bucharest (2009-2015)

Marin RUSĂNESCU[1], Carmen Otilia RUSĂNESCU[2]

[1] Valplast Industry Bucharest

[2] Polytechnic University of Bucharest, Faculty of Biotechnical Engineering

Abstract: *In this paper we have analyzed seasonal mean temperatures, semi-annual, annual number of days that exceed certain thresholds, thermal hourly average temperatures, temperature extremes absolute in Bucharest in the winter season; period under review is 2009-2015.*

Keywords: *Seasonal mean temperatures, schedules, absolute extreme, semestrials*

1. Introduction

Temperature variations influence the dispersion and transport of pollutants and have health effects. Temperature decreases with altitude, when a layer of cold air is absorbed in a layer of warm air, there is a thermal inversion, and the pollutants accumulate on the surface of the earth. Once this happens and ozone depletion. This layer serves to filter out ultraviolet radiation. When ultraviolet radiation are not stopped occurs greenhouse effect, increases the average temperature of the planet. Thermal inversion layer acts as a cap preventing the dispersion and transport of pollutants.
Characteristics of general circulation of the atmosphere, manifested through intensification or permanent reductions of atmospheric circulation over Bucharest together with changes in the direction of being transported air masses with physical properties different, plus the fluctuations of solar radiation in a year or from one year to another, leading to irregular variations of air temperature, observable both in the monthly averages and at the annual media (Sterie Ciulache, 1997).
General circulation of the atmosphere prints a dynamic climate; it is often characterized by temperate oceanic air masses with frequencies especially during summer synoptic and two synoptic transition periods. Azores anticyclone Ridge at the transition between autumn and winter brings moisture, precipitation and moderate temperatures in summer cooler air drives that determine rainfall.
Tropical maritime air masses are involved in hot and humid tropical-maritime movements from the south-west and south. They are moving to the Balkans bringing rainfall in the first half of the year and cold sudden and massive warming. And summer rainfall causes changeable weather.
Tropical continental air masses are common in summer; they are due to movements from the south and southeast. These hot, dry air masses cause high heating.
In this paper, the data are processed monthly, Seasonal, half yearly air temperature at the weather station at the Biotechnical Faculty of Engineering, Polytechnic University of Bucharest the range 2009-2015. Bucharest appears as an urban heat island due fuels burned in the city, because of the heating surfaces of asphalt, bricks, due to the number of inhabitants (Gugiuman and Contrău, 1975). Comprising mostly horizontal section and vertical assumes the shape of a bell urban (phenomenon horn) climbing in altitude up to several times the height of the assembly building (Iojă, 2009). Urban heat island presents seasonal and diurnal variations in temperature and ratio values of the area affected (Iojă, 2009). In Bucharest with the expansion of built areas (especially in the north of the city) at the expense of green areas (potential consumer of thermal energy through processes of evapotranspiration), witnessing an increase in thermal values to the suburbs. This contributes to the fact that in the last 20 years has increased the volume of traffic (the explosion fleet); heat island effects are higher where the green has the lowest percentage. The air temperature may be important for some chemical reactions that cause pollutants to be transformed into other sometimes much more dangerous than those from which they originated. If Bucharest concentrations of ozone exceed since March and April, thanks to the intensification of solar radiation under the influence that certain pollutants (especially nitrogen oxides resulting from

activities in industry traffic) reacts with atmospheric oxygen causing photochemical reactions, from which the ozone.

2. Results and discussion

Average temperatures in the winter season have been analyzed.

Bucharest is located in a temperate continental climate; the four seasons are underway normal. Atmospheric temperature was monitored weather station: AWS / EV from the Biotechnical Faculty of Engineering measurement range from -30 ^{0}C to + 60 ^{0}C.
We analyzed term average temperatures in Bucharest being analyzed period 2009-2015 (data processed based on data from the weather station of the Biotechnical Faculty of Engineering, Polytechnic University of Bucharest. We analyzed the evolution of the multi-annual average temperatures of winter. It is noted that the trend of development is increasing, except for 2012, which has a tendency of decreasing trend (Figure 1).
Average yearly temperature in winter season is calculated from the monthly averages between December and February.
We analyzed the average temperatures of the winter months: December - the current year and January, February next year. These temperatures were statistically analyzed individually, each string separately, then string sets of values we calculated average temperature of winters. The string average temperatures of winters we performed statistical processing as (Figures 1, 2, 3, 4). For every season we calculated the annual average, standard deviation, range. We calculated the difference between the highest and the lowest value of average temperatures string Seasonal called amplitude (Figure 5).
Averages multi positive average temperature of winter were obtained in Bucharest in years: 2011 (0.5 ^{0}C), 2013 (0.8 ^{0}C) 2014 (0.9 ^{0}C), 2015 (2.3 ^{0}C), the smallest term average were obtained years: 2009 (-0.2 ^{0}C), 2010 (-0.2 ^{0}C) 2012 (-2.1 ^{0}C). It is noted that the standard deviation does not exceed 1.6ºC, the lowest of which is 0.1 ºC. (Figure 4) The lowest temperature in winter was recorded in January 2009 being - 19.7 ^{0}C, and the highest temperature value in the winter season, was recorded in December 2012 was 19.4 ^{0}C. The amplitude ranges from 1.0 ^{0}C in 2014 and 2.8 ^{0}C in the winter season (Figure 5).
The warmest winter in 2015 (4.4 ^{0}C) followed by 2011 (3.9 ^{0}C). The lowest average winter temperature was recorded in 2012 (-5.3 ^{0}C), followed by 2009 with -2.8 ^{0}C, 2010 ^{0}C -2.7 (coldest winters in Bucharest in the period under review).
The thermal regime winters at all the analyzed period (2009-2015) had periods of increased temperature and lowering it. The trend is to increase the average temperature of winters, warmer winters so in Bucharest than in the 1994 2008. Given the wide variability of the thermal regime, we can expect, as before, on winters, severe or moderate.

Average temperatures in spring season

It is observed in Figure 1 Spring season considering that the lowest values of average temperature were obtained in Bucharest in years: 2011 (12.1 ^{0}C), 2013 and 2015 (12.3 ^{0}C). The highest average temperature values were obtained in spring season in Bucharest in years: 2012 (14 ^{0}C) followed by 2010 (13.3 ^{0}C), 2009 (13 ^{0}C).
Spring season peak in January 2009 was 35.4 ^{0}C, while the minimum was recorded in March 2012 being -5.2 ^{0} C (Figure 3). Analyzing square standard deviation values, it is noted that it has lower values than the winter season, which is between 0.5 ºC and 1.3 ºC (Figure 4).
By analyzing the amplitude values, it notes that are higher than in the winter season, with values between 7.5 ºC 14 ºC in 2013 and 2014. Looking at the variation and evolution trend of the average temperature of the spring season it is observed that the trend for this season is the temperature rise (Figure 5).

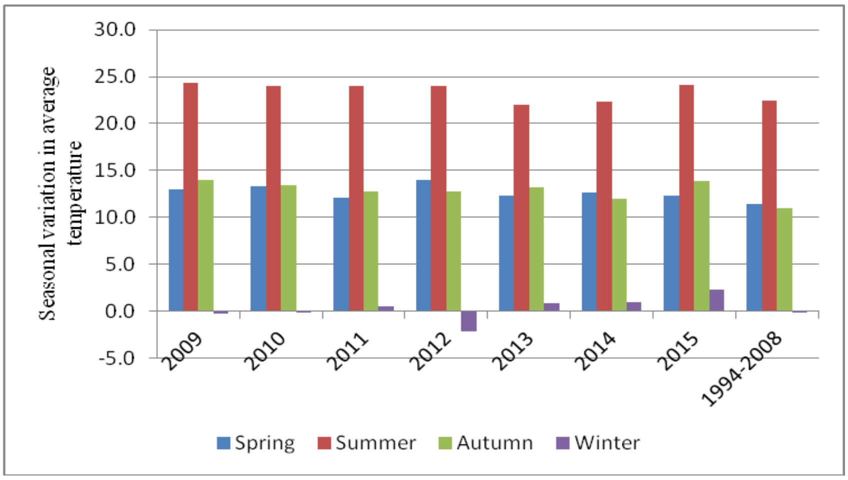

Fig. 1. Seasonal mean temperatures in Bucharest; analyzed period 2009-2015 compared to the period 1994-2008

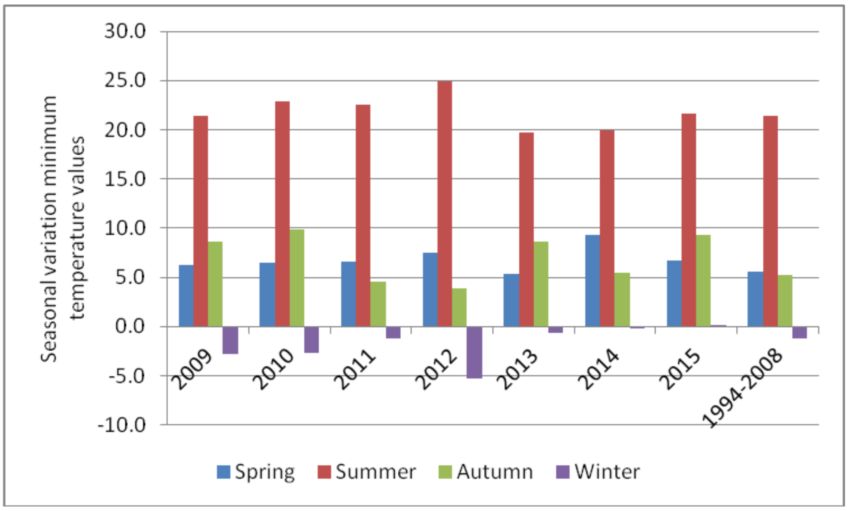

Fig. 2. Seasonal variation minimum temperatures in the range from 2009 to 2015 in Bucharest, compared to the period 1994-2008

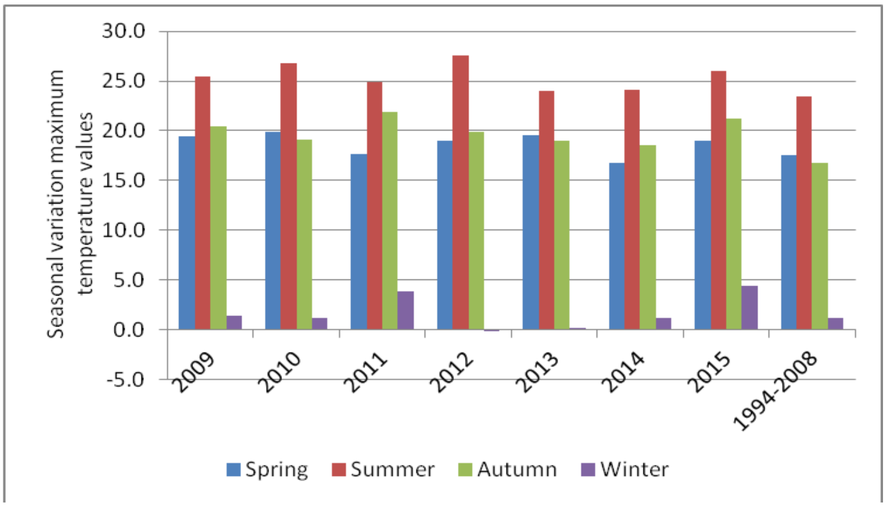

Fig. 3. Seasonal variation in maximum temperatures in Bucharest between 2009-2015 compared to the period 1994-2008

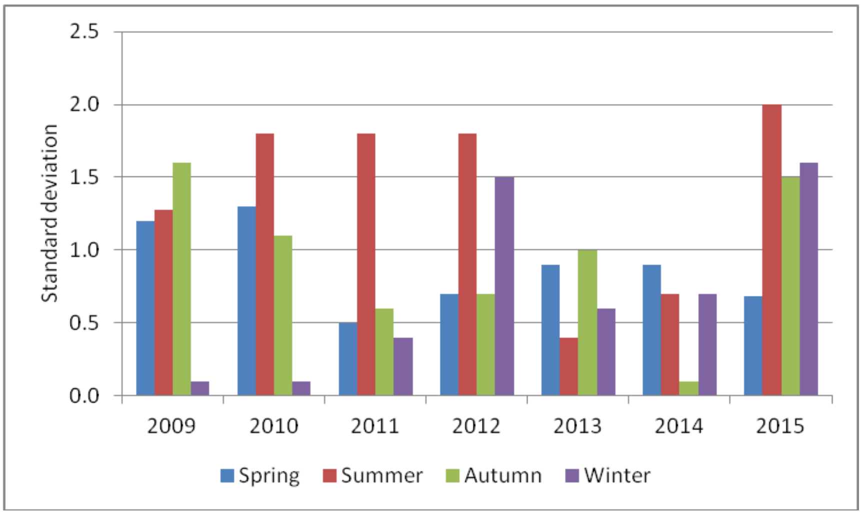

Fig. 4. Standard deviations from Bucharest temperatures between 2009-2015 compared to 1994-2008

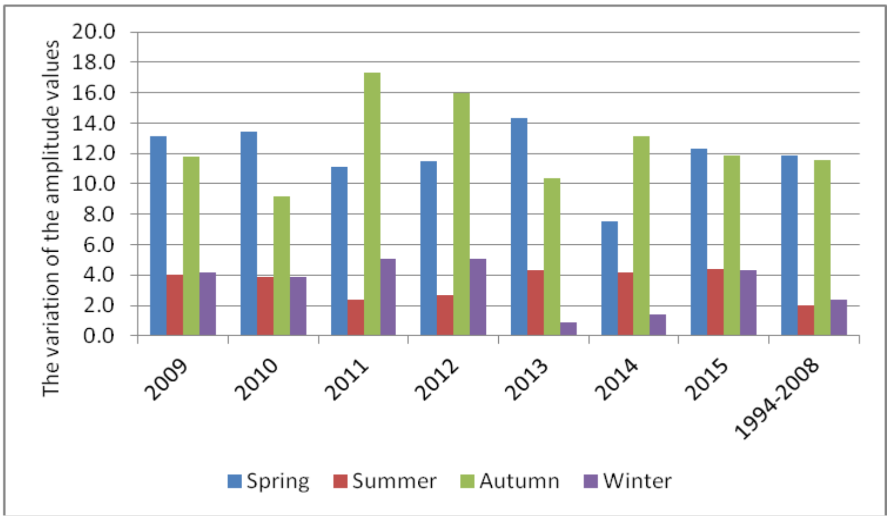

Fig. 5. Variations amplitudes in Bucharest between 2009-2015 compared to 1994-2008

Average temperatures in summer season

It is noted that the average annual values of summer temperatures are about two times higher than the spring season.

It is noted that the standard deviation is between 0.4 ^{0}C and 1.8 ^{0}C in summer season. The lowest values of average temperature of the summer season are observed in Bucharest in years: 2013 (21.9^{0}C) 2014 (22.4^{0}C). The highest values of average temperature of the summer season are observed in Bucharest in years: 2009 (24.3^{0}C), followed by years: 2010, 2011, and 2012 (24.^{0}C) (Rusănescu, 2016).

Warmest summer was in 2012 (27.6 ^{0}C) followed by 2010 (26.8^{0}C), 2015 (26^{0}C), 2009 (25.4^{0}C). These years were years of extremely hot under (Sandu, 2013).

The maximum recorded temperature in the range 2009-2015 summer seasons was in August of 41.5 ^{0}C, followed by July 2014, all of which is 40.9 ^{0}C, while the lowest temperature was 10.3 ^{0}C in June 2013 (Figure 3).

Evolution of the average temperature of the summer season is growing in the years 2012, 2010, 2015.

Average temperatures in the autumn season

Notice in figure 1 that averages multiannual average temperatures of winter season ranges from 11.9 ^{0}C in 2014 and 13.9 ^{0} C in 2015. The standard deviation is between 0.1-1.6ºC (Figure 4).

Annual mean air temperatures

The average annual temperature of the air has variable heat changes caused by the movement of air, hot or cold fronts. Above the plains, the average annual temperature is relatively evenly distributed. Average annual temperatures are influenced by local factors such as altitude, the layout of landforms, ridges orientation, inclination slopes, vegetation coverage, showing an uneven distribution.
In the first half cold temperature is regulated by the atmospheric circulation (air advection). Average yearly temperature semester cold, calculated from monthly averages over the interval from October to March has turned positive, reaching values between 3.3-5.7 °C. The average temperature hot semester calculated from the monthly averages between April and September is between 19.1 °C - 21.4 °C.
The variation in average temperatures, maximum and minimum year in Bucharest in 2009, 2010, 2011, 2012, 2013, 2014, 2015 - In the period under review there has been a slight increase in annual average air temperature compared to the annual average standard 1961 1990. During the year the average monthly air temperature records a maximum in July and a minimum in January and one in February.

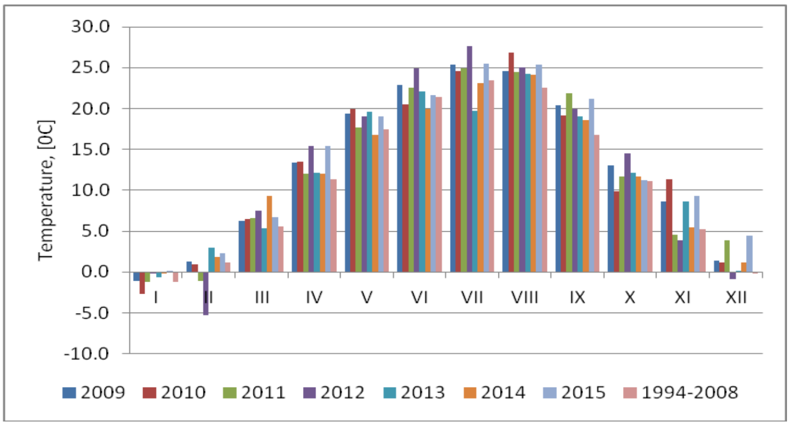

Fig. 6. Variation in average annual temperatures range from 2009 to 2015 in Bucharest, compared to the period 1994-2008

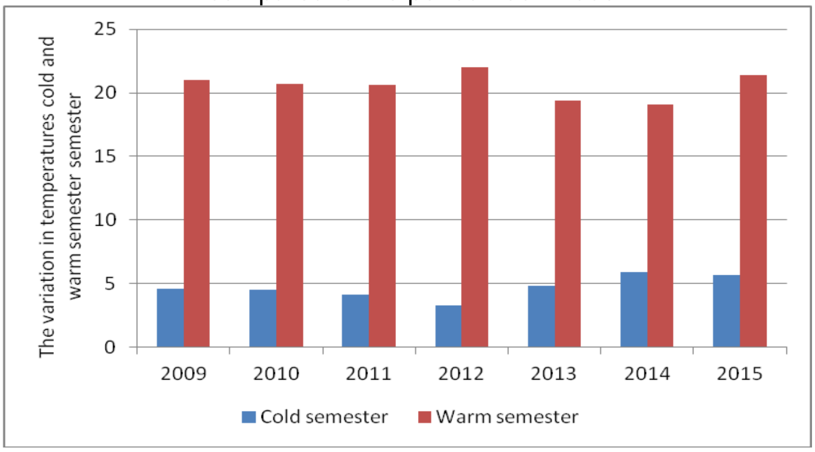

Fig. 7. Semester average temperatures in Bucharest, analyzed period 2009-2015

Average annual amplitude is an indicator that reflects the value of thermal contrast between the warmest month and coldest of the year and that express the degree of continentalism climate of a region. As obvious from Figure 5, the amplitude of the annual average air temperature in Bucharest increases in 2012 (32.9 ^{0}C), the lowest being in 2014 (23.3 ^{0}C).
The annual change resulting from the analysis of monthly air temperature averages denoted the continental climate, with a minimum in February (-5.3 °C), followed by a rise in values until August where heat peaks (26.8 °C) after lowering temperatures on a downward trend since January.

Temperatures average hourly

Hourly average air temperature values are influenced by the movement of air and surface characteristics of assets, against which produce heat and cool air in 24 hours.
In January, the lowest values of average temperature zones in Bucharest are after sunrise (8pm) reaching the maximum at around 15 when solar radiation intensity begins to decrease (Figures 8-11).
In July the temperatures drop hourly until around May, after growing highs at 14-17 when solar radiation intensity begins to decrease.
For any local temperature variation has a daily phenomenon called diurnal variation. After reaching a minimum around sunrise sunlight, temperature increases, reaching the maximum value from 14 and 17 of that afternoon, then it falls to sunrise the following day (Figure 3). Control of the diurnal cycle is provided by the sun. There appear sudden changes in weather deviations of daily variation in air temperature [6]. Studying the evolution of air temperature during the day we made the observations in the time range 1-24 in two days in different seasons. At noon (13 pm), air temperature throughout the year remains positive (Figure 3).

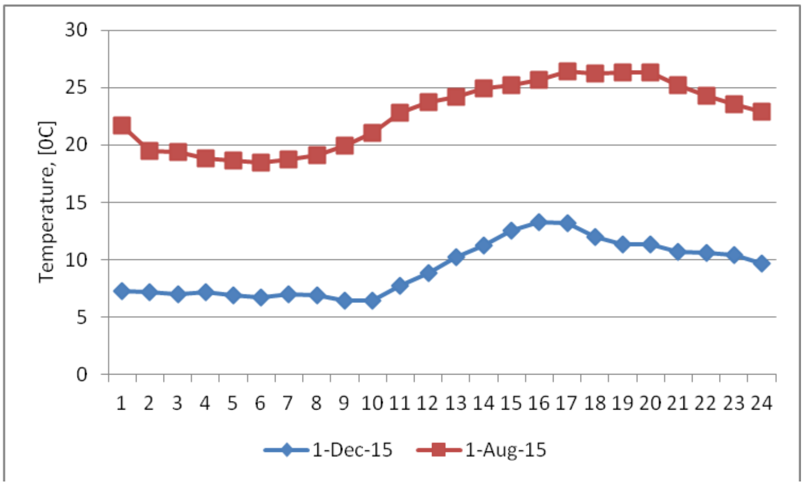

Fig. 8. Temperature variation days December 1, August 1, 2015
(a winter day, a summer day)

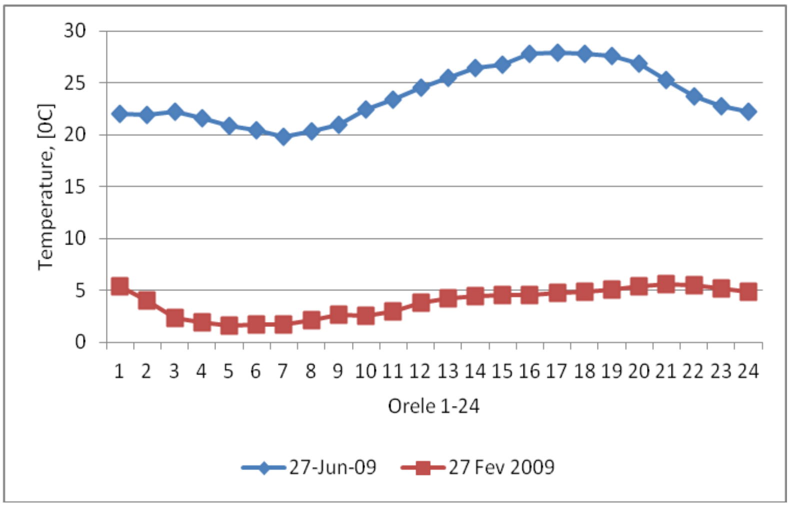

Fig. 9. Variation of temperature in the days June 27, February 27, 2009
(a summer day, a winter day)

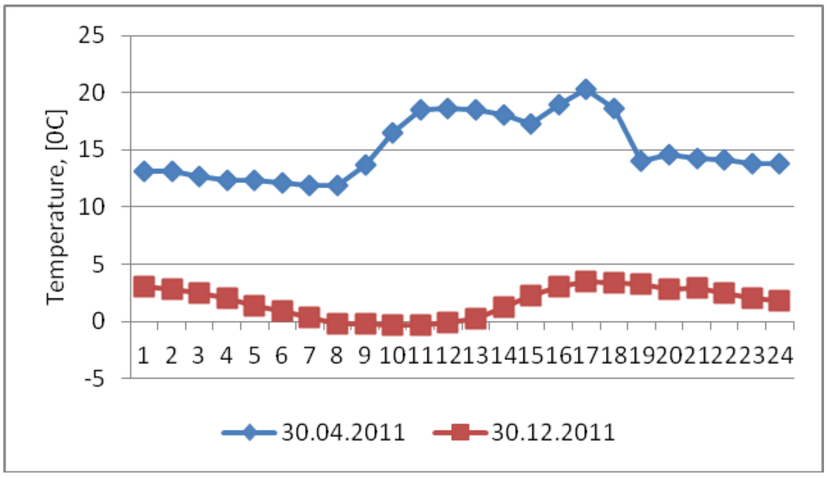

Fig. 10. Variation in temperature days 30.04.2011, 30.12.2011

If the soil is covered with vegetation, diurnal temperature variations amplitude changes in that rich vegetation decreases the amplitude of these variations.
Negative temperature values begin to appear during the night (1 am), at this time in December and the shift towards positive values occurs in March (Figure 11).

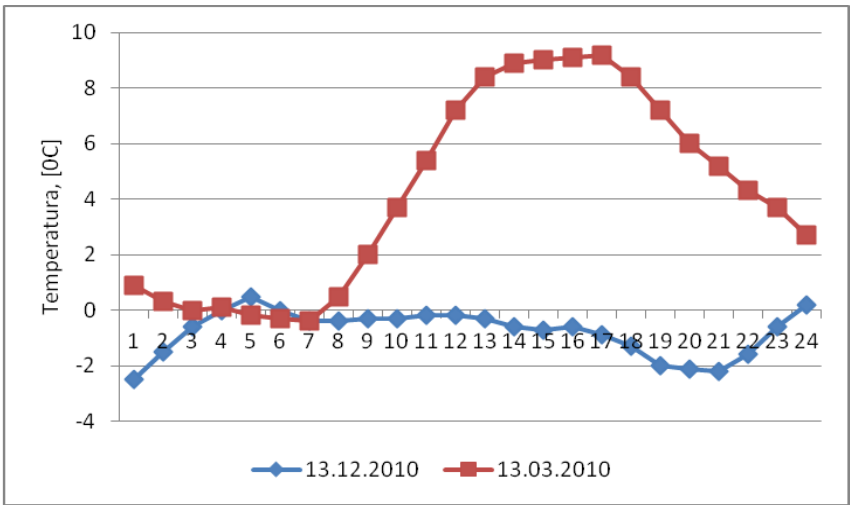

Fig. 11. Changes in air temperature on 13.12.2010 and 13.03.2010 in Bucharest

Negative temperature values begin to occur in the morning (hour 7) at this time, also in December, moving towards positive values occurs one month later in April;
In the evening (hour 19), negative values reappear temperature between December and February (Figure 10).

Absolute extreme temperatures

Highs and lows are achieved instant values of air temperature, with unique character in the history of meteorological station analyzed, occurring at a time. Extreme temperatures are recorded at intervals of extremely high, this parameter indicates the real limits between oscillating actual values of the air temperature in a certain place on a long period of years, so that has great theoretical and practical importance in assessing climate of regions.
Bucharest geographical position at the junction with the tropical air polar determines the contrasts between winter and summer. Thermal amplitudes grow (Figure 5).
Lows absolute regime annually produced in the winter months due to advections cold air home Arctic or continental moved from the eastern outskirts of anticyclones develop over Europe Northern the Arctic and North Atlantic, while installing above the Mediterranean, Aegean and Black Sea baric low pressure systems (cyclones). Due to these invasions of cold air, continentalized,

there is a sudden increase in air pressure, which leads to the establishment of the anticyclone regime in Romania. Nocturnal radiative cooling, the regime intensified anticyclone conditions (for clear, cold air, low in water vapor) and the presence of snow, the emergence of temperature inversions in winter nights. Absolute minimum air temperature in January 2009 was recorded at the weather station at the Biotechnical Faculty of Engineering of the Polytechnic University of Bucharest, with a temperature of -19.7 ^{0}C, followed by January 2010 with a temperature of -19.2 ^{0}C, with a temperature January 2015 by -16.1 ^{0}C under the influence of a thick layer of snow (Figure 2)

Absolute maximum temperature values were recorded in Bucharest: August 2012 (41.5 ^{0}C), 2012 (40.9 ^{0}C); in April 2013 (32.2 ^{0}C), May 2009 (35.4 ^{0}C), October 2012 (32.7 ^{0}C) - Figure 3.

The highest recorded temperature variations winter days, and the lowest recorded temperature variations on summer days.

Fluctuations in the general circulation of the atmosphere are much lower average temperatures in July variation of July compared to the annual average of this month is in the range of 19.7 ^{0}C and 25.5 ^{0}C compared to 22.15 ^{0}C.

The number of days with temperatures some

Knowing the number of days with certain temperatures is important for agriculture; offer a snapshot of the air temperature in Bucharest.

The number of days below freezing (t ≤0 ^{0}C) of the analyzed period 2009-2015 was 427 in Bucharest, the temperature was below 0 ^{0}C in the months from December to February, in March were fewer days with this temperature.

The number of summer days (t ≥25 ^{0}C) in the analyzed period from 2009 to 2015 in Bucharest was 627. Most summer days with temperatures above 25 ^{0}C were 2015 (134 days) months: June, July, August, September, and sometimes into May.

The number of tropical days (t ≥30 ^{0}C) in the analyzed period from 2009 to 2015 in Bucharest was 317 days with temperatures above 30 ^{0}C were in June, July, August, and September.

In the analyzed period were 49 hot days (t max≥35 ^{0}C) in August 2012 were recorded and three days with temperatures above 40 ^{0}C (Figure 12).

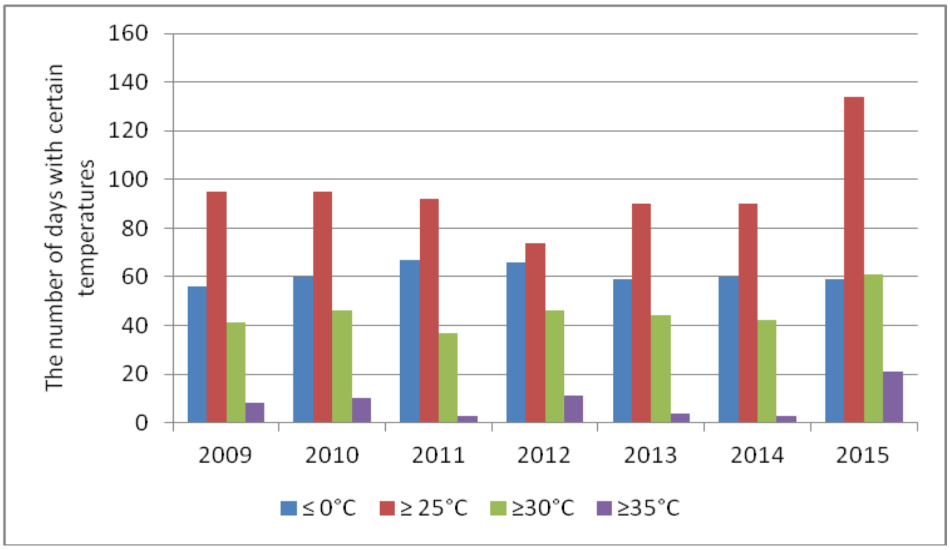

Fig. 12. The frequency of days with different temperatures characteristic Bucharest in 2009-2015

3. Conclusions

By analyzing the thermal variation of the seasonal air temperature observed annual average air temperature increase in winter season, spring, summer and autumn.

An important feature of the trends in the thermal regime in the mid-latitudes is warming, highlighted value growth in average annual regime. Another feature is that the springs and autumns start

earlier. After processing temperatures average values per year, it is observed that if the annual values are very close together (12.1-13.5 °C).
It appears that the warming trend manifested in mean annual temperatures largely due to trend more pronounced warming of the cold season. The increasing trend of annual average temperature of the planet is a topic of current research specialists from around the world, which became apparent at the end and beginning of the new century in our country, but this state is actually considered much of specialists as a normal, non-periodic oscillations being the effect of air temperature, conclusion resulting from the processing undertaken on a large number of weather stations with long strings of data.

References

[1] I. Iojă, “Metode și tehnici de evaluare a calității mediului în aria metropoliatană a municipiului București” 2009;
[2] V. Tufescu, “Modelarea naturală a reliefului şi eroziunea accelerată”, Editura Academiei Republicii Socialiste România, Bucureşti, 618 p., 1966;
[3] Clima Romaniei - Administraţia Naţională de Meteorologie, Ed. Academiei Române, Bucureşti, 2008;
[4] A. Vlăduţ, “Ecoclimatic indexes within the Oltenia plain*”,* Forum geografic.- Studii și cercetări de geografie și protecția mediului, Year 9, No. 9/ 2010, pp. 49-56;
[5] A. Vlăduţ, “Deficitul de precipitaţii în Câmpia Olteniei în perioada 1961-2000”, Forum Geografic – Studii şi cercetări de geografie şi protecţia mediului, Year III, No. 3, Editura Universitaria, Craiova, pp. 99-104, 2004;
[6] C.-O. Rusănescu, I. N. Popescu, M. Rusanescu, L. David , “Analysis of variation in relative humidity in autumn 2009”, In: International Journal of Energy and Environment, Issue 4, Volume 4, 2010, pp.113-121, ISSN: 1109-9577;
[7] Scientific Journal of the National Meteorological Administration, Bucharest, 2012-2013;
[8] C.-O. Rusănescu, G. Paraschiv, Gh. Voicu, M. Rusănescu, “Comparative analysis of atmospheric temperature values, relative humidity in 2009 and 2010 in west side of Bucharest city”, In: Bulletin UASVM Agriculture, 68(2)/2011, Print ISSN 1843-5246; Electronic ISSN 1843-5386, pp. 130-138;
[9] V. Sorocovschi, T. Tudose, H. Selagea, P. Roman, “Variația în cursul anului și repartiția teritorială a precipitațiilor medii din Podișul Someșean”, Geographia Napocensis, Year IV, No. 2/2010;
[10] C.-O. Rusănescu, M. Rusănescu, “Some aspects regarding the global warming”, In: Hidraulica no. 4 (2013), pp. 7-11;
[11] C.-O. Rusănescu, “Îndrumar de meteorologie și climatologie”, Editura Matrix Rom, Bucuresti, 2013;
[12] N. Mărunţelu, L. Istode, A. Coman, “Indicii ecometrici, instrumente moderne folosite pentru monitorizarea evoluției ecosistemelor, conservarea biodiversității şi optimizarea conceptului de casă ecologică”, București, 2013.

Theoretical Approaches Regarding the VENTURI Effect

Assistant professor **Fănel Dorel ȘCHEAUA**[1]

[1)] "Dunărea de Jos" University of Galați, fanel.scheaua@ugal.ro

Abstract: *In fluid mechanics there are situations when the fluid flow is carried out inside pipelines with different values of the main flow section. Based on the research works it was therefore demonstrated that when the fluid passes from a larger to a smaller section an increase in flow velocity is obtained together with a decrease of fluid static pressure. This phenomenon it is known as the VENTURI effect. This particular effect is based on both the fluid continuity principle, but also on the principle of conservation of mechanical energy, or BERNOULLI'S principle. This principle shows that inside a specific flow region, a decrease in static pressure appears when it is achieved an increase in fluid velocity. In this paper are presented the theoretical foundations regarding fluid flow inside a special model called the VENTURI tube where the effect can be emphasized. A three-dimensional model of the VENTURI tube was constructed with Solid Edge V20 and analyzed using ANSYS CFX for highlighting the fluid flow inside. The results are presented in terms of velocity and pressure of the working fluid.*

Keywords*: fluid flow, 3D modelling, computational fluid dynamics (CFD)*

1. Introduction

In the XVII century Isaac Newton published his works related to the laws of motion. He is considered the father of physics. Later in XVIII century Daniel Bernoulli published the fluid mechanics principle that describes mathematically how the static pressure changes when fluid flow rate is modifying in time. This principle describes an incompressible fluid flow and it is based on the conservation of energy law.
The Italian physicist Giovanni Battista VENTURI (1746-1822) had made research works in the field of fluid mechanics and published his results in 1797. These results are related to fluid flow inside a constricted tube where he observed that the fluid motion is achieved with a higher velocity in the region having small section area but in the same time with a smaller value recorded for static pressure. In the region with a greater section area the fluid velocity was smaller while the static pressure increased.

2. Daniel Bernoulli's principle

The theoretical approaches that led to the principle formulated by Daniel Bernoulli in 1700's are presented hereinafter.
Daniel Bernoulli published his research regarding fluid mechanics in 1738. He was a mathematician that created a formula that mathematically explains how an increase in a fluid's flow rate results in a decrease of static pressure exerted by that fluid. This equation is based on the Law of Conservation of Energy. In order for the fluid to increase its speed, it must convert its potential energy into kinetic energy. As kinetic energy (velocity) increases, potential energy (static pressure) decreases. [2]
In a permanent flow regime of an ideally, incompressible fluid, subjected to the action of conservative forces, Daniel Bernoulli's equation, as a load equation has the form: [4]

$$\frac{v^2}{2g}+\frac{p}{\gamma}+z=C \tag{1}$$

Where:

- $\frac{v^2}{2g}$ - kinetic load;

- $\frac{p}{\gamma}$ - piezometric load;
- z - position load.

By multiplying equation (1) with fluid specific height and the fluid weight the pressure and energy equation are obtained.
The Bernoulli equation describing the pressure values within an ideal incompressible fluid can be written as: [4]

$$\frac{\rho v^2}{2} + p_{st} + \gamma z = C \tag{2}$$

The energy equation can be written as: [4]

$$G\frac{\rho v^2}{2} + Gp_{st} + G\gamma z = C \tag{3}$$

For a barotropic fluid (compressible), the Bernoulli equation as a load equation can be written as: [4]

$$\frac{v^2}{2g} + \int \frac{dp}{\gamma(p)} + z = C \tag{4}$$

Along a fluid streamline the total pressure can be assumed as: [4]

$$p_s + \frac{\rho v^2}{2} = p_t \tag{5}$$

Where:
p_s - static pressure;
$\frac{\rho v^2}{2}$ - dynamic pressure.

3. VENTURI tube model CFD analysis

A model is constructed for the VENTURI tube and analyzed using ANSYS CFX in order to emphasize the fluid flow parameters represented by air velocity and pressure.

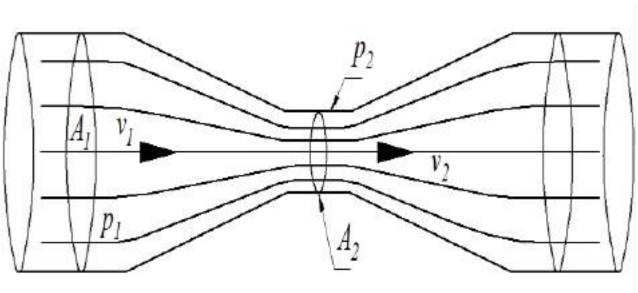

Fig. 1. VENTURI tube mathematical model

For the two main fluid regions can be written: [3]

$$\left(p_s + \frac{\rho v^2}{2}\right)_1 = \left(p_s + \frac{\rho v^2}{2}\right)_2 \tag{6}$$

It is expected that at the modification of fluid flow velocity through the tube interior pressure will change its value in a certain region.

The VENTURI tube model constructed was launched into numerical analysis using ANSYS CFX software to observe the flow parameters of the working fluid (air) circulated through the tube. The results are presented in terms of pressure and velocity of the working fluid, specific values being recorded in different fluid regions within the analyzed model.

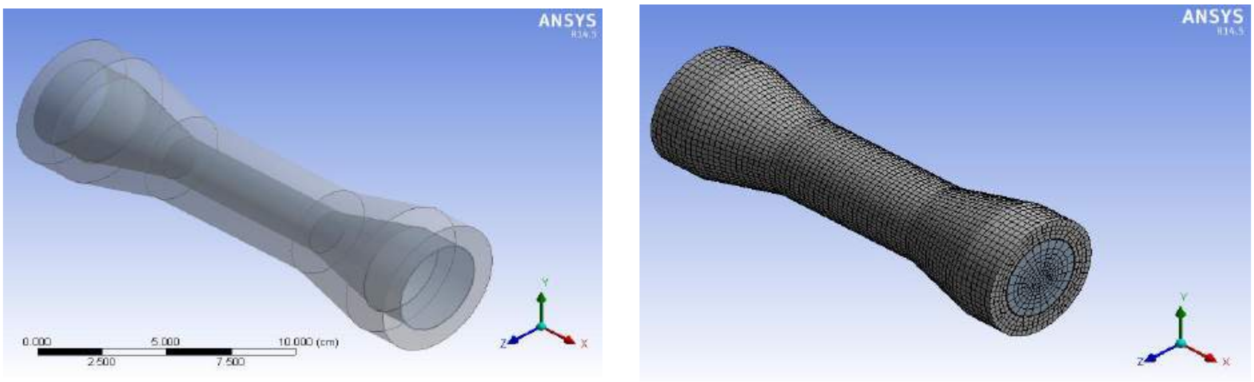

a) Imported model b) Model mesh

Fig. 2. The VENTURI tube three-dimensional model

A mesh was achieved for the three-dimensional model of the VENTURI tube having a total of 25987 nodes and 21987 elements of tetrahedral form.
The analysis of fluid flow through the VENTURI tube was made for the air at 25 degrees Celsius, with the declared static pressure value at the inlet in the range of (1.1, 1.3 and 1.9 bar), while the reference pressure was 1 atm.
Three sets of values were obtained for the parameters that describe fluid flow through the tube interior, being represented by pressure and velocity values on fluid regions. The obtained results are presented for the three cases in the following.

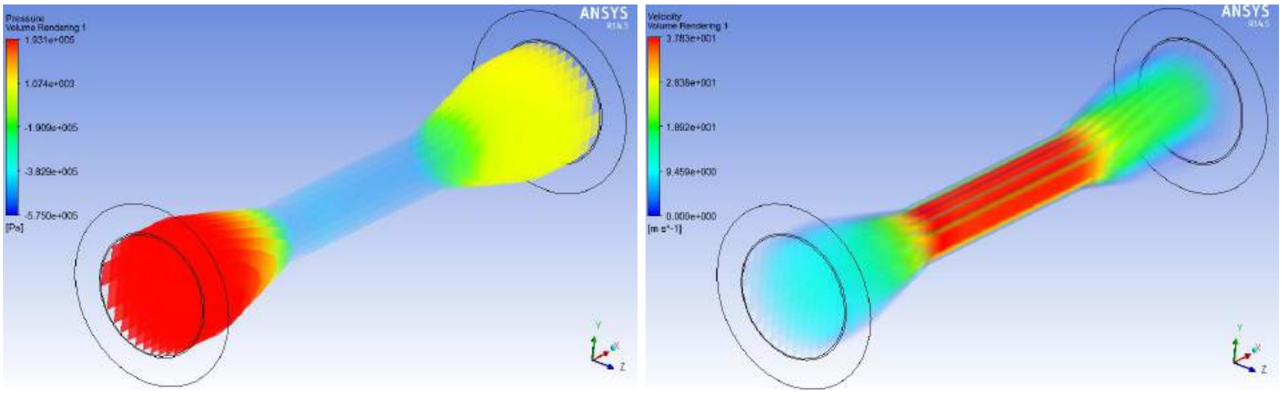

a) The values for static pressure b) Velocity values

Fig. 3. The obtained results for Case 1

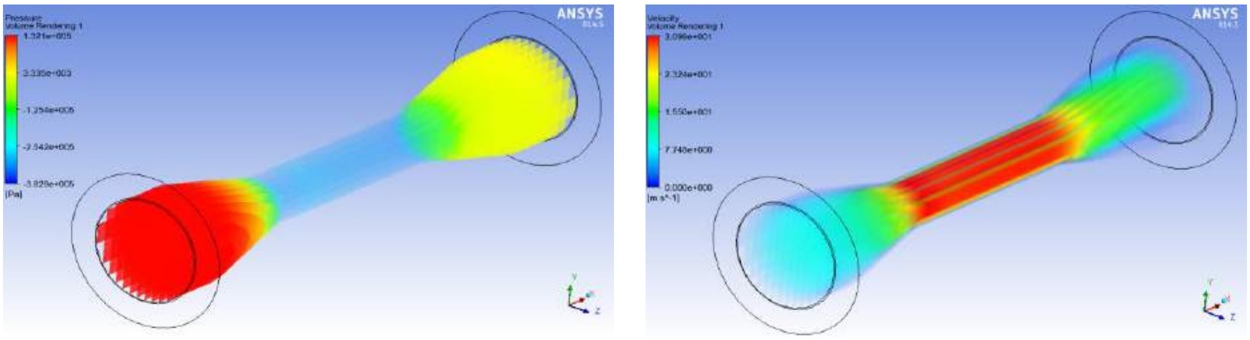

a) The values for static pressure b) Velocity values

Fig. 4. The obtained results for Case 2

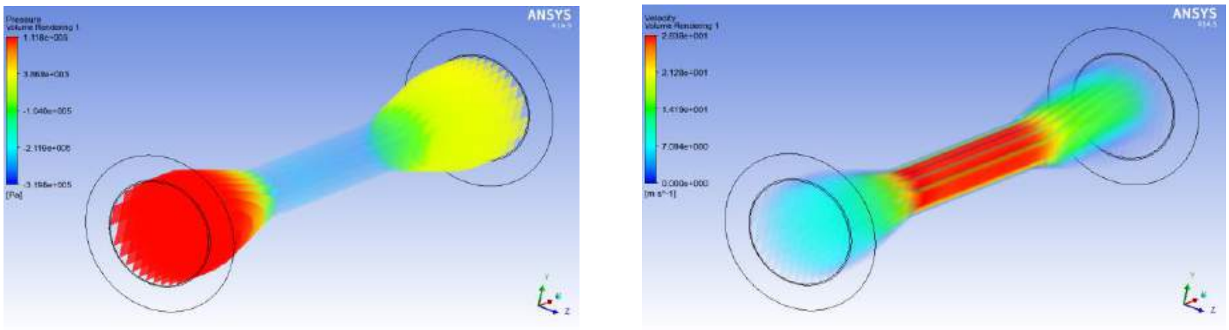

a) The values for static pressure b) Velocity values

Fig. 5. The obtained results for Case 3

In Figures 3-5 are shown the values recorded for the static pressure and flow velocity of the working fluid inside the tube being noted the high levels of the inlet pressure for the large diameter section and the fluid velocity values are low. In the middle section the fluid velocity achieve high values while the static pressure reaches low values.

TABLE 1: Diagrams of the fluid velocity and static pressure values for the three cases

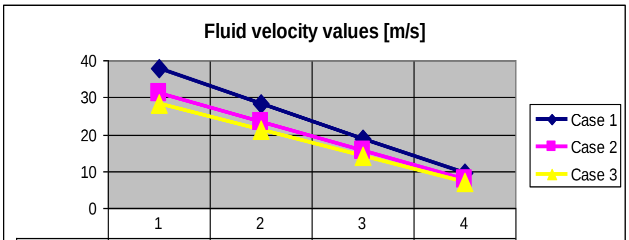

	1	2	3	4
Case 1	37.83	28.38	18.92	9.459
Case 2	30.99	23.24	15.5	7.748
Case 3	28.38	21.28	14.19	7.094

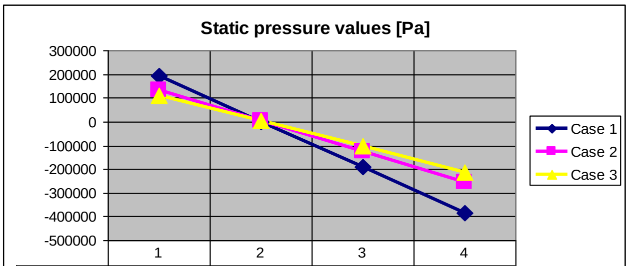

	1	2	3	4
Case 1	193100	1074	-190900	-382900
Case 2	132100	3335	-125400	-254200
Case 3	111800	3868	-104000	-211900

In Table 1 are presented the results diagrams for the three analyzed cases highlighting the maximum and minimum static pressure and velocity values of fluid flow through the tube.

4. Conclusions

A three-dimensionally model of a VENTURI tube was achieved and analyzed in this paper. This model can provide a solution to determine the fluid flow rate in a hydraulic or pneumatic installation using manometers mounted on different sections of the tube. Based on different pressure values recorded can be determined the flow rate for the working fluid circulated through the respective section.

Also by means of the VENTURI tube can be achieved the mixture of two different fluids due to the low pressure values recorded in the middle section where the fluid flow velocity values are high, and as a result a fluid (which may be a liquid or gas) may be absorbed and transported further into the hydraulic system circuit.

This property of making the mixture of two different fluids is used in automobile carburettors where is realized the mixture of liquid fuel and air, or the development of the ejectors also using the mixture of the two fluids.

References

[1] https://www.comsol.com/blogs/exploring-the-venturi-effect/
[2] https://answers.yahoo.com/question/index
[3] http://www.grc.nasa.gov/WWW/K 12/airplane/bern.html
[4] Vasilescu, Al., A., Mecanica fluidelor, Ministerul Educatiei și Învățământului, Universitatea din Galați, Galați, 1979

UNIUNEA EUROPEANĂ

Instrumente Structurale 2014-2020

Comunicat de presă

București, 23.09.2016

Începerea proiectului POC - axa G:
TEHNOLOGII ECO-INOVATIVE DE VALORIFICARE A DEȘEURILOR DE BIOMASĂ

INSTITUTUL NAȚIONAL DE CERCETARE-DEZVOLTARE PENTRU OPTOELECTRONICĂ - INOE 2000 – Filiala INSTITUTUL DE CERCETĂRI PENTRU HIDRAULICĂ ȘI PNEUMATICA București, cu sediul în str. Cuțitul de Argint nr. 14, sector 4, derulează, începând cu data de 23.09.2016, proiectul "TEHNOLOGII ECO-INOVATIVE DE VALORIFICARE A DEȘEURILOR DE BIOMASĂ (ECOVALDES)", cofinanţat prin **Fondul European de Dezvoltare Regională**, în baza contractului de finanţare încheiat cu **Autoritatea Națională pentru Cercetare Științifică și Inovare** în calitate de Organism Intermediar (OI), în numele şi pentru **Ministerul Fondurilor Europene (MFE)** în calitate de **Autoritate de Management (AM)** pentru Programul Operaţional Competitivitate (POC).

Valoarea totală a proiectului este de 7.551.957 lei, din care **asistenţa financiară nerambursabilă** este de 5.768.454 lei.

Proiectul se implementează în regiunile **București-Ilfov** și **Sud-Est**, pe o durată de **54 luni**.

Obiectivul proiectului este dezvoltarea interacțiunii INOE 2000 – IHP cu întreprinderile de producție pentru transferul de cunoștinte în subdomeniul tehnologiilor eco-inovative de valorificare a deșeurilor de biomasă. Ca obiective specifice, proiectul urmărește:

a) Stimularea transferului de cunoștinte către unitățile de producție interesate în domeniul de expertiză al INOE 2000-IHP;

b) Accesul întreprinderilor interesate la facilitățile, instalațiile si echipamentele de cercetare de care dispune INOE 2000-IHP;

c) Transfer de competențe de cercetare industrială pentru linii tehnologice de valorificare a deșeurilor de biomasă vegetală compuse din echipamente de tocare, presare, uscare și ardere prin procedeul TLUD;

d) Cercetare industrială în parteneriat INOE 2000 – IHP cu întreprinderi, în scopul pregătirii fabricației de echipamente mecano-hidraulice componente ale liniilor tehnologice de valorificare a deșeurilor de biomasă vegetală.

Beneficiarii actuali sunt în principal entităţi din categoria IMM-urilor, cu care INOE 2000-IHP a colaborat atât în calitate de partener în diferite proiecte şi programe de cercetare, cât şi ca furnizor de servicii directe: cercetare, proiectare, asistență tehnică, execuție modele experimentale sau prototipuri.

Proiect cofinanţat din **Fondul European de Dezvoltare Regională** prin **Programul Operaţional Competitivitate (POC) 2014-2020**

Date de contact:
Nume persoană contact: Dr. Ing. Gabriela MATACHE
Funcţie: Director de proiect
Tel.: 021 3363991, Fax: 021 3373040 e-mail: fluidas@fluidas.ro

UNIUNEA EUROPEANĂ

Instrumente Structurale 2014-2020

Comunicat de presă

București, 02.09.2016

Demarare proiect POC - Axa E:
CREAREA UNUI NUCLEU DE COMPETENŢĂ DE ÎNALT NIVEL ÎN DOMENIUL CREŞTERII EFICIENŢEI DE CONVERSIE A ENERGIILOR REGENERABILE ŞI A AUTONOMIEI ENERGETICE PRIN UTILIZAREA COMBINATĂ A RESURSELOR

INSTITUTUL NAȚIONAL DE CERCETARE-DEZVOLTARE PENTRU OPTOELECTRONICA - INOE 2000, cu sediul în localitatea Măgurele, Bucuresti-Ilfov, str. Atomiştilor, C.P. 077125 nr. 409, județul Ilfov, România, telefon 0214574522, fax 0314056397, derulează, începând cu data de 02.09.2016, proiectul “**CREAREA UNUI NUCLEU DE COMPETENŢĂ DE ÎNALT NIVEL ÎN DOMENIUL CREŞTERII EFICIENŢEI DE CONVERSIE A ENERGIILOR REGENERABILE ŞI A AUTONOMIEI ENERGETICE PRIN UTILIZAREA COMBINATĂ A RESURSELOR**“, cofinanţat prin PROGRAMUL OPERAŢIONAL COMPETITIVITATE, în baza contractului de finanțare nr. 37/2016 încheiat cu INSTITUTUL NAȚIONAL DE CERCETARE-DEZVOLTARE PENTRU OPTOELECTRONICĂ-INOE 2000.

Valoarea totală a proiectului este de 5.735.282,21 lei, din care **asistenţa financiară nerambursabilă** este de 5.700.282,2 lei.

Proiectul se implementează la sediul filialei INOE 2000-IHP în localitatea Bucureşti, sector 4, str. Cuţitul de Argint nr. 14, C.P. 040558, pe o durată de **36 luni**.

Obiectivul proiectului este crearea unui nucleu de competentă ştiinţifică şi tehnologică, de înalt nivel, în domeniul creşterii performanţelor de conversie pentru tipurile de energie regenerabilă care se găsesc în cantităţi importante pe teritoriul României (solară, biomasă, eoliană, hidro). Nucleul astfel creat va avea ca obiectiv prioritar participarea la competiţiile naţionale, dar mai ales internaţionale în domeniu.

Beneficiar: INOE 2000-IHP. Potenţiali beneficiari ai rezultatelor proiectului: persoane publice sau private care vor utiliza sistemele combinate, persoane angajate în fabricarea, vânzarea, montarea, întreţinerea şi exploatarea produselor.

Rezultate prevăzute: Indicatorii de realizare preconizati a fi realizati constau în: noi cercetători în entitatea care beneficiază de sprijin (ENI), publicaţii științifice rezultate din proiect, co-publicaţii științifice public-private, propuneri de proiecte depuse pentru Orizont 2020, cereri de brevet, rapoarte de încercare/testare, metodologii de testare, cărţi tehnice, referenţiale, studii tehnice, studii de fezabilitate, prototipuri realizate, documentatii complete de introducere în fabricatie, proiecte tehnice ce pot fi dezvoltate, standuri realizate, modele experimentale realizate, modele demonstrative, workshop-uri pe teme de energie regenerabilă, modele la scară realizate și testate.

Proiect cofinanţat din **Fondul European de Dezvoltare Regională** prin **Programul Operaţional Competitivitate (POC) 2014-2020**

Date de contact:
Nume persoană contact: Dr. Ing. Cătălin DUMITRESCU
Funcţie: Director INOE 2000 - IHP
Tel.: 021 3363991, Fax: 021 3373040 e-mail: dumitrescu.ihp@fluidas.ro


http://hidraulica.fluidas.ro